Chem Soc Rev

This article was published as part of the

2008 Chemistry at Surfaces issue

Reviewing the latest developments in surface science

All authors contributed to this issue in honour of the 2007 Nobel Prize winner Professor Gerhard Ertl

Please take a look at the issue 10 table of contents to access the other reviews

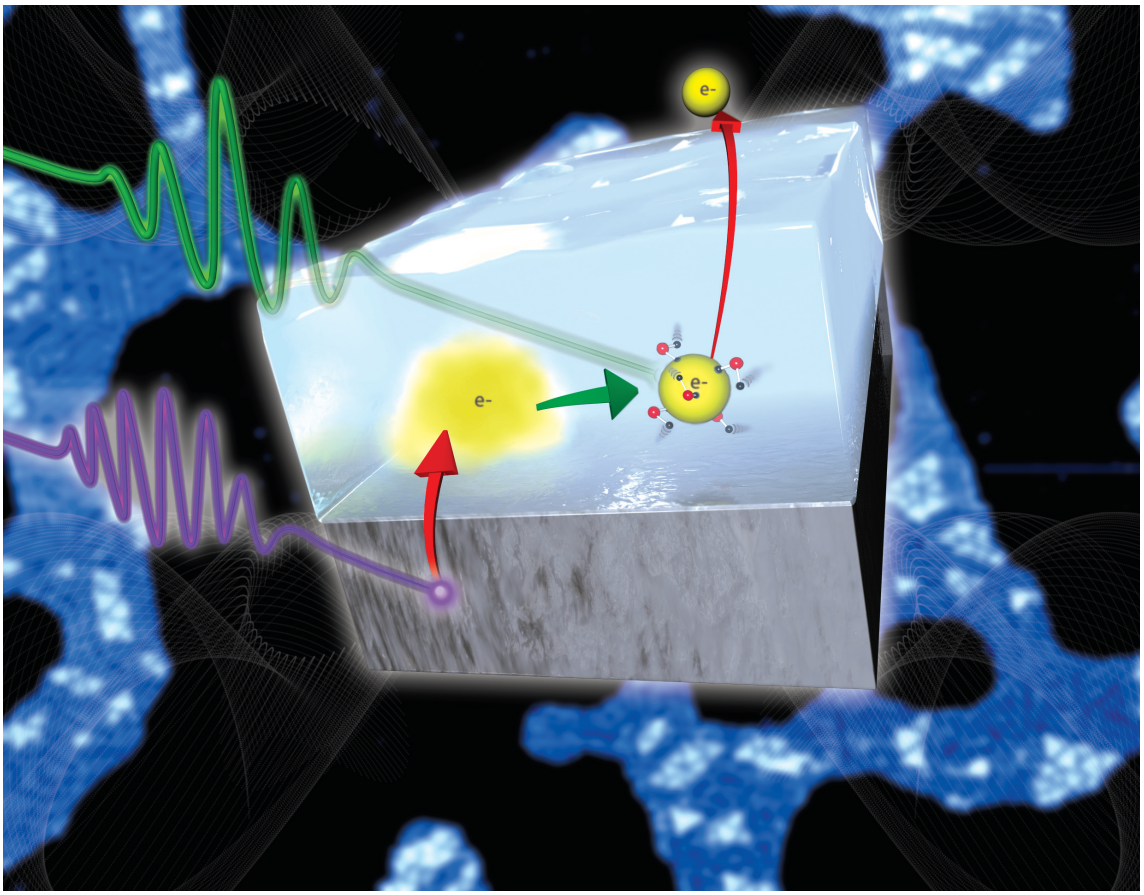

Chem Soc Rev

Chemical Society Reviews

www.rsc.org/chemsocrev

Volume 37 | Number 10 | October 2008 | Pages 2141–2360

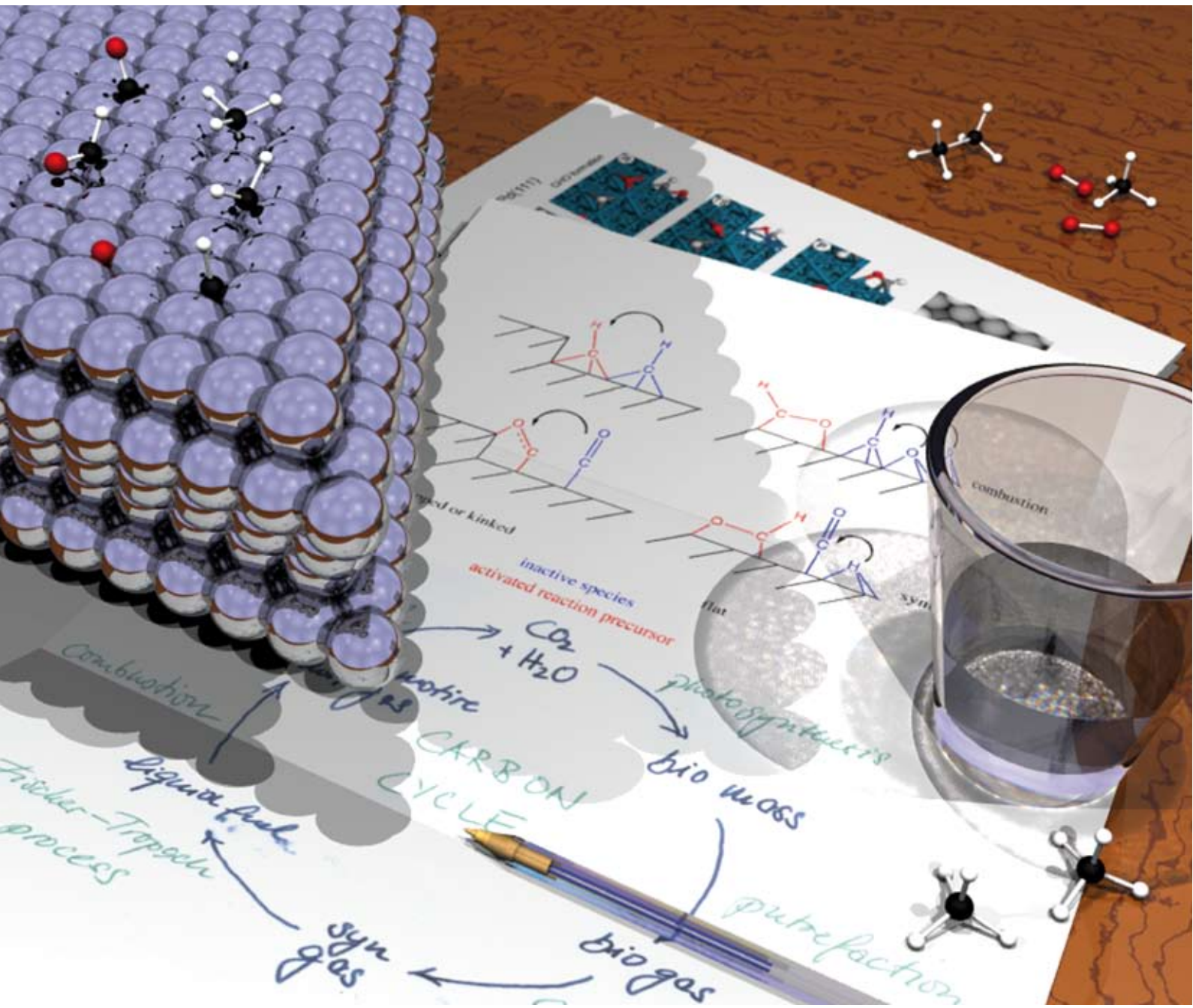

ISSN 0306-0012

CRITICAL REVIEW
Oliver R. Inderwildi and Stephen J. Jenkins
In-silico investigations in heterogeneous catalysis—combustion and synthesis of small alkanes

TUTORIAL REVIEW
Gabor A. Somorjai and Jeong Y. Park
Molecular surface chemistry by metal single crystals and nanoparticles from vacuum to high pressure

RSC Publishing

In-silico investigations in heterogeneous catalysis—combustion and synthesis of small alkanes†

Oliver R. Inderwildi and Stephen J. Jenkins*

Received 16th June 2008
First published as an Advance Article on the web 8th September 2008
DOI: 10.1039/b719149a

In this *critical review*, we cover first-principles density functional calculations relevant to alkane oxidation and synthesis over transition metal catalysts. For oxidation, we focus upon Pt, Rh, Pd and Ni surfaces, while for synthesis we consider Co, Ru, Fe and Ni. Throughout, we emphasise the insight to be gained by thinking of each kind of reaction as the inverse of the other, with the directionality determined simply by the choice of metal catalyst and the reaction conditions. We highlight particularly the role of low-coordination sites (steps, kinks, *etc.*) and the emerging consensus over the importance of the formyl intermediate in facilitating the rate-determining step (249 references).

1. Acronyms

ARPES	Angle-resolved photoemission spectroscopy
BtL	Biomass-to-liquid (process)
DFT	Density functional theory
(HR)EELS	(High resolution) electron energy loss spectroscopy
FT	Fischer–Tropsch (process)
FP-LAPW	Full-potential linearised augmented-plane wave
GGA	Generalised gradient approximation
GtL	Gas-to-liquid (process)
LAAD	Laser assisted associative desorption
LDA	Local density approximation
LEED	Low energy electron diffraction
NEB	Nudged elastic band method
NEXAFS	Near edge X-ray absorption fine structure
PBE	Perdew–Burke–Ernzerhof (GGA functional)
PES	Potential energy surface
PW91	Perdew–Wang 91 (GGA functional)
RAIRS	Reflection absorption infra-red spectroscopy
RPBE	Revised PBE (GGA functional)
STM	Scanning tunnelling microscopy
UPS	Ultraviolet photoelectron spectroscopy
XPS	X-Ray photoemission spectroscopy

Department of Chemistry, University of Cambridge, Lensfield Road, Cambridge, UK CB2 1EW. E-mail: sjj24@cam.ac.uk
† Part of a thematic issue covering reactions at surfaces in honour of the 2007 Nobel Prize winner Professor Gerhard Ertl.

2. Introduction

Climate change is arguably the most severe threat currently faced by mankind;[1] moreover, overwhelming evidence now exists to link anthropogenic greenhouse gases to its recent acceleration.[2,3] Of these, the most influential is CO_2, whose predominant man-made emission source is the combustion of fossil fuels.[4] Whether the unprecedented meteorological disasters experienced in recent years, such as Hurricane Katrina in the United States or widespread flooding in the UK and Europe during the summer of 2007, can yet be directly linked to anthropogenic influences remains more controversial. Nevertheless, these hitherto rare events will doubtless become commonplace in the future if the atmosphere's greenhouse gas concentration continues to rise. Looking beyond such

Oliver R. Inderwildi

Oliver Inderwildi is a postdoctoral research fellow in the Reactive Solid Surfaces group in the Department of Chemistry at Cambridge University, and a College Research Associate at Trinity Hall. He read chemistry at Heidelberg and Amsterdam Universities and subsequently joined the Interdisciplinary Centre for Scientific Computing specialising in computer simulations of emission control catalysts.

Stephen J. Jenkins

Stephen J. Jenkins heads the Reactive Solid Surfaces group in the Department of Chemistry at the University of Cambridge, where he holds a Royal Society University Research Fellowship. He received his BSc and PhD degrees in Theoretical Physics from the University of Exeter in 1991 and 1995, respectively, and is a Fellow of St Edmund's College.

headline-grabbing phenomena, even subtle modification of weather patterns should be expected to have far-reaching geopolitical consequences. Models indicate, for instance, that the current drought plaguing the Darfur region of the Sudan may have been caused by relatively small changes in the global climate;[3] this drought is credited with exacerbating ethnic and cultural tensions, terminating centuries of peaceful coexistence with a civil conflict that may have cost as many as 400 000 lives to date.[5] But if the Darfur conflict can be identified as the first to be driven by the local effects of global climate change, it is unlikely to be the last.[6] For a comprehensive overview of the causes and consequences of climate change induced by emission of greenhouse gases, the interested reader is referred to a recent book by Walker and King.[2] For a similarly comprehensive analysis of the outlook and limitations of long-term climate modelling, we refer to the excellent articles by Allen and co-workers.[7]

Owing to these potentially devastating effects upon our global environment, and their inevitable consequences for prospects of our peaceful coexistence on this planet, it is of paramount importance to move urgently to a carbon-neutral economy (*i.e.* one based upon utilisation of fuels that do not stem from fossil deposits, such as oil fields). One route towards such an economy may be the conversion of biomass into liquid fuels (*i.e.* liquid hydrocarbons). Biomass, which is generated from CO_2 and H_2O by photosynthesis, can thus be converted into liquid fuels that are again combusted to H_2O and CO_2. In this scheme, energy is ultimately extracted from sunlight, *via* a short-period carbon cycle, without release of fossil carbon from reserves into the atmosphere.

Plant biomass is presently the only sustainable source of organic carbon.[8] There are two routes for converting plant biomass into liquid fuels, one biological and the other chemical.[9] In the biological route, enzymes and microorganisms are utilised to yield mainly alcohol; in the chemical route abiological catalysts, mainly based on transition metals, are utilised to yield a mixture of liquid hydrocarbons, commonly referred to as biodiesel.

The essential problem is to convert biomass, which consists of sugar polymers and contains significant amounts of oxygen, to shorter building blocks (carbon chain length between around five to sixteen atoms), with a significantly lower oxygen content. This has to be done without losing significant amounts of the biomass energy content in order to achieve feasibility.

In the biological route, the starch and cellulose is broken down to glucose, utilising enzymes, and this sugar is subsequently fermented to alcohol. During the fermentation oxygen is partially removed from the sugars by CO_2 formation, but alcohol as a fuel suffers from a low energy density compared to liquid hydrocarbons and is also hygroscopic (a too high water content would further lower the energy density provided by the fuel or even make it unusable). The main argument against these fuels, however, is that they are derived from edible biomass and hence fuel production would compete with food production, which—in turn—could lead to severe socio-economic problems.[10]

In the chemical route, in contrast, inedible biomass such as harvest leftovers is gasified (oxidised) to synthesis gas (CO & H_2) and subsequently the synthesis gas is converted to a mixture of liquid hydrocarbons using the so-called Fischer–Tropsch process. Fischer–Tropsch synthesis—a gas-to-liquid (GtL) process—was already used to circumvent oil embargoes towards the Axis during World War II[11] or towards the South African regime during the Apartheid[12] by converting coal into synthesis gas, which was subsequently liquefied to synthetic fuels. These liquid hydrocarbons could then be used as fuels for internal combustion engines. Essentially the same technology remains in use today. In Fig. 1, however, we propose a hybrid carbon cycle in which biomass is converted to natural gas (mainly methane) *via* putrefaction (biological) while three of the six steps are carried out utilising heterogeneous catalysis (1–3). In step 1, natural gas is converted to synthesis gas using processes such as steam reforming or catalytic partial oxidation, commonly catalysed by platinum-group metals; in step 2, this synthesis gas is liquefied using the Fischer–Tropsch process, commonly using metals such as iron, cobalt or ruthenium; in step 3, automotive catalytic converters, usually complex multi-component systems,[13] are used to convert the toxic exhaust, which contains CO, hydrocarbons, soot and nitrous oxides, into CO_2 and water with near-to-zero pollutant concentrations. This purified exhaust can then be utilised by plants to grow (*i.e.* to produce biomass).

This carbon cycle stresses the importance of heterogeneous catalysis for future societies. In the event that all the steps become economically feasible, the depicted cycle would be a possibility to provide energy for applications such as individual transportation, without significantly increasing the amount of green-house gas in the atmosphere *and*, equally importantly, using inedible biomass. For a more comprehensive overview of the state-of-the-art in biofuel synthesis, the interested reader is referred to several excellent review and highlight articles published in recent years.[14]

What at first glance looks like a closed cycle that essentially harvests energy from sunlight, actually also demands energy. The Fischer–Tropsch synthesis (step 2 in Fig. 1), for instance, is a high-pressure process that is carried out at elevated temperature and hence practical implementation of this step consumes energy, lowering the feasibility of the proposed

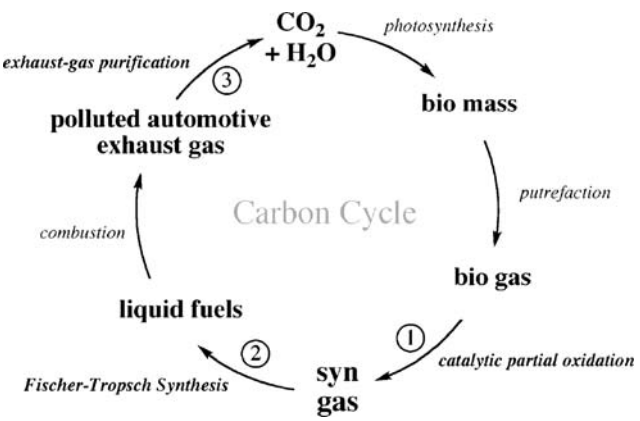

Fig. 1 Carbon cycle, the catalytic steps are numbered. Reprinted from ref. 75, Copyright Wiley-VCH Verlag GmbH & Co.KGaA. Reproduced with permission.

carbon cycle. In the oxidation of natural gas (step 1), *via* whatever means, a considerable proportion of its energy is released in the form of heat, also lowering the feasibility of this carbon cycle. The necessary energy inputs can, of course, be derived by combustion of a fraction of the manufactured fuel, but the overall efficiency (and hence economic viability) will be reduced. The catalytic steps in the cycle have therefore to be improved until the whole has a positive energy balance, with solar energy powering the photosynthetic step. In order to improve the catalytic steps, the processes in the catalysts have to be fully understood. While processes on various time and length scales influence the activity of a catalyst, the most crucial factor is the kinetics of the chemical reactions on the surface of metal (or metal oxide) particles.

Surface scientists have made considerable progress in elucidating surface reaction mechanisms by studying low-index and stepped metal surfaces under ultra high vacuum (UHV) conditions since the 1960s, which was recognised by the 2007 Nobel Prize for Chemistry awarded to Gerhard Ertl. Adjunct to the methods used by experimentalists,[15] theoretical studies carried out during the past ten years utilising density functional theory (DFT) calculations have brought significant insight into reaction mechanisms on transition metal surfaces.[16–18] DFT is a technique based on the Hohenberg–Kohn theorem (Nobel Prize for Chemistry awarded to Walter Kohn in 1998), which proves that for calculation of the electronic ground state properties a knowledge of the electron density is as good as knowledge of the many-electron wave function; the total energy of a system can consequently be expressed as a functional of the electron density. Since the electron density of a system can be computed far more easily than the many-electron wavefunction, DFT made total energy calculations of larger systems (including initially jellium and later metal surfaces) computationally feasible.

The first DFT calculations of jellium surfaces were published in the late 1960s and the early 1970s by Lang and co-workers.[19] Subsequently, the adsorption of atomic adsorbates such as oxygen and hydrogen on jellium surfaces was studied in the same group.[20] By the late 1970s, Goddard and co-workers had studied the adsorption of atoms on cluster models of metal surfaces.[21] In 1980, Lang and Nørskov published the first paper concerned with molecular adsorption on realistic slab models of metal surfaces,[22] which the present authors consider to be a milestone on the way to elucidation of reaction mechanism by means of DFT. Later in the 1980s, Hoffmann *et al*. published transition states for the dissociation of H–H and C–H bonds on clusters mimicking Ni{111} and Ti{0001} using his extended Hückel method, and explained adsorption on metal clusters using frontier orbital theory, both marking further milestones on the way to a theoretical approach for reaction mechanism development.[23]

The next barrier to be scaled in the field of DFT was the development of algorithms that locate the transition state of a reaction on the potential energy hypersurface; this allowed computational chemists to study reactions and leads to studies that report complete branches of complex reaction mechanisms.[24] Apart from simple interpolation methods, constrained minimisation was one of the first methods to determine accurate transition states (as for instance in ref. 25 and 26); subsequently, methods such as quadratic synchronous transit evolved,[27] which lead to equally accurate transition states (especially when combined with constrained conjugate gradient refinements[28]) while automating, to some degree, the selection of an appropriate reaction coordinate. Recently, many DFT codes employ methods such as the nudged elastic band method to determine transition states in cases where the reaction coordinate may be complex and not readily apparent *a priori*.[29] An improved version of this algorithm, the climbing image nudged elastic band method is expected to improve the results of NEB calculations still further.[30] Highly accurate hybrid eigenvector-following methods (as for instance applied in the OPTIM code) give probably the most accurate transitions states, with root-mean-square force values close to zero, while being rather computationally time consuming.[31]

The first DFT-based determination of a transition state for a dissociation reaction on a realistically modelled metal surface was, we believe, presented by Hammer *et al*.[32] in 1992, who studied the dissociative adsorption of hydrogen on Al{110}.[4] Since then an enormous number of studies have investigated surface reaction mechanisms on metallic[16,33–38] as well as oxidic surfaces[39] and even on metal particles supported on oxides.[40] It is hence difficult to provide a comprehensive overview of *all* the reaction mechanisms developed by DFT calculations. This review is instead focussed only upon the insight gained through DFT calculations into hydrocarbon formation and combustion processes over transition metal surfaces.

The article is subdivided into two main parts: first, the conversion of hydrocarbons on transition metal surfaces as relevant for steps 1 and 3 in our example carbon cycle; and second, the synthesis of hydrocarbons from carbon oxides (CO_x). We deliberately neglect the synthesis of hydrocarbons by hydrogenation of aromats, alcohols and other oxygen-containing organic substances. The review of hydrocarbon synthesis will moreover focus on the initial steps of the hydrocarbon synthesis as these are the steps which are well studied. Studies of longer chain hydrocarbons on surfaces are rather scarce due to the complexity of the adsorption system; furthermore, the initial steps appear to be the rate determining steps, justifying our focus.

2.1 Hydrocarbon oxidation on transition metal surfaces

Although the Haber–Bosch process—the synthesis of ammonia from "air"—is commonly referred to as the first heterogeneously catalysed process utilized on an industrial scale, heterogeneous oxidation processes were applied (albeit on a smaller scale) somewhat earlier. About 1900, the "lead chamber" method to produce sulfuric acid was replaced by a heterogeneously catalysed process in which platinum was utilized to oxidize SO_2 with air.[41] The Haber–Bosch process, however, remains *the* breakthrough in large-scale synthesis using heterogeneous catalysis *and* high-pressure chemistry, going online in 1913. Shortly thereafter, in 1915, the catalytic oxidation of ammonia over Pt for the production of nitric acid, as proposed by Ostwald, was commercialized. This can be set as the first large-scale oxidation process using heterogeneous catalysis, the next important step being realisation of

the water–gas shift reaction ($CO + H_2O \rightarrow CO_2 + H_2$), which in turn promoted implementation of the Haber–Bosch process (because hydrogen could now be produced from coal on a large scale *via* gasification and subsequent water–gas shift reaction). Water–gas shift was at first carried out using iron oxide as a catalyst, but later employed copper, which enabled engineers to carry out the reactions at more ambient temperatures. Thereafter, World War II "catalysed" catalyst development, because both sides were in need of war-relevant products such as gunpowder, high-octane fuels for airplanes or indeed regular fuels to circumvent embargoes, *vide infra*.

Nowadays, many large-scale oxidation processes are heterogeneously catalysed, as for instance the partial oxidation of alkenes to alcohols or epoxides,[42] or of methane (natural gas) to synthesis gas.[43] Also in the control of emissions from combustion engines, as for instance in cars, oxidation catalysis plays an important role: in the well-known three-way catalyst, CO and unburnt hydrocarbons are removed by oxidation on transition metals; in this case rhodium, platinum, iridium and palladium are the metals of choice.[44] Other important tasks for oxy-catalysts are the preferential oxidation (PROX) of CO from syngas[45] or the selective partial oxidation of alkanes into higher-value oxygenated compounds.[46] For readers interested in experimental studies of hydrocarbon fragments on transition metal surfaces, we refer to excellent review articles by Zaera.[47] An excellent theoretical study of the molecular adsorption of saturated alkanes was published by Öström *et al.*;[48] this article also discusses the difficulty of describing these systems by means of DFT and is therefore recommended by the present authors.

2.2 Hydrocarbon synthesis on transition metal surfaces

The main process for production of hydrocarbons from synthesis gas is the so-called Fischer–Tropsch process, already mentioned in the general introduction. This process is well-established and has been utilized on an industrial scale for more than 80 years.[12] In 1943, for example, more than seven million tons of liquid fuel was synthesised using the Fischer–Tropsch process, which enabled Nazi Germany to keep its war machinery going even though it was cut off from crude oil supplys due to the ascendancy of allied naval forces after 1942. Today it is once again of vital economic interest because it can also be utilised to convert biomass into liquid fuels.[12] It is thus a potential source of highly clean, carbon-neutral fuels, which could help to mitigate global warming due to CO_2 emissions, *vide supra*.

The initial publication of the Fischer–Tropsch process reported the activity of the transition metals iron and cobalt as active components, and indeed both metals are still used in industrial applications nowadays.[12,49] Later, other metals, such as nickel and ruthenium were introduced as FT catalysts, yielding liquid hydrocarbons with longer carbon chain length than obtained using iron or cobalt as a catalyst. Iron suffers from deactivation by water, which is formed as a side product in the FT synthesis.[12] Cobalt does not, and was already applied in the pioneer plant at Ruhrchemie as early as 1935.[12] State-of-the-art cobalt catalysts are designed to produce wax (composed of paraffins), which is subsequently cracked to yield liquid hydrocarbons. Using this combination of FT synthesis and hydrocracking, a diesel fuel selectivity of up to 80% can be achieved.[50] A drawback of both cobalt and iron, however, is that those metals need promoters, making the catalyst synthesis more difficult and mechanistic studies more demanding.[12] One metal that does not need any promoting agents is ruthenium, and this metal has further advantages: it is the most active of FT catalysts, works at the lowest temperature, and produces the highest molecular weight hydrocarbons. This is probably one of the reasons why Ru is the best studied metal, with regard to the FT process.

It is noteworthy that the metals that catalyse the formation of hydrocarbons in a one-step reaction are the ferromagnetic metals Fe, Co and Ni as well as the platinum-group metal Ru. Presumably the same electronic feature that favours ferromagnetism, namely an exceptionally high density of states at the Fermi level in the spin-compensated system, also favours the chemical steps in the FT synthesis. Another reaction for the synthesis of hydrocarbons from syngas is the so-called methanation reaction, in which methane is produced, mainly using a nickel-based catalyst.‡ The authors, however, regard the methanation reaction as a special case of the Fischer–Tropsch synthesis that just happens to be highly selective towards the C_1-hydrocarbon methane. The obvious assumption is that on nickel surfaces hydrogenation reactions can be significantly faster then C–C coupling reactions, making the reaction very selective towards methane production.

3. Catalytic alkane oxidation

The combustion of hydrocarbons on transition metal surfaces implies an evolution of the relevant carbon-containing species through four distinct stages, namely: (i) adsorption of the hydrocarbon; (ii) possible partial or complete dissociation of the adsorbed hydrocarbon; (iii) oxidation of the dissociation products, possibly followed by further dissociation steps; and (iv) desorption of the oxidation products. The initial adsorption may, in principle at least, be either molecular or (partially) dissociative in nature; subsequent dissociation may involve dehydrogenation and/or carbon–carbon scission; oxidation may occur *via* reaction with adsorbed oxygen adatoms (O) or involve intact adsorbed molecular dioxygen (O_2); and the final balance of the desorbed products is inevitably influenced by all of the above considerations.

In this section, we review the current theoretical literature[51]§ relating to alkane oxidation on platinum, rhodium, palladium and nickel surfaces. For the most part, this amounts to a series of studies concerning alkane dissociation (we summarise the dissociation in Fig. 2), in many of which the relevance to oxidation is implicit rather than overt. In addition, some studies of oxygen adsorption are also cited, for

‡ With increasing reaction temperature the selectivity in the FT synthesis changes from formation of liquid hydrocarbons to methane production. This tendency is most pronounced on Ni, but also observed with Co and Ru to a lower degree. Fe is selective towards liquid hydrocarbons even at very high temperature.[12]

§ An excellent overview of the experimental literature, particularly in regard to initial adsorption, is given in a relatively recent review by Weaver, Carlsson and Madix.[51]

obvious reasons. Only in a relatively small number of cases have studies been published that consider coadsorption of the key reactants and that explicitly explore the detailed mechanism of the oxidation process itself. Where available, such material is particularly highlighted in the following discussion. For each element, we further organise our review according to the structure of the surfaces involved, recognising the distinction between flat, stepped and kinked surfaces,[52,53] in particular, as a crucial factor in determining surface reactivity.

3.1 Platinum

Flat Pt surfaces: {111}, {100}. Studies relevant to alkane oxidation on the flat surfaces of Pt have largely been confined to the {111} facet, the {100} surface being almost entirely neglected to date. Regarding methane adsorption and dissociation, initial experimental studies from Zaera[54] reported spectroscopic evidence for methyl (CH_3) and methylene (CH_2) moieties on the surface upon heating adsorbed methyl iodide above around 200 K, while subsequent results from

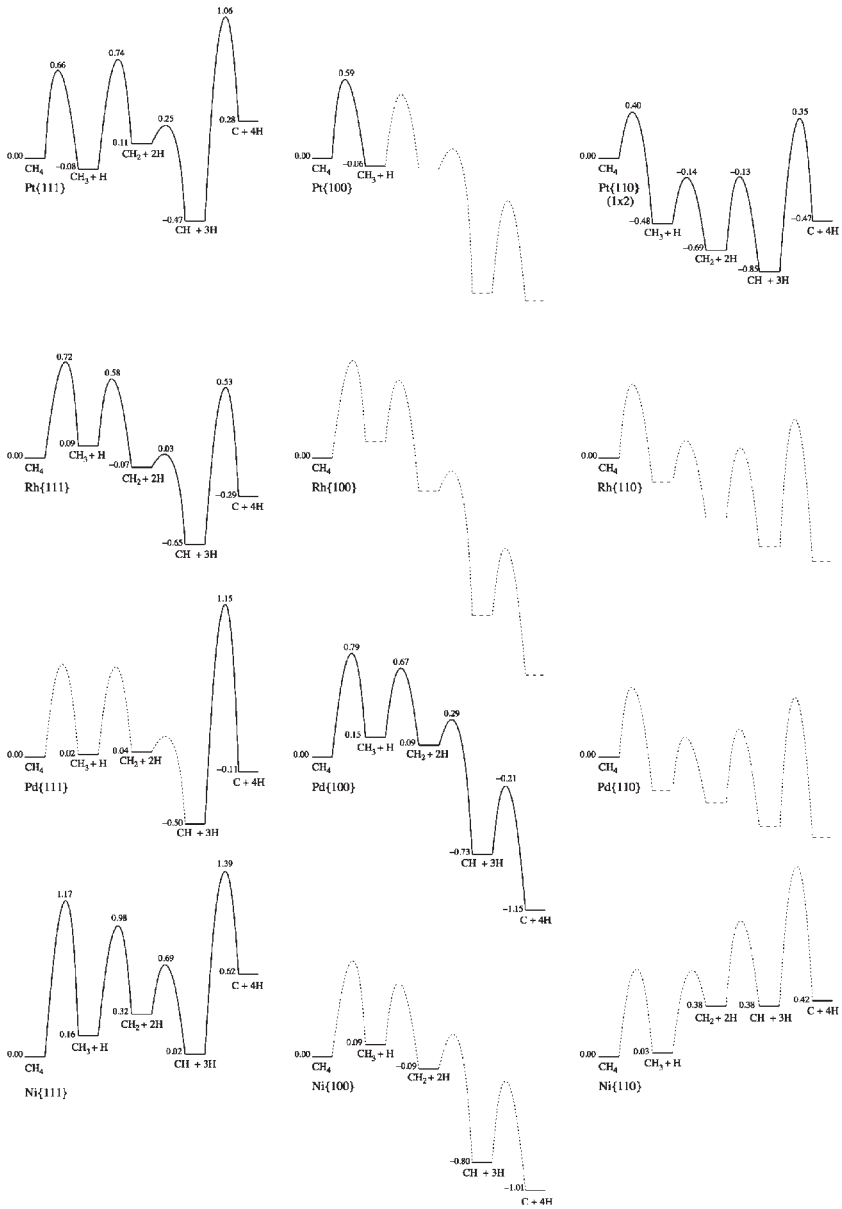

Fig. 2 Solid horizontal lines indicate DFT energies, relative to gas-phase methane above the clean surface, on the assumption that all the hydrogen atoms generated remain on the surface, adsorbed distant from the hydrocarbon fragment (*i.e.* H and CH_x adsorption calculated on separate slabs); marked energies are in eV per original methane molecule, and the intermediate is indicated with a label. The high points of solid curved lines indicate DFT barriers, obtained in the forward direction; marked energies are derived by taking the quoted barrier and adding it to the energy of the more hydrogenated intermediate, so again these are measured relative to the energy of gas phase methane above the clean surface. Broken, unmarked lines are plausible guestimates based on interpolation between extant data from extant adjacent systems (for the energies of intermediates) and Brønsted–Evans–Polanyi arguments (for the activation barriers). Data for Pt was taken from ref. 25, 26, 36, 67, 68, 80 and 81; Rh data was taken from ref. 115; Pd data was taken from ref. 75, 132 and the present work; and Ni data came from ref. 158 and 159.

other groups[55] were interpreted as possibly indicating the formation of ethylidyne (CCH_3) *via* carbon–carbon coupling at high coverage. In contrast, recent supersonic molecular beam XPS studies[56,57] suggest that methyl (CH_3) decomposes on the surface at temperatures exceeding 250 K to form methylidyne (CH), and provide no confirmation of a carbon–carbon coupling reaction. RAIRS studies by Trenary and co-workers[58] indicate that methylene (formed by decomposition of diiodomethane) is unstable against dehydrogenation to methylidyne (CH) at temperatures above 130 K.

The first credible application of DFT to alkane adsorption on Pt{111} can be traced to the groups of Goddard[59–61] and Dumesic,[62] whose cluster calculations revealed a clear preference for methyl (CH_3) to bind at the atop site, for methylene (CH_2) to bind at the bridge site, and for methylidyne (CH) to bind at the threefold coordinated hollow site (specifically, the *fcc* hollow site in the work of the Dumesic group[62]). Such predictions are consistent with expectations, dating back at least to the tight-binding calculations of Minot, Van Hove and Somorjai in the early 1980s,[63] that suggest completion of carbon tetravalency¶ as a driving force for adsorption site selection amongst hydrocarbon fragments on this surface. Realistically, however, the small size of the clusters employed (only eight Pt atoms, in a single layer, for the work of Goddard and co-workers;[59–61] ten Pt atoms in three layers for that of Dumesic and co-workers[62]) means that these early results have indicative value only, from a modern perspective.‖ Nevertheless, the prediction that methyl (CH_3) should prefer the atop site was swiftly confirmed by more reliable periodic slab calculations reported by Papoian *et al.*,[66] and later work in a similar vein has consistently concurred with all the cluster-based site assignments.[65,67,68]

Taking matters somewhat further, Michaelides and Hu[67,68] were the first to calculate transition states for the dehydrogenation of methane on Pt{111}. They obtained barriers of 0.66 eV for the initial dissociative chemisorption process ($CH_4 \rightarrow CH_3 + H$); 0.82 eV for the methyl-to-methylene reaction ($CH_3 \rightarrow CH_2 + H$); 0.14 eV for the methylene-to-methylidyne reaction ($CH_2 \rightarrow CH + H$); and 1.53 eV for the methylidyne-to-carbon reaction ($CH \rightarrow C + H$). These provide a very strong argument in support of the notion that methylene (CH_2) is almost certainly *not* a majority product of methane dehydrogenation on this surface, since a temperature sufficient to allow formation of methylene from methyl (CH_3) would certainly also allow even more rapid decomposition of methylene to methylidyne (CH), pre-dating the clearest experimental evidence for that view[56–58] by some years.

Meanwhile, the adsorption of oxygen on Pt{111} has been the subject of several DFT studies within the past decade or so.[65,69–72] Eichler and Hafner[72] explored the potential energy surface for O_2 chemisorption, concluding that the most tightly-bound molecular precursor for dissociative adsorption symmetrically bridges between two nearest-neighbour Pt atoms, with an adsorption heat of 0.85 eV; a second chemisorbed precursor state was also found, with an adsorption heat of 0.76 eV and a tilted orientation located above the *fcc* hollow site. The barrier to dissociation was estimated (with fixed substrate atoms) as 0.18 eV relative to the energy of the gas-phase molecule (hence perhaps in the range 0.95–1.05 eV relative to the precursor states). The precise numerical values are slightly different in a subsequent publication from the same group,[71] but qualitatively the results are the same (the molecular precursor reported in the later work has a binding energy of 0.72 eV in the bridging geometry, and the dissociation barrier is 0.90 eV relative to this). Bocquet *et al.*[69] found very similar molecular states, but with lower adsorption heats and relative energy-ordering marginally reversed (0.65 eV adsorption heat for the tilted molecule above the *fcc* hollow site; 0.64 eV for the symmetric bridged species). These discrepancies are likely caused by the different unit cells and k-point samplings used in the two works (a $c(4\times2)$ cell with $3 \times 4 \times 1$ sampling for Eichler *et al.*,[71,72] but a (2×2) cell with $5 \times 5 \times 1$ sampling for Bocquet *et al.*[69]). Oxygen adatoms preferentially occupy the *fcc* hollow site, with a dissociative adsorption heat of 2.16 eV per original O_2 molecule according to Bocquet *et al.*[69] or 1.65 eV according to Eichler *et al.*[71] The actual *process* of dissociative adsorption, on the other hand, has been simulated (at normal incidence) by Groß *et al.*[73] using a tight-binding model with parameters based upon DFT calculations; trapping into the chemisorbed precursor states emerges as their favoured scenario, even at high incident translational energy (where conversion of that energy into rotational and vibrational modes is responsible for a considerably longer surface lifetime than might otherwise have been expected). Trapping is found to be significantly suppressed, however, in their further calculations conducted at higher angles of incidence.[74] Since adsorption of oxygen on Pt{111} is known to be dissociative above around 150 K,[71,72] while most evidence points to the dissociation product of methane on the same surface being methylidyne (CH) for temperatures exceeding 250 K,[56–58] it seems reasonable to assume that real catalytic oxidation on this surface (typically occurring at temperatures *significantly* above room temperature) will proceed *via* a reaction involving oxygen adatoms and commencing either with the oxidation of methylidyne ($CH + O \rightarrow CHO \rightarrow CO + H$) or with the dissociation of methylidyne ($CH + O \rightarrow C + O + H \rightarrow CO + H$). Accordingly, Inderwildi *et al.*[75] have very recently conducted DFT calculations comparing these two different pathways, finding that both methylidyne oxidation ($CH + O \rightarrow CHO$) and methylidyne dissociation ($CH \rightarrow C + H$) have the same energy barrier (1.12 eV); the former reaction is thermochemically favoured, however, being

¶ Although we follow Somorjai and co-workers in using the word "tetravalency" to denote a situation where carbon possesses a total of four neighbouring atoms at bonding distance in a tetrahedral arrangement, we should stress that we make no strong claims about bond order, or even about the degree of covalency, where metal–carbon bonds are involved.

‖ Indeed, we remain somewhat unconvinced even by more recent cluster calculations, using 35-atom three-layer models for the surface.[64] Once again, these provide reasonable adsorption geometries, but the energetic ordering of hydrocarbon fragments seems, to us at least, incorrect; assuming that H adatoms resulting from dehydrogenation adsorb distant from the remaining fragment, methyl (CH_3) is found to be more stable than methylene (CH_2), methylidyne (CH) and carbon (C), which clearly contradicts reliable and widespread experimental evidence for thermal decomposition. In contrast, recent periodic slab calculations,[65] making the same assumption about the location of H adatoms, place methylidyne (CH) as the most stable surface species, in line with the most up-to-date experimental observations.

exothermic by 1.18 eV, where the latter is endothermic by 0.59 eV. Once created, the adsorbed formyl (CHO) is trivially dehydrogenated to carbon monoxide (CO) over a barrier of just 0.57 eV. We believe, therefore, that oxidation of methane over Pt{111} occurs without substantial involvement of carbon adatoms, proceeding instead *via* a formyl pathway.

Adsorption of C_2 species on Pt{111} has been investigated within DFT by rather fewer groups. Papoian *et al*.[66] reported on slab-based calculations showing that ethyl (CH_2CH_3) binds preferentially in an atop fashion, in accord with earlier cluster-based calculations by Kua and Goddard.[61] The initial dissociative adsorption of ethane ($CH_3CH_3 \rightarrow CH_2CH_3 + H$) was found to be slightly endothermic, by 0.18 eV;[66] the same group had obtained 0.05 eV exothermicity for the initial dissociative adsorption of methane ($CH_4 \rightarrow CH_3 + H$). It seems likely, however, that ethyl would dissociate further on the surface, but subsequent dehydrogenation was not considered by Papoian *et al*.[66] Contemporary calculations conducted on *extremely* thin slabs (*i.e*. two atomic layers) were reported by Watwe *et al*.,[76] in which ethyl (CH_2CH_3), ethene (CH_2CH_2), ethylidene ($CHCH_3$), vinyl ($CHCH_2$), ethylidyne (CCH_3) and vinylidene (CCH_2) species were investigated; favoured adsorption sites were consistent with the completion of carbon tetravalency, in line with the pattern previously established for the dissociation products of methane on the same surface. In a subsequent study,[77] the same group presented results obtained with thicker slabs (*i.e*. three atomic layers) for the cases of ethene (CH_2CH_2) and ethylidyne (CCH_3), reporting no particular discrepancy with the earlier work. More recent DFT results from Essen *et al*.[78] also relate to the adsorption of ethene (CH_2CH_2), but hydrogenation and dehydrogenation products were not investigated. Adsorption of ethyne (CHCH) has been investigated by Medlin and Allendorf,[79] who report a preference for binding in the *fcc* hollow site, with the C–C bond projecting along a surface [110] direction and tilted from the horizontal by around 22° (they report a very similar *fcc* hollow site structure on Pd{111}, and an analogous *hcp* hollow site structure on Rh{111}, but bridge site adsorption is apparently preferred on Ni{111}).

Before leaving the flat Pt surfaces, we note that a small amount of DFT-based work has been carried out on Pt{100}. Moussounda *et al*.[80] report adsorption geometries and energetics for physisorbed methane (CH_4), finding a slight preference for atop adsorption with a heat of around 0.06 eV. Furthermore, several of the same authors[81] subsequently went on to study the dissociation of methane ($CH_4 \rightarrow CH_3 + H$), reporting a barrier of around 0.53 eV relative to the physisorbed molecule (*i.e*. 0.59 eV relative to the gas-phase molecule). Such a barrier is intermediate between the values of 0.66 eV calculated by Michaelides and Hu[67,68] on Pt{111} and 0.40 eV calculated by Anghel *et al*.[36] on Pt{110}-(1 × 2), perhaps reflecting a trend in the coordination number of the top-layer metal atoms (9 for Pt{111}, 8 for Pt{100} and 7 for Pt{110}[52]).

Stepped Pt surfaces: {110}. Amongst the stepped surfaces of Pt, only the {110} facet has received sustained attention in regard to hydrocarbon dissociation and oxidation. This surface is, however, probably the most heavily studied of all stepped surfaces in this context, so an extended discussion would seem to be in order.

Early experimental work by Weinberg and co-workers, in the mid 1980s, reported only weak molecular adsorption below 150 K for ethane and propane on the missing-row reconstructed Pt{110}-(1 × 2) surface, whilst *n*-butane and *n*-pentane were found to undergo partial dissociation at around 200 K.[82] These studies involved background dosing, however, and so the details of adsorption and dissociation mechanisms remained obscure. Subsequent work in the Madix group,[83–85] almost a decade later, employed supersonic molecular beam techniques to investigate the adsorption of methane, ethane and propane on the same substrate, but at surface temperatures in the range 500–1400 K where background dosing would be ineffective. Both methane and ethane were believed to adsorb by direct dissociation,[85] albeit with a higher barrier than found by the same group on Pt{111}.[86] In agreement with the original background-dosing studies, intact molecular adsorption of ethane and propane was reported in supersonic beam experiments conducted at a surface temperature of 95 K.[84,87]

During the present decade, a succession of detailed experiments on alkane dissociation and oxidation over Pt{110}-(1 × 2) have emerged from the Cambridge group, again making use of the supersonic molecular beam technique to extract detailed information on the adsorption and reaction dynamics of methane[88–92] and ethane.[93,94] Throughout the same period, parallel theoretical efforts have addressed the adsorption and/or dissociation of methane,[25,26,36,91] ethane[34,35,95] and oxygen[96] on the same surface, by means of DFT calculations whose results we summarise below.

Addressing initial hydrocarbon adsorption first, calculations are consistent with the experimental observation that partial dissociation is necessary for adsorption at all but the lowest surface temperatures. Anghel *et al*. have reported DFT transition states for adsorption by partial dissociation for methane[36] ($CH_4 \rightarrow CH_3 + H$) and ethane[35] ($C_2H_6 \rightarrow C_2H_5 + H$), obtained using a highly-accurate eigenvector-following transition-state-search algorithm. Physisorption of the intact hydrocarbon prior to partial dissociation was negligible in these calculations, although some small additional van der Waals binding, not fully captured within DFT, would presumably be present in reality. In the case of methane, two low-energy dissociation pathways were identified, each involving a transition state in which the nascent methyl moiety (CH_3) binds in atop fashion to one of the surface ridge atoms; the pathways differ in the ultimate destination of the leaving H atom (ridge bridge site, or threefold-coordinated microfacet site) but *both* have barriers close to 0.40 eV relative to the gas-phase methane molecule.[36] Similar results were obtained for ethane, where two pathways leading to atop binding of ethyl (C_2H_5) on a ridge atom, again differing only in the destination of the leaving H atom, were found to have barriers essentially equal to those for dissociative methane adsorption.[35]

Initial dissociative adsorption over calculated barriers in the region of 0.4 eV offers a perfectly adequate explanation for the experimental observation of direct adsorption at translational energies above that value for both methane[88] and ethane.[94] The apparent absence of any lower-energy pathway, however,

argues against the suggestion proffered by Walker and King[88] that adsorption at lower translational energy takes place *via* a steering mechanism; the dependence of sticking probability upon vibrational excitement of the impinging molecule was viewed as evidence against a precursor-mediated process. In light of their theoretical results, however, Anghel *et al*. have argued that, for a very weakly physisorbed precursor, some memory of the molecule's original vibrational state might be retained for an appreciable time.[36] Furthermore, the transition state geometries of methane and ethane suggest that not only stretch but also deformation modes ought to contribute to vibrationally-enhanced adsorption,[35,36] a notion strongly supported by recent experiments.[94] On balance, we favour the view that alkane adsorption on this surface is precursor-mediated at low translational energies; that it is direct for higher translational energies is not in any doubt.

Once methyl has formed on the Pt{110}-(1 × 2) surface, experiments suggest that it rapidly dissociates *via* methylene (CH_2) into either methylidyne (CH) or carbon (C); the complete dissociation is favoured in ultra-high vacuum conditions only for surface temperatures exceeding 450 K.[92] Comprehensive DFT calculations by Petersen *et al*. confirm that methylidyne is the lowest-energy surface product, if one insists that all hydrogen removed from the original methane molecule remains adsorbed in the form of isolated H adatoms distant from the hydrocarbon fragment.[25,26] The methyl-to-methylene reaction ($CH_3 \rightarrow CH_2 + H$) is found to occur over a barrier of 0.34 eV, *via* a transition state in which the nascent methylene moiety already essentially occupies the ridge bridge site that it will eventually settle into. Two pathways were identified for the methylene-to-methylidyne reaction ($CH_2 \rightarrow CH + H$), having barriers of 0.56 eV and 0.77 eV, in both of which the nascent methylidyne moiety in the transition state has already moved close to its ultimate location in an *fcc*-like threefold-coordinated site on the {111} microfacet. Finally, the methylidyne-to-carbon reaction ($CH \rightarrow C + H$) has a computed barrier of 1.20 eV, corresponding to a transition state in which the hydrogen atom has moved towards a ridge atop site, leaving the carbon atom in the same threefold microfacet site where it began. Where these calculated barriers can be compared with experimental estimates, the agreement is excellent.[26] It is interesting to note that, whilst the barrier to methyl dissociation is substantially lower than the comparable value obtained by Michaelides and Hu on Pt{111} (0.34 eV on the stepped surface *vs*. 0.83 eV on the flat[67,68]), as is that for methylidyne dissociation (1.20 eV on the stepped surface *vs*. 1.53 eV on the flat[67]), the barrier to methylene dissociation is actually significantly higher (0.56 eV minimum on the stepped surface *vs*. 0.14 eV on the flat[67]).

The story that emerges from DFT calculations of ethyl dissociation is in some ways similar to that described above for methyl, but far more complex. In all, Anghel *et al*.[34] have reported optimised structures for nine different C_2 species adsorbed on Pt{110}-(1 × 2), namely: ethyl (H_2CCH_3), ethene (H_2CCH_2), ethylidene ($HCCH_3$), ethylidyne (CCH_3), vinyl ($HCCH_2$), ethyne (HCCH), vinylidene (CCH_2), ethynyl (CCH) and di-carbon (C–C). Favoured adsorption sites for all the hydrocarbon species are consistent with completing carbon tetravalency. By assuming the surface to be in equilibrium with gas-phase hydrogen and ethene, it is possible to construct a free energy diagram for these species, as a function of temperature and the gas-phase partial pressures. Invoking reasonable ultra-high vacuum pressures, the DFT results of Anghel *et al*.[34] predict ethene (H_2CCH_2) and ethylidyne (CCH_3) to be the thermodynamically preferred species at 300 K (consistent with prior experiments by Stuck *et al*.[97]), but ethynyl (CCH) to be the more stable species in the range 400–600 K, with complete dehydrogenation being favourable only at still higher temperatures (these latter two statements being consistent with the experiments of Harris *et al*.[93]). Moreover, this free energy approach allows tentative predictions to be made across the ''pressure gap'', simply by adjusting the gas-phase partial pressures accordingly. Thus, Anghel *et al*.[34] suggest that, close to atmospheric pressure, ethene (H_2CCH_2) will be the thermodynamically preferred species for temperatures throughout the range 300–600 K, with ethylidyne (CCH_3) becoming increasingly competitive at higher temperature. In a subsequent analysis of the reaction barriers for this system, the same authors identified three subsets within their data:[95] low barriers, in the range 0.29–0.42 eV, for initial ethane dissociation to ethene (H_2CCH_2) and ethylidene ($HCCH_3$); medium barriers, in the range 0.72–1.10 eV, for dehydrogenation of ethene or ethylidene *via* vinyl ($HCCH_2$) or ethylidyne (CCH_3) to vinylidene (CCH_2) and ethyne (HCCH); and high barriers, greater than 1.45 eV, for dehydrogenation to products with fewer than two hydrogen atoms per molecule.

As regards the adsorption of oxygen on the Pt{110} surface, Petersen *et al*.[96] have reported DFT calculations of molecular adsorption, demonstrating a preference for binding in a bridged geometry with O_2 lying along the ridge of the missing-row reconstruction. The calculated adsorption heat of 1.48 eV is quite high for molecular oxygen, and certainly considerably higher than the values in the range 0.64–0.85 eV reported by others for the Pt{111} surface.[69,71,72] The authors concluded from their results that ridge bridge sites would be occupied at low coverage, while binding at less strongly-bound sites on the microfacets could occur at higher coverage;[96] such a state of affairs is consistent with experimental evidence from NEXAFS[98] and ARPES[99] studies conducted directly on the adsorbed oxygen molecules themselves, but contradicts an alternative interpretation of preferential trough adsorption based upon photoemission from coadsorbed xenon.[100] Alignment of the most strongly-bound molecular oxygen species with the step edge seems, however, to be a general feature on stepped platinum surfaces, having been observed in NEXAFS results not only for Pt{110}-(1 × 2),[98] but also on Pt{311},[101] Pt{331}[102] and Pt{211};[103] it would be hard to avoid the inference that molecular oxygen adsorbs *actually at* the step in all these cases.

At surface temperatures above around 200 K, oxygen adsorbs dissociatively on Pt{110}-(1 × 2), and the matter of where the resulting O adatoms bind has been addressed by two groups, with differing conclusions. Helveg *et al*.[104] report calculations showing a preference for the *fcc*-like site on the {111} microfacet, while Janin *et al*.[105] interpret their results as indicating binding in a ridge bridge site. Although both groups employ DFT in their work, the latter study was carried out on

relatively small clusters, whereas the former was a periodic slab calculation. Unpublished results from our own group concur with the assignment of the same threefold microfacet site;[106] we therefore conclude that this is indeed essentially the correct location for the adatoms, although with the caveat that the energy difference between *fcc*-like and *hcp*-like microfacet sites is rather small. It should be noted that, whilst STM images of the adsorption site are symmetrical,[104,105] this is not in itself evidence for a symmetrical adsorption site, since the barrier for hopping between microfacet sites across the ridge bridge site may be very low.[104]

Calculations and experiments are thus in broad agreement that the dominant surface species at moderate temperatures will be methylidyne (from decomposition of methane) and oxygen adatoms (from dissociation of molecular oxygen). As yet unpublished calculations by Petersen *et al.*[107] have indicated a low barrier to the direct oxidation of methylidyne by adsorbed oxygen adatoms (CH + O → CHO), which is likely to prove the dominant route for CO production on this surface, just as we believe to be the case for the Pt{111} surface.[75] Such a mechanism would certainly be consistent with the interpretation of temperature programmed reaction experiments[90] on Pt{110}-(1 × 2), where metastable adsorbed molecular oxygen was thought to be responsible for oxidation of carbon adatoms at high temperature (*c*. 650 K) forming predominantly CO_2, but oxygen adatoms were thought to react with adsorbed methylidyne at lower temperature (*c*. 510 K) creating first a short-lived formyl intermediate (CHO) *en route* to the rather more desirable formation of CO.

We conclude this section by noting some intriguing recent supersonic molecular beam experiments on methane decomposition over the Pt{553} and Pt{322} surfaces.[57] Although both surfaces are stepped, the nature of that step is rather different in the two cases: for the {553} surface, located between {111} and {111} in a stereographic projection, the step-edge geometry is highly reminiscent of that found on the {110} surface, whilst for the {322} surface, located between the {111} and {100} poles, the step-edge geometry is more similar to that of the {311} surface.[52,53] That is, whilst the {553} surface exhibits only threefold coordinated hollow sites adjacent to the step edge, the {322} surface displays both threefold and fourfold hollows in proximity to the step. Through the use of temperature-programmed XPS, Papp *et al.*[57] have demonstrated that methyl decomposition (*via* methylene, to methylidyne) at the step sites of the Pt{553} surface occurs at temperatures up to around 100 K lower than on the Pt{111} surface, but that the step sites of Pt{322} reduce the reaction temperature by only about 50 K. On the other hand, the reaction temperature of terrace-bound methyl on both stepped surfaces is reduced by about 50 K, and the formation of surface carbon begins, for both substrates, some 100 K lower in temperature than on the {111} substrate. Notably, the initial sticking probability of methane at low surface temperatures (below 130 K) is reported by the same authors to be virtually identical for the {111}, {553} and {322} surfaces,[57] whereas an earlier study had noted a substantial increase in this parameter for the Pt{533} surface (steps similar in nature to those of Pt{322}), albeit at a surface temperature of 600 K.[108] Clearly there remain significant open questions concerning the effect of steps on initial alkane adsorption and on subsequent alkyl dehydrogenation, and further careful theoretical efforts in this direction would doubtless prove extremely fruitful; the Pt{311} surface, having significant structural affinity with Pt{110},[52,109] but featuring steps more akin to the {322} surface, would be an admirable starting point for such work.

3.2 Rhodium

Flat Rh surfaces: {111}. Just as was the case for the flat Pt surfaces, the first DFT studies of alkanes on flat Rh surfaces were based on the cluster approach. Chen *et al.*[110] used a ten-atom Rh cluster to model adsorption of methyl (CH_3) on Rh{111}, concluding that the favoured adsorption location was a threefold coordinated hollow site. Kua and Goddard,[59] on the other hand, presented results from an eight-atom cluster, employed to model all of the dissociation products of methane (CH_4) on Rh{111}, finding very similar behaviour as for the same species on Pt{111}: methyl (CH_3) was found to bind at an atop site, methylene (CH_2) at a bridge site, and methylidyne (CH) at a threefold coordinated hollow site. Of these, methylidyne was the favoured product (in the scenario where the hydrogen atoms resulting from dissociation remain adsorbed, but distant from the hydrocarbon fragment).

Amongst slab-based DFT calculations, the first to address alkane dissociation on Rh{111} appears to have been that of Mavrikakis *et al.*,[111] which concurred with the atop site preference of methyl (CH_3), by a margin of at least 0.1 eV over the bridge site, and at least 0.4 eV over the hollow sites (all at 0.25 ML coverage, within a (2 × 2) unit cell). In contrast, a subsequent study by Liu and Hu[38] determined the *fcc* hollow site to be most stable, by a margin of around 0.1 eV over the atop site (at 0.25 ML coverage, within a (2 × 2) unit cell), while another by Walter and Rappe[112] determined the *hcp* hollow site to be most stable, by a margin of more than 0.3 eV over the atop site (at 0.33 ML coverage, within a $(\sqrt{3} \times \sqrt{3})R30^\circ$ unit cell). The lack of consensus over precisely which hollow site might be preferred is, perhaps, not too disturbing, and may even be explained by a coverage-dependent site-switch, but the more significant discrepancy between hollow and atop site predictions must raise serious doubts over the reliability of at least one set of results. Fortunately, further calculations by Xiao and Xie[113] suggest a resolution. They considered 0.25 ML coverage, within a (2 × 2) unit cell, just like Mavrikakis *et al.*[111] and Liu and Hu,[38] reporting results essentially in accord with those of the latter authors. They also noted, however, that this was true only if methyl in the hollow site was allowed to adopt a geometry in which the C–H bonds point towards neighbouring atop sites, without which freedom the results of Mavrikakis *et al.*[111] were essentially reproduced. The clear atop preference reported in the earlier work may therefore turn out to be essentially steric in origin, resulting from incomplete sampling of possible adsorption geometries. At any rate, a marginal preference for methyl adsorption at the *fcc* hollow site has been found in all of the more recent calculations[114–116] carried out for this system with either PW91[117] or PBE[118] exchange–correlation functionals; Yang *et al.*[116] note, however, that use of the RPBE[119] functional can (just) reverse the calculated energy-ordering of atop and

hollow sites, but that experimentally-observed softening of the asymmetric methyl stretch mode[120] can only be reproduced within the hollow site model.

Dissociation products of methyl (CH_3) have been studied recently by Bunnik and Kramer[115] and by Yang *et al.*[116] Both groups report that methylene (CH_2) preferentially occupies the *fcc* hollow site at 0.25 ML coverage, while methylidyne (CH) prefers the *hcp* hollow site at the same coverage. Energy differences between the *fcc* and *hcp* models are rather small, however, so it is probably best not to be too dogmatic in specifying which hollow site is occupied; Bunnik and Kramer,[115] for example, report a switch in preference from *fcc* to *hcp* hollow site for methylene (CH_2) at 0.11 ML coverage (*i.e.* within a (3×3) unit cell). Regarding thermochemistry, both groups also agree that the most stable surface species is adsorbed methylidyne (CH), with a heat of formation from gas-phase methane of 0.65 eV (Bunnik and Kramer[115]) or 0.83 eV (Yang *et al.*[116]), calculated on the assumption that hydrogen derived from the reaction remains adsorbed on the surface but distant from the hydrocarbon fragment. In both studies, adsorbed carbon (C) is approximately 0.3–0.4 eV less stable than methylidyne, and adsorbed methylene (CH_2) is approximately 0.2–0.3 eV less stable than adsorbed carbon, working upon the same assumption; adsorbed methyl (CH_3) is actually unstable relative to rehydrogenation to form gas-phase methane. Yang *et al.*[116] provide the additional information that all their adsorbed carbon-containing species are destabilised by 0.2–0.3 eV in the presence of coadsorbed CO, which renders methylene (CH_2) thermochemically unstable against recombinative desorption, but does nothing to alter the overall stability of methylidyne (CH) relative to other surface species.

Barriers for the initial dissociative adsorption of methane ($CH_4 \rightarrow CH_3 + H$) have been calculated by three groups, with remarkable agreement in the nature of the transition state (the nascent methyl fragment occupies an atop site, with hydrogen leaving in the direction of either an adjacent hollow site[38,114] or bridge site[115]) and the activation energy (variously 0.67 eV,[38] 0.69 eV[114] or 0.72 eV[115]). Further dehydrogenation has been studied systematically by Bunnik and Kramer,[115] who found barriers of 0.49 eV for the methyl-to-methylene reaction ($CH_3 \rightarrow CH_2 + H$), 0.10 eV for the methylene-to-methylidyne reaction ($CH_2 \rightarrow CH + H$), and around 1.18 eV for the methylidyne-to-carbon reaction ($CH \rightarrow C + H$); the carbon atom remained close to the *fcc* hollow site in all of the transition states. Kokalj *et al.*[114] had previously reported a barrier of 0.42 eV for methyl decomposition ($CH_3 \rightarrow CH_2 + H$), while Inderwildi *et al.*[121] have recently reported a barrier of 1.28 eV for methylidyne decomposition ($CH \rightarrow C + H$). In comparison with the Pt{111} surface, therefore, the barrier to initial dissociation is rather similar (0.67–0.72 eV on Rh[38,114,115] *vs.* 0.66 eV on Pt[67,68]), as is the barrier to formation of methylidyne from methylene (0.10 eV on Rh[115] *vs.* 0.14 eV on Pt[67,68]), while the barriers to the formation of methylene from methyl, and to the formation of carbon from methylidyne, are notably lower (0.42–0.49 eV and 1.18–1.28 eV, respectively on Rh,[114,115,121] *vs.* 0.82 eV and 1.53 eV, respectively on Pt[67,68]).

Early DFT calculations for oxygen adsorption on Rh{111} were performed by Chen *et al.*,[70] using a ten-atom three-layer cluster model; the *fcc* hollow site was preferred for the O adatom, but finite size effects render such a conclusion highly tenuous. Somewhat more convincingly, Loffreda *et al.*[122] performed slab-based DFT calculations, finding a preference for the *fcc* hollow site at adatom coverages ranging from 0.25 ML to 1.00 ML, although their two-layer slabs with frozen substrate geometry appear a little lacking by current standards (albeit reasonable for their time). Subsequent calculations from the Scheffler group, however, confirm the fundamentals revealed by the first studies, and offer substantial further insights into the nature of bonding in the preferred sites.[123,124] Walter *et al.*,[125] meanwhile, provided details of calculations for molecularly chemisorbed O_2 on Rh{111}, with results favouring the *fcc* and *hcp* sites, described as very similar to those found previously by Eichler and Hafner[72] on the Pt{111} surface. Inderwildi *et al.*[126] have identified a different end-on bound species located in the *fcc* site, and have furthermore shown that a small precoverage of adatoms enhances dissociation. With increasing adatom coverage above 0.25 ML, however, the molecular adsorption heat is reported to drop, while dissociation apparently becomes less exothermic and occurs over an increasingly high activation barrier. The authors consequently conclude that oxygen uptake on this surface is kinetically self-limiting, since the dissociation barrier exceeds the molecular adsorption heat for adatom coverages above about 0.7 ML.

Coadsorption of oxygen (O) and methyl (CH_3) has been studied by Walter and Rappe,[112] who find that softening of the symmetric methyl stretch modes is reduced by the presence of coadsorbed adatoms (coverage of 0.33 ML for each species). This change is, it seems, driven by charge transfer that strengthens the C–H bonds whilst weakening the C–Rh bond; possible effects on dissociation and desorption barriers are not, however, discussed.

We are aware of very few studies relating to actual oxidation reactions for alkanes on Rh{111}. Liu *et al.*[127] have calculated a barrier of 1.57 eV for the oxidation of carbon adatoms ($C + O \rightarrow CO$), which combined with the significant endothermicity of the methylidyne-to-carbon step ($CH \rightarrow C + H$) is probably enough to rule out a carbidic route to alkane oxidation on this surface. At the other extreme, Fratesi and de Gironcoli[128] have investigated the potential of Rh{111} for direct low-temperature conversion of methane (CH_4) to methanol (CH_3OH), but conclude that no plausible mechanism exists. Oxidation of adsorbed methyl (CH_3) by oxygen adatoms (O) involves a barrier of 1.59 eV, while oxidation by adsorbed hydroxyl (OH) involves a barrier of 1.85 eV; in contrast, the same group[114,128] calculate a barrier of just 0.4–0.5 eV for dehydrogenation of methyl to methylene (CH_2). Even the introduction of a surface defect, in the form of a Rh adatom, only reduces the barriers to 1.56 eV (oxidation by O) and 1.65 eV (oxidation by OH). Clearly, dehydrogenation to methylene (CH_2) and thence methylidyne (CH) will utterly dominate any possibility of oxidation to methanol (CH_3OH).

Our own contribution to the matter of methane oxidation on Rh{111} took the dehydrogenation of methyl (CH_3) *via* methylene (CH_2) to methylidyne (CH) as its starting assumption.[121] From this *ansatz*, the competing processes considered in our model included methylidyne decomposition

(CH → C + H); hydrogen abstraction from methylidyne by coadsorbed oxygen (CH + O → C + OH); hydrogen abstraction from methylidyne by coadsorbed hydroxyl (CH + OH → C + H_2O); oxidation of atomic carbon (C + O → CO); methylidyne oxidation (CH + O → CHO); formyl decomposition (CHO → CO + H); and oxidation of carbon monoxide (CO + O → CO_2). Crucially, the direct oxidation of methylidyne (CH) to create formyl (CHO) was found not only to have a lower barrier than either dehydrogenation or hydrogen abstraction by coadsorbed oxygen (1.15 eV *vs.* at least 1.28 eV), but also to be thermochemically much more favourable (0.14 eV exothermic *vs.* at least 0.67 eV endothermic). The only plausible route to form surface carbon (C), as opposed to surface formyl (CHO), would thus be hydrogen abstraction from methylidyne by coadsorbed hydroxyl (OH), with an activation barrier of 1.26 eV and an exothermicity of 0.17 eV, but this eventuality is precluded by the rapid consumption of hydroxyl through reaction with hydrogen adatoms (H + OH → H_2O; reaction barrier of just 0.35 eV). Decomposition of formyl (CHO) to yield adsorbed carbon monoxide (CO) is entirely favourable, having a reaction barrier of 0.30 eV and an exothermicity of 1.33 eV. Once a reaction network becomes this complicated, however, it is clear that qualitative reasoning may become unreliable, so quantitative modelling is required if solid conclusions are to be drawn. Given starting coverages of 0.2 ML CH and 0.7 ML O, realistic microkinetic simulations (based upon the DFT-calculated barriers) show that surface CO is formed at 400 K exclusively *via* the formyl (CHO) route, with negligible formation of surface carbon. Detailed features of experimental reaction studies are reproduced by inclusion of the formyl pathway, such as the time-evolution of the balance between H_2 and H_2O production, and between CO and CO_2 production.[121]

Stepped Rh surfaces: {211}. Disappointingly few first-principles studies exist that are relevant to alkane oxidation on stepped Rh surfaces. Liu and Hu[38] have reported calculations for the dissociation of methane to methyl (CH_4 → CH_3 + H) on Rh{211}, finding an increased binding energy for the product methyl relative to flat Rh{111} (0.28 eV more stable) and a substantially decreased reaction barrier (0.32 eV *vs.* 0.67 eV). They have also modelled the effect of surface kinks by removing one in three of the step-edge Rh atoms from Rh{211}, whereupon they determine that methyl bound at one of the resulting kink sites has similar adsorption heat to the stepped surface, but that the reaction barrier is decreased still further to 0.20 eV. On the basis of these results, Liu and Hu[38] reasonably suggest that dissociation on nominally flat surfaces may be dominated by step and kink defects. Similarly, in the same work the authors report a substantial decrease in the barrier towards oxidation of carbon adatoms (C + O → CO) at steps and kinks, from 1.84 eV on flat Rh{111}, to 1.18 eV on stepped Rh{211}, and 1.09 eV on artificially-kinked Rh{211}. They argue, however, that whilst the barrier reduction for methane dissociation is due mainly to electronic effects (relating to low coordination of metal atoms at the step or kink), the barrier reduction for carbon oxidation is due mainly to geometrical effects (such as steric considerations affecting the approach to bond formation). Kokalj *et al.*[114] have calculated the initial dissociative adsorption barrier of methane (CH_4 → CH_3 + H) to be 0.42 eV, in plausible agreement with the work of Liu and Hu,[38] but have also calculated the barrier towards methyl decomposition into methylene (CH_3 → CH_2 + H) to be 0.40 eV, which is only very slightly lower than the barrier of 0.42 eV calculated by the same group on Rh{111}.

To our knowledge, the next dehydrogenation step, from methylene-to-methylidyne (CH_2 → CH + H), has not yet been studied theoretically on any stepped or kinked Rh surface. However, the final dehydrogenation of methylidyne-to-carbon (CH → C + H) has been calculated on Rh{211} by McAllister and Hu[129] as part of a study aimed at the hydrogenation reactions of carbon, nitrogen, oxygen and sulfur adatoms. They report that the dehydrogenation of methylidyne (CH) on Rh{211} is actually slightly exothermic (by 0.18 eV), which contrasts markedly with the endothermicity (of 0.3–0.4 eV) calculated by other authors for the same reaction on Rh{111}.[115,116] The barrier for the reaction is also substantially reduced, to just 0.65 eV, from values in the range 1.18–1.28 eV on the flat {111} surface.[114,115,121] In contrast, Bhattacharjee *et al.*[130] have recently calculated a rather larger barrier of 1.04 eV for methylidyne dissociation on Rh{211}, finding lower barriers only if starting from adsorption geometries considerably less stable than the preferred fourfold hollow site. They therefore argue that oxidation on the stepped surface is, once again, unlikely to occur *via* a carbidic route. Instead, they propose that direct oxidation of methylidyne (CH + O → CHO) occurs with a barrier of just 0.75 eV and an exothermicity of 0.62 eV (compared with a barrier of 1.15 eV and an exothermicity of 0.14 eV on Rh{111}[121]); subsequent dissociation of formyl (CHO → CO + H) then occurs with a very low barrier of 0.14 eV and an exothermicity of 0.90 eV (0.30 eV and 1.33 eV, respectively for the flat surface[121]).

Current understanding of methane oxidation on stepped Rh surfaces is thus rather incomplete. What seems safely established is that, relative to Rh{111}, the presence of steps at the Rh{211} surface reduces the barrier towards initial dissociative adsorption (0.32–0.42 eV on the stepped surface[38,114] *vs.* 0.67–0.72 eV on the flat[38,114,115]), but does little to the barrier for methyl dissociation (0.40 eV on the stepped surface[114] *vs.* 0.42–0.49 eV on the flat[114,115]). The barrier to methylene dissociation on Rh{211} is, at present, unknown, but methylidyne dissociation is activated by either 0.65 eV[129] or 1.04 eV,[130] both lower than the range of 1.18–1.28 eV on Rh{111}. Direct oxidation of methylidyne (CH) to formyl (CHO) is *at least* competitive with the carbidic route, and we believe it to be dominant.[130]

3.3 Palladium

Flat Pd surfaces: {111}, {100}. So far as we are aware, the only DFT slab calculations for the adsorption of methane on Pd{111} were those carried out by Paul and Sautet in the late 1990s.[131] This early work indicated that methyl (CH_3) binds preferentially at the atop site, methylene (CH_2) at the bridge site, methylidyne (CH) at the *hcp* hollow site, and carbon (C)

at either the *hcp* or *fcc* hollow site. These site preferences are rather similar to those found on Pt{111} (and differ from those found on Rh{111}) but the thermochemical trend is completely different. Whereas methylidyne (CH) is the favoured surface species for both Pt{111} and Rh{111} (in the case where hydrogen resulting from dissociation remains on the surface, but distant from the hydrocarbon fragment), for Pd{111} the preference is apparently for methyl (CH_3). Indeed, the initial dissociative adsorption of methane ($CH_4 \rightarrow CH_3 + H$) was found to be endothermic by 0.27 eV; decomposition of methyl to methylene ($CH_3 \rightarrow CH_2 + H$) was endothermic by 0.23 eV; dehydrogenation to methylidyne ($CH_2 \rightarrow CH + H$) was exothermic by just 0.10 eV; and the final decomposition to form carbon adatoms ($CH \rightarrow C + H$) was endothermic by 0.35 eV. Such results are highly puzzling, in light of experimental evidence suggesting decomposition of adsorbed methyl to less hydrogen-rich surface species. Paul and Sautet[131] suggest that hydrogen transfer between hydrocarbon fragments is responsible for this apparent discrepancy, since disproportionation reactions such as $2CH_3 \rightarrow CH_4 + CH_2$ and $CH_3 + CH \rightarrow CH_4 + C$ are nearly thermoneutral in their scheme, and the overall reaction $4CH_3 \rightarrow 3CH_4 + C$ is substantially exothermic. On the other hand, one must note that these slab results are entirely at odds with cluster calculations by Kua *et al.*[59] that indicate the methane-to-methyl step ($CH_4 \rightarrow CH_3 + H$) to be essentially thermoneutral, the methyl-to-methylene step ($CH_3 \rightarrow CH_2 + H$) to be only mildly endothermic by 0.08 eV, the methylene-to-methylidyne step ($CH_2 \rightarrow CH + H$) to be strongly exothermic by 0.60 eV, and the methylidyne-to-carbon step to be strongly exothermic by 0.58 eV. Despite reservations about the accuracy of cluster calculations for surface thermochemistry, it must be said that such figures are more in line with expectations than those from the slab calculations. Since no more recent slab calculations have been carried out for this system (to our knowledge), we have carried out our own, finding remarkably close agreement with the results of the cluster calculations. We find both the methane-to-methyl ($CH_4 \rightarrow CH_3 + H$) and methyl-to-methylene ($CH_3 \rightarrow CH_2 + H$) steps to be marginally endothermic (0.02 eV in each case), while the methylene-to-methylidyne step ($CH_2 \rightarrow CH + H$) is strongly exothermic (0.54 eV) and the methylidyne-to-carbon step is quite strongly endothermic by 0.39 eV.

Another interesting point of comparison may be found, however, in the work of Zhang and Hu[132] on dissociative methane adsorption at the Pd{100} surface. Their slab calculations with the PW91 functional[117] reveal mildly endothermic (0.15 eV) initial adsorption ($CH_4 \rightarrow CH_3 + H$), followed by a methyl-to-methylene step ($CH_3 \rightarrow CH_2 + H$) that is very slightly exothermic (0.06 eV), a methylene-to-methylidyne step ($CH_2 \rightarrow CH + H$) that is highly exothermic (0.82 eV), and finally a methylidyne-to-carbon step ($CH \rightarrow C + H$) that is also exothermic (0.42 eV). Thus the favoured species on Pd{100}, according to these calculations, is atomic carbon. Calculated barriers are 0.79 eV for initial adsorption ($CH_4 \rightarrow CH_3 + H$); 0.52 eV for the methyl-to-methylene step ($CH_3 \rightarrow CH_2 + H$); 0.20 eV for the methylene-to-methylidyne step ($CH_2 \rightarrow CH + H$); and 0.52 eV for the methylidyne-to-carbon step ($CH \rightarrow C + H$). Use of the RPBE functional slightly destabilises all the surface species, but does not significantly change the overall picture.[132] On this basis, it would be reasonable to suppose that dehydrogenation all the way to carbon takes place even at quite moderate temperatures on this surface, but that methyl might be kinetically stable at sufficiently low temperature. It is hard to imagine a scenario where methylene or methylidyne could be the majority species, since any surface temperature sufficient to overcome the barrier to methyl decomposition would also be sufficient to overcome the methylene-to-methylidyne and methylidyne-to-carbon barriers.

Adsorption of oxygen on both Pd{111} and Pd{100} has been the subject of considerable interest, not least because of the potential for surface oxide formation. The first slab-based DFT calculations for O adatoms on these surfaces were reported by Hammer *et al.*,[119] and showed the *fcc* hollow site to be the most stable location on Pd{111}, while the fourfold hollow site was most stable on Pd{100}. Dissociative adsorption heats were very similar for the two surfaces.[119] A short while later, Eichler *et al.*[71] presented the first DFT study of molecular adsorption and dissociation on Pd{111}, identifying two of the three experimentally observed vibrational frequencies with surface-parallel molecules bound in bridge and *fcc* hollow sites; the barrier to dissociation from the latter site (the most stable intact geometry) was found to be 1.11 eV, somewhat higher than the barrier reported in the same work for Pt{111} (0.90 eV) and much higher than that reported for Ni{111} (0.22 eV). Honkala and Laasonen, by way of comparison, reported a barrier in the range 0.87–1.00 eV for dissociation from a similar molecular state on Pd{111}, with the precise value somewhat dependent on the size of unit cell employed.[133]

Overlayers of atomic oxygen on Pd{111} have also been studied by Todorova *et al.*,[134] for atom coverages in the range 0.25–1.00 ML; the *fcc* hollow site was found to be consistently favoured over the *hcp* hollow site, and both were more stable than the bridge and atop sites. Beyond around 0.75 ML, however, calculations from the same group indicate a thermodynamic preference for the incorporation of subsurface oxygen.[124] Further work by Reuter and Scheffler[135] analysed the stability of surface oxide layers as a function of gas-phase pressure and composition (*i.e.* $CO : O_2$ ratio), concluding that there exists a range of conditions for which the surface oxide phase is stable and the bulk oxide is not. The surface oxide phase should be understood as distinct from either the chemisorbed oxygen phase or the sub-surface oxygen phase (in both of which the Pd atoms remain in an essentially metallic state), but crucially also differs from the bulk oxide phase (in which thermodynamics would favour oxidation of the entire sample, and the oxide growth is limited only by kinetics). Such a surface oxide had recently been reported in STM experiments,[136] where an incommensurate overlayer was believed to achieve a stoichiometry of Pd_5O_4, and was simulated within DFT on that basis in both the original work and the later thermodynamic analysis.[135,136] Todorova *et al.*[137] subsequently argued that subsurface oxygen should be viewed as a metastable precursor to formation of the surface oxide phase.

A rather similar scenario pertains to the Pd{100} surface, where LEED studies had suggested a structure for the

observed ($\sqrt{5} \times \sqrt{5}$)R27° phase akin to a rumpled plane of PdO{001} epitaxed upon the metallic substrate material.[138] A combination of STM, XPS and DFT, however, subsequently demonstrated that such a model was inconsistent with the newly-acquired data.[139] Instead, it was concluded that a strained PdO{101} plane epitaxed to Pd{111} could explain all the observations.[139] Note that neither {001} nor {101} are thermodynamically favoured facets for PdO, which is predicted to expose preferentially the {100} plane with some minority {101} facets;[139] this fact underlines the extent to which the surface oxide phase may be expected to display different structural, electronic and indeed chemical characteristics from the bulk oxide.

The particular relevance of these studies to the oxidation of alkanes is that oxidised particles (either bulk oxide, or exposing only a surface oxide) are strongly implicated in the high activity of Pd towards methane combustion.[140,141] Accordingly, Li *et al.*[142] have calculated barriers for the initial dissociative adsorption of methane ($CH_4 \rightarrow CH_3 + H$) over PdO{100}, PdO{001} and PdO{110} surfaces (note that PdO is tetragonal, so that the {100} and {001} facets are distinct, as are the {110} and {101} facets). The presence of oxygen vacancies was found to be important, with undercoordinated Pd atoms being particularly active towards dissociation; the reaction in each case yields methyl (CH_3) bound to a Pd atom, with the leaving hydrogen atom (H) bound to one of the lattice oxygen atoms.[142] In fact, some experimental evidence suggests that the most active sites in real catalysts may actually comprise small particles of metallic Pd embedded in an oxide environment.[140] This might, at first, appear puzzling, since the calculated barrier of 1.65 eV for methylidyne dissociation ($CH \rightarrow C + H$) on Pd{111}[75] is actually rather higher than on Pt{111}, Rh{111}, and indeed Ni{111}. If this were a necessary step in the combustion of methane, one would conclude that Pd-based catalysts ought to be amongst the worst for this reaction, when they are actually amongst the best. Once again, the answer may lie in the formyl species (CHO) which King and co-workers[75] determine can be formed on Pd{111} by oxidation of methylidyne ($CH + O \rightarrow CHO$) over a barrier of just 0.78 eV, and which dehydrogenates ($CHO \rightarrow CO + H$) over a barrier of just 0.36 eV. Taken together, these barriers indicate a higher activity for Pd than for the other three metals, so long as sufficient oxygen can be supplied; the role of the oxide may therefore be simply to supply the latter reactant *via* a spillover effect.

Stepped and kinked Pd surfaces: {110}, {211}, {320}. Unlike those of Pt and Rh, the stepped surfaces of Pd seem thus far to have been entirely neglected as regards first-principles calculations relevant to hydrocarbon dissociation. Nevertheless, some interesting quantum mechanical molecular dynamics simulations have been reported,[143,144] based upon a tight-binding model for adsorbates, coupled with semi-empirical interatomic potentials for the substrate. In these studies, Paavilainen, Nieminen and co-workers have addressed the initial dissociation of methane ($CH_4 \rightarrow CH_3 + H$) over the stepped Pd{110} surface[143,144] and the kinked Pd{320} surface.[144] Surprisingly, they find that the effective activation energy on the more open {320} surface appears to be *higher* than on the {110} surface, which fact they attribute to steering of the molecule *away* from active sites in the case of Pd{320}. Accurate first-principles calculations for the transition states of these systems would clearly constitute a highly-desirable adjunct to these intriguing simulations.

Regarding the dissociative adsorption of oxygen on stepped Pd surfaces, DFT calculations have recently been reported by Lahti *et al.*[145] for the {211} case. In addition to mapping out a potential energy surface for O_2 dissociation constrained to six different combinations of orientation and impact site, molecular dynamics simulations were also performed; the results of these indicate molecular adsorption occurs with O_2 bridging between two adjacent metal atoms along the step edge, while non-activated dissociation can occur close to the fourfold hollow site immediately below the step edge. The stepped Pd{211} surface is concluded to be more reactive towards oxygen dissociation than either of the two flat surfaces, Pd{100} and Pd{111}, where, in the latter case at least, molecular adsorption is weak and the dissociation itself is an activated process.[145] Earlier calculations by Junell *et al.*,[146] reporting potential energy surfaces for the stepped Pd{110} surface, had revealed molecular chemisorption minima corresponding to several different adsorption geometries, the most favourable being a ridge bridge site similar to that found by Petersen *et al.*[96] on Pt{110}-(1 × 2); the smallest barrier to dissociation was found to be 0.17 eV relative to the gas-phase molecule, and occurs with the O–O bond lying along the trough.[146] Note that the clean Pd{110} surface is unreconstructed, in contradistinction to the missing-row reconstruction of the clean Pt{110} surface.

3.4 Nickel

Flat Ni surfaces: {111}, {100}. Oxygen adsorption on the Ni{111} surface has been investigated theoretically in a number of studies, including those reported by Eichler *et al.*,[71] Yamagishi *et al.*[147] and Li *et al.*[148] Experimental studies[149] have revealed (2 × 2) and ($\sqrt{3} \times \sqrt{3}$)R30° chemisorbed overlayers upon dissociative adsorption, and the published calculations agree on a slight preference for the *fcc* hollow site over the *hcp* hollow site for both 0.25 ML[71,148] and 0.33 ML[147,148] adatom coverages with the corresponding periodicities. The magnetic moment of the top-layer Ni atoms is reduced by the influence of the adsorbate,[148] while the small residual moment on the adatom itself is ferromagnetically aligned with respect to the net spin of the substrate.[147] For the Ni{100} surface, calculations on a $c(2 \times 2)$ overlayer with O adatoms in fourfold hollow sites have been reported by Hong *et al.*,[150] and very recently by Harrison *et al.*,[151] and the structural parameters obtained in both works are in generally very good agreement with the most convincing LEED experiments.[152]

Early slab-based DFT calculations relevant to methane dissociation on Ni{111} were reported by Michaelides and Hu.[153–155] These indicated preferential adsorption of methyl (CH_3) in either the *fcc* or *hcp* hollow sites,[153] stabilised by three-centre (Ni–C–H) bonding and consequent softening of the C–H stretch modes analogous to that observed in similar geometries on Rh{111}. Methylene (CH_2) was also found to

adsorb in the hollow sites,[154] while the methyl-to-methylene reaction ($CH_3 \rightarrow CH_2 + H$) was found to be 0.51 eV endothermic (in the case of fully-separated products) with a barrier of 1.06 eV.[155] At least in respect of the preferred adsorption sites of dehydrogenation products, the Ni{111} surface can thus be seen to bear a stronger resemblance to Rh{111} than to either Pd{111} or Pt{111}.

At around the same time, Watwe *et al.*[156] reported the methyl-to-methylene reaction ($CH_3 \rightarrow CH_2 + H$) to be exothermic by 0.03–0.12 eV (the exact value depending upon the functional used in the calculations). The methylene-to-methylidyne reaction ($CH_2 \rightarrow CH + H$) was reportedly 0.45–0.54 eV exothermic, and the methylidyne-to-carbon reaction ($CH \rightarrow C + H$) 0.45–0.55 eV endothermic. In all cases, the PW91 functional provided results that were marginally more favourable for dehydrogenation than those obtained with the RPBE functional. The strongest dependence upon the functional was found, however, for the initial dissociative adsorption of methane ($CH_4 \rightarrow CH_3 + H$): the PW91 functional yielded a 0.19 eV exothermic reaction, while the RPBE functional suggested 0.42 eV endothermicity; the activation barrier for this latter process was 1.32 eV, with the RPBE functional. The RPBE barrier for the methyl-to-methylene reaction ($CH_3 \rightarrow CH_2 + H$) was reported as 0.70 eV; that for the methylene-to-methylidyne reaction ($CH_2 \rightarrow CH + H$) was 0.29 eV; and that for the methylidyne-to-carbon reaction ($CH \rightarrow C + H$) was 1.44 eV. It is important to note, however, that all of the above results were obtained from spin-unpolarised calculations. Whilst they provide a more *complete* survey of the reaction scheme than the work of Michaelides and Hu,[153–155] their accuracy must therefore be considered somewhat questionable. A subsequent spin-polarised study, from an overlapping set of authors, also noted that at least the initial dissociation barrier could be altered by using a larger unit cell and allowing more than one surface layer to relax, but did not report in detail on the parameters for the later dehydrogenation stages.[157]

Perhaps the most comprehensive DFT study of methane decomposition over flat Ni surfaces is that reported recently by Wang *et al.*[158,159] On Ni{111}, they first found initial dissociative adsorption of methane ($CH_4 \rightarrow CH_3 + H$) to be 0.16 eV endothermic, the methyl-to-methylene reaction ($CH_3 \rightarrow CH_2 + H$) to be also 0.16 eV endothermic, the methylene-to-methylidyne reaction ($CH_2 \rightarrow CH + H$) to be 0.30 eV exothermic, and the methylidyne-to-carbon reaction ($CH \rightarrow C + H$) to be 0.60 eV endothermic.[158] Methylidyne (CH) is thus the most stable surface species on Ni{111}, in line with the results described above for the Pt{111}, Rh{111} and Pd{111} surfaces. In a later publication, the same group[159] reports activation barriers of 1.17 eV for the initial dissociative adsorption of methane ($CH_4 \rightarrow CH_3 + H$), 0.82 eV for the methyl-to-methylene reaction ($CH_3 \rightarrow CH_2 + H$), 0.37 eV for the methylene-to-methylidyne reaction ($CH_2 \rightarrow CH + H$) and 1.37 eV for the methylidyne-to-carbon reaction ($CH \rightarrow C + H$). The major differences between Ni and the other three metals thus appear to be (i) that the surface intermediates are thermochemically less stable relative to gas-phase methane, and (ii) that the barriers to the first three dehydrogenation steps (between methane and methylidyne) are somewhat greater.

Despite these differences, however, the reforming of methane by CO_2 on Ni{111} seems to proceed *via* a similar route to that noted above for methane oxidation on Pt{111}, Rh{111} and Pd{111}. Wang *et al.*[159,160] have conducted comprehensive calculations on oxygenated intermediates and the barriers between them. The barrier towards oxidation of methylidyne ($CH + O \rightarrow CHO$) is found to be slightly lower than that for methylidyne decomposition (the barrier is quoted as 0.80 eV, but this is relative to a coadsorbed geometry lying considerably higher in energy than the fully-separated adsorbates; relative to the lowest energy for the well-separated reactants, the effective barrier would be 1.26 eV, which is still lower than the value of 1.37 eV for methylidyne dissociation). Moreover, the oxidation of methylidyne to create formyl (CHO) is only mildly endothermic relative to the fully-separated reactants (0.30 eV), whereas methylidyne dissociation is more strongly endothermic (0.60 eV). Dehydrogenation of formyl ($CHO \rightarrow CO + H$) then occurs over a low barrier (0.29 eV) and is strongly exothermic (by 1.12 eV). The combination of barrier heights and thermochemical considerations is believed to lead to an overall kinetic preference for the formyl pathway.[159,160]

On the Ni{100} surface, Wang *et al.*[158] obtain results differing more than somewhat from those found by the same authors on Ni{111}. Firstly, they find that although most species favour the fourfold hollow site (which might have been guessed by analogy), the methyl moiety (CH_3) actually favours the bridge site. Furthermore, they report the initial dissociative adsorption of methane ($CH_4 \rightarrow CH_3 + H$) to be 0.09 eV endothermic, the methyl-to-methylene reaction ($CH_3 \rightarrow CH_2 + H$) to be 0.18 eV exothermic, the methylene-to-methylidyne reaction ($CH_2 \rightarrow CH + H$) to be 0.71 eV exothermic, and the methylidyne-to-carbon reaction ($CH \rightarrow C + H$) to be 0.21 eV exothermic. The most stable species on Ni{100} is thus atomic carbon, in line with the results described above for Pd{100}. It is intriguing to speculate whether this is a common feature of the *fcc*-{100} surfaces, so further investigation of Pt{100} and Rh{100} might prove very interesting in this regard.

Stepped Ni surfaces: {110}, {211}. As one would expect, first-principles DFT studies relevant to alkane oxidation over stepped Ni surfaces are rather thinner on the ground than those for the flat surfaces. Nevertheless, Wang *et al.*[158] have provided a complete thermochemical sequence for dissociation of methane on Ni{110}. Favoured adsorption sites are short-bridge for methyl (CH_3) and methylene (CH_2), long-bridge for methylidyne (CH), and fourfold hollow (*i.e.* atop relative to a trough atom) for atomic carbon (C). The initial dissociative adsorption of methane ($CH_4 \rightarrow CH_3 + H$) is reported to be almost thermoneutral (0.03 eV endothermic), and therefore very slightly more favourable than on either the Ni{111} surface or the Ni{100} surface (0.16 eV and 0.09 eV endothermic, respectively). The methyl-to-methylene reaction ($CH_3 \rightarrow CH_2 + H$), in contrast, is found to be 0.35 eV endothermic, whereas it is only 0.16 eV endothermic on Ni{111}, and actually 0.18 eV exothermic on Ni{100}. Both the methylene-to-methylidyne reaction ($CH_2 \rightarrow CH + H$) and the methylidyne-to-carbon reaction ($CH \rightarrow C + H$) are nearly thermoneutral (0.00 eV and 0.04 eV endothermic,

respectively), differing markedly from the Ni{111} case (where methylidyne is strongly favoured) and the Ni{100} case (where atomic carbon is strongly favoured). On the basis of these results (and in the absence of data on the reaction barriers) it seems possible that methyl may be the majority species on the Ni{110} surface.

Adsorption of oxygen on Ni{110} has been calculated by Li *et al.*,[148] whose results suggest a preference for O adatoms to occupy long-bridge sites at 1.0 ML coverage, but short-bridge sites at the (probably more achievable) 0.5 ML coverage. To some degree, therefore, we may anticipate that oxygen adatoms (O) and methyl moieties (CH_3) will compete for the same sites on Ni{110}, so coadsorption studies would form a highly desirable adjunct to the existing literature. It seems likely that the greater binding energy of oxygen will, in effect, block the most reactive sites for methane dissociative adsorption, and may also reorder the thermochemistry of subsequent dehydrogenation.

Abild-Pedersen *et al.*[161] have meanwhile performed DFT calculations on the dissociation of methane on the stepped Ni{211} surface, in which the initial dissociative adsorption occurs over a barrier of 0.91 eV (*cf.* 1.09 eV from the same group for the Ni{111} surface[157]) and with an endothermicity of 0.08 eV (*cf.* 0.16 eV from Wang *et al.*[158] for dissociative adsorption on Ni{111}). The initial reaction ($CH_4 \rightarrow CH_3 + H$) is thus kinetically and thermochemically more favourable at the step than on the flat surface. Abild-Pedersen *et al.*[161] further demonstrate that atomic sulfur or carbon will adsorb preferentially at the fourfold hollow site beneath the step-edge, raising the activation barrier for dissociative adsorption above that found for the Ni{111} surface.

The methyl moiety (CH_3) resulting from dissociation of methane over Ni{211} is bound, at least initially, at the step edge in a short-bridge site, in contrast to the hollow site favoured on Ni{111}, but similar to the geometry adopted on Ni{110}. Bengaard *et al.*[157] previously reported a preference for methyl (CH_3) binding at a step-edge atop site, for methylene (CH_2) binding at a step-edge bridge site, and for methylidyne (CH) and atomic carbon (C) binding at the fourfold hollow site beneath the step edge. In addition, their schematic energy diagram[157] (they do not tabulate their precise energetic results) seems to show the initial dissociation reaction ($CH_4 \rightarrow CH_3 + H$) as quite strongly endothermic both on Ni{111} (around 0.5 eV) and on Ni{211} (around 0.4 eV), which seems to be markedly at odds with the results of Wang *et al.*[158] for Ni{111} (0.16 eV endothermic) and Abild-Pedersen *et al.*[161] for Ni{211} (0.08 eV endothermic). The origin of these apparent discrepancies remains obscure to us at the present time. Bengaard *et al.*[157] show the methyl-to-methylene reaction ($CH_3 \rightarrow CH_2 + H$) as nearly thermoneutral on Ni{211}, with the methylene-to-methylidyne reaction ($CH_2 \rightarrow CH + H$) and the methylidyne-to-carbon reaction ($CH \rightarrow C + H$) each exothermic by around 0.3 eV. Atomic carbon would thus be thermochemically favoured on the Ni{211} surface, but the barrier to the last dehydrogenation step would be around 0.9 eV, compared to around 0.6 eV for each of the previous two.

Although not strictly falling within the remit of the present work, we should also note in passing the calculations published recently by Vang *et al.*[17] on the dissociative adsorption of ethene (C_2H_4) on Ni{111} and Ni{211}; the intermediates deriving from ethene are, of course, a large subset of the possible products from the dissociative adsorption of ethane (C_2H_6), and the work represents a rare DFT study of C_2 species surface chemistry. In very brief summary, the Ni{211} step edge is more active for ethene dissociation than the flat Ni{111} surface, and indeed is the only locale where C–C bond scission may be kinetically nearly competitive with dissociation of the C–H bonds. The thermochemically favoured species on Ni{111} is ethyne (C_2H_2), whilst on Ni{211} methylidyne (CH) is slightly more stable.[17]

Once again, the results obtained thus far for the stepped Ni surfaces are enough to show that intriguing differences from the flat surfaces are likely to be found, but they also show that considerable further work will be necessary before a complete and indisputable picture emerges.

4. Catalytic alkane synthesis

The synthesis of hydrocarbons on transition metal surfaces implies an evolution of the relevant hydrocarbon building block through three distinct stages, namely: (i) adsorption of CO (molecular or dissociative); (ii) dissociative adsorption of hydrogen; (iii) hydrogenation of CO either by cleavage and subsequent hydrogenation or direct hydrogenation followed by C–O bond scission. In the case of the methanation reaction, the C_1 species is hydrogenated to methane, while in the case of the classic Fischer–Tropsch process, the C_1 building blocks undergo C–C coupling reactions either with other C_1 species or with longer hydrocarbon chains. This polymerization proceeds until a chain is terminated by, for instance, hydrogenation to up to saturation, recombination of alkyl adsorbates or by beta-elimination forming alkenes. The relative rates of hydrogenation and C–C coupling reactions will determine the distribution of alkanes (alkenes) produced. In the case of the classic methanation catalyst Ni, hydrogenation is obviously much faster than C–C coupling, which is the only possible explanation for the selectivity towards methane. Selectivity issues will form a particular focus of our discussion. In this section, we review the current theoretical literature relating to alkane synthesis on cobalt, ruthenium, iron and nickel surfaces. This includes studies of CO adsorption and dissociation, hydrocarbon hydrogenation reactions together with the few existing DFT investigation into C–C coupling and termination. Once again, we sub-divide our review according to the structural properties of the surfaces involved, which here include the very particular facets available on *bcc* or *hcp* crystals but not *fcc*.

4.1 Cobalt

Flat Co surfaces: {0001}. The flat, low-index Co{0001} surface is by far the most thoroughly studied cobalt surface. Many excellent experimental and theoretical studies are concerned with the adsorption of CO and hydrogen on this facet of cobalt and mentioning all the relevant publications would go far beyond the scope of the present work; we therefore restrict ourselves to highlighting novel and particularly comprehensive studies related to the FT synthesis.

Klinke and Broadbelt, for instance, studied the adsorption of hydrogen on Co{0001} using FP-LAPW calculations. They determined adsorption energies for two different coverages, namely 0.5 ML and 1.0 ML. Hydrogen is most stable in the hollow positions and the adsorption energy for the *fcc* and *hcp* positions was approximately 2.88 eV at both coverages.[162] These values are only slightly above the experimental value of 2.6 eV reported by Christmann.[163] Gong *et al.*[174] also studied the adsorption of H on Co{0001} but using the less accurate plane-wave pseudopotential set-up. They also determine the most stable site to be the *fcc* site and the adsorption energy calculated with the plane-wave pseudopotential approach is −2.94 eV, overestimating the experimental value by 11.3% while the more accurate, but computationally more expensive, FP-LAPW calculation overestimates it by 11.1%. Hence, the plane-wave pseudopotential calculations are only very slightly less accurate, while they are computationally by far less expensive.

Papp presented a very thorough study of the chemisorption of CO on Co{0001} using LEED, UPS, EELS and Auger measurements.[164] He determined atop adsorbed CO to be stable on this cobalt facet up to 450 K, in contrast to stepped cobalt surfaces on which dissociation is observed above 300 K.[164] Lahtinen *et al.* carried out a LEED study on the adsorption of CO on Co{0001}, determining that the molecule adsorbs atop, perpendicular to the surface, with the carbon atom bonding to a Co atom.[165] The optimum length for the C–O bond is 1.17 ± 0.06 Å and that for the C–Co distance 1.78 ± 0.06 Å.[165] Pick calculated the same overlayer using a plane-wave DFT approach and determined the C–O bond length to be 1.17 Å for CO in the atop position[166] which is in very good agreement with the Lahtinen *et al.* LEED result; the calculated Co–C separation (1.75 Å) is slightly shorter than the experimental value of 1.78 ± 0.06 Å, but still within the error limits of the LEED analysis.[166] It is noteworthy that Pick's results indeed determine the atop site to be energetically favoured over the two threefold sites, which implies that overbinding of CO in high-coordination sites is not terribly pronounced on Co{0001}.

Ge and Neurock subsequently simulated the adsorption and dissociation of CO on Co{0001}.[167] The authors report a very good agreement between calculated and experimentally determined adsorption energies.[167] Dissociation of CO on Co{0001} traverses a rather late transition state and the reaction has a barrier of 2.40 eV, higher than the adsorption energy of CO.[167] This is in agreement with previous experimental studies, which cannot observe dissociation on this facet.[168] Gong *et al.*[169] also studied CO dissociation on Co{0001} and they determine the lowest barrier to be 1.04 eV relative to the CO molecule in the gas phase and 2.64 eV relative to the most stable adsorbed state. Therefore this study also concluded that CO should desorb from Co{0001} rather than dissociate.[169]

Oosterbeek, however, showed experimentally that FT can indeed be carried out on this facet of cobalt; it converts CO in the presence of hydrogen, not to long chain hydrocarbons, but to methane,[170] which is in agreement with previous results by Geerlings *et al.*[171] But how is CO converted to methane on this surface when it preferentially desorbs rather than dissociates? Very recently, DFT simulations of the reactions of CO and hydrogen on Co{0001} could shed light onto this paradox: Inderwildi *et al.* find values for the dissociation and desorption barriers of CO on Co{0001}[75] very similar to Gong *et al.*'s values,[169] with a dissociation barrier more than 1 eV higher than the desorption barrier, implying that the adsorbed molecule desorbs rather than dissociates.[24] In this study, however, direct hydrogenation of CO leading to oxymethylidyne (CHO, formyl) was also considered, and it was determined that this step requires a much smaller activation barrier of merely 1.31 eV. This barrier is not only lower than the dissociation barrier but also considerably lower than the desorption barrier. The study moreover shows that the CHO product (formyl species) is adsorbed with both the carbon *and* the oxygen atom bound to the surface: cleavage of the C–O bond (*i.e.* CHO → CH + O) is therefore facilitated, with a significantly lower barrier of 1.00 eV than for direct CO dissociation where the barrier is 2.82 eV. These results showed that the hydrogenation route is the main reaction pathway on Co{0001}. Moreover, the subsequent hydrogenation of the CHO species to CH_2O was studied[75] and it was found that this step only requires an activation barrier of 0.45 eV, and that dissociation of the CH_2O species requires an activation barrier of 0.85 eV, while the dissociation of the CHO species requires 1.00 eV.[75] Thus, hydrogenation of the CO species to CHO and CH_2O successively weakens the C–O bond, which leads to lower activation barriers for its cleavage (CO: 2.82 eV; CHO: 1.00 eV; and CH_2O: 0.85 eV), the relevant structures are shown in Fig. 3. An energy diagram of the different pathways is shown in Fig. 4. An obvious alternative reaction is the hydrogenation of the oxygen atom of the CHO species leading to the surface alcohol species CHOH. This reaction, however, has an activation barrier of 0.81 eV and is therefore less likely than CH_2O formation.[75] Jenkins and King have previously speculated that polarisation of CO by co-adsorbed K promotor may enhance production of CHOH, although they had not considered the alternative production of CHO and CH_2O.[172]

Regarding the surface stability of C_1 hydrocarbon species, Ge *et al.* studied the adsorption of methylidyne (CH) and methylene (CH_2) on Co{0001}.[173] According to their study methylidyne is the most strongly bound C_1 species on this cobalt facet, with an adsorption energy of 6.42 eV relative to CH in the gas-phase. It is adsorbed in a hollow position, with the *hcp* hollow being slightly more stable than the *fcc* hollow in this case. One might expect that methylene (CH_2) would adsorb in the bridged position where it can adopt a tetrahedral geometry, but the DFT calculations by Ge *et al.* determined that the most favourable adsorption site is again the *hcp* hollow, being 0.25 eV more stable than the bridged position.[173] Hydrocarbons on Co{0001} thus violate the "completion of carbon tetravalency" rule-of-thumb (which the reader will recall holds on Pt{111} and Pd{111}, but not on Rh{111} and Ni{111}).

Gong *et al.* not only studied the adsorption of the C_1 fragments methylidyne (CH) and methylene (CH_2), but also methyl (CH_3) on Co{0001}, and found that for all three the *hcp* hollow site is the most stable,[174] supporting the earlier results by Ge *et al.*[173] The energies of the co-adsorption systems of $CH_x + yH$ ($x + y = 4$) are as follows: the most

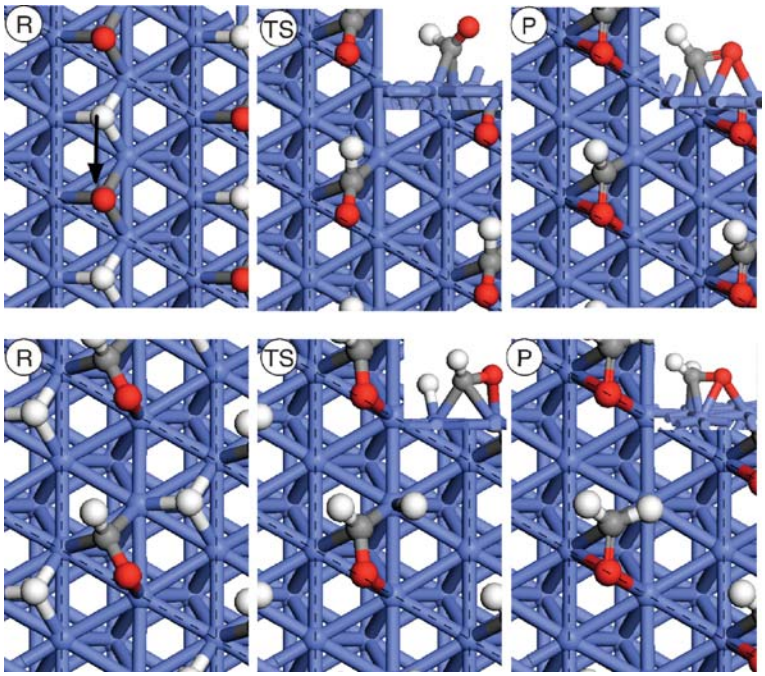

Fig. 3 Reactant (R), transition state (TS) and product (P) of the hydrogenation of CO (top) and CHO (bottom) on Co{0001}; side views are shown as insets. Cobalt is shown as blue, oxygen as red, hydrogen as white and carbon as grey. Reprinted from ref. 24, Copyright ACS Publications. Reproduced with permission.

stable species is the CH species, the least stable species is carbon co-adsorbed with hydrogen, while CH_2 is the second least stable species, and CH_3 the second most stable; adsorption energies are −5.99 eV for CH, −3.85 eV for CH_2 and −1.89 eV for CH_3 relative to the gas-phase neutral radicals. In a subsequent study, Hu and co-workers studied methyl on the surface and confirm the results by Gong *et al.*:[174] CH_3 is bound to the *hcp* position with a Co–C bond length of 2.1 Å. The adsorption energy in this study is slightly higher (2.00 eV)[175] than in the earlier study by Gong *et al.* (1.89 eV), which can most likely be attributed to a slightly different calculation setup (the earlier work utilises the CASTEP computer code with a plane-wave basis set, the recent work, SIESTA with a localised basis set).

Moving to C_2 species, Gong *et al.* assumed that vinyl ($CHCH_2$) is an essential intermediate in the hydrocarbon polymerization process[176] and therefore studied adsorption of this species on Co{0001}. They reached the conclusion that vinyl prefers *hcp* hollow sites, in which the less saturated group resides directly in the hollow position whereas the other binds at the adjacent atop site, leading to a tetrahedral structure of both carbon atoms. The adsorption energy of this species was determined to be 2.35 eV. In a study concerned with olefin selectivity, Hu and co-workers also calculated the structure and stability of ethyl (CH_2CH_3) on the Co{0001} surface.[177] This species is (with an adsorption heat of 1.6 eV) considerably less strongly bound to the surface than vinyl, owing to a smaller number of Co–C bonds due to the higher degree of

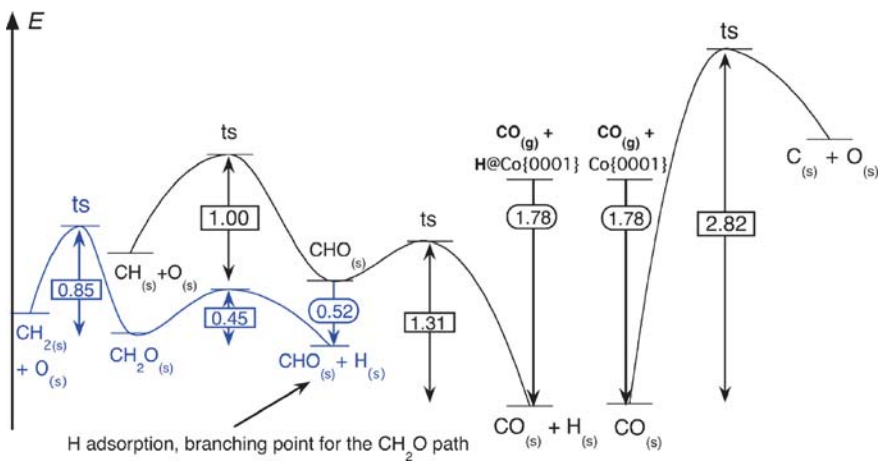

Fig. 4 Energy diagram for CO dissociation and hydrogenation on Co{0001}. Reprinted from ref. 24, Copyright ACS Publications. Reproduced with permission.

saturation. The Co–C bond length of ethyl is 2.2 to 2.3 Å, which is considerably greater than for methyl (2.1 Å) again indicating the weaker bonding of this species to the surface. The differences in distance and bonding are very similar to those of longer chain alkyl species calculated by the same group.[177]

For C_{3+} species, indeed, Cheng *et al*. recently studied the adsorption of a variety of longer-chained alkyl groups (C_3 to C_6) on Co{0001}.[177] In all cases, the most stable structure of the *n*-alkyl species is adsorbed in the *hcp* hollow site with the carbon chain normal to the cobalt surface. The Co–C bond distance is very similar in all C_{2+} cases (2.2 to 2.4 Å), but considerably longer than in the case of CH_3, implying that the strength of the surface bond is independent of the chain length in the case of longer alkyl chains. The calculated chemisorption energies confirm this assumption; chemisorption energies range from 1.60 to 1.62 eV and hence it can be concluded that the Co–C bond strength does not change in the growth process for C_{3+} species. Nevertheless, the Co–C bond strengths of methyl (2.00 eV) and vinyl (2.35 eV) are considerably higher.

DFT predicts the carbon chain of the alkyl species to be normal to the surface. However, this is most likely due to the neglect of van der Waals interactions by DFT. In a realistic FT catalyst, however, the alkyl species will quite likely be normal to the surface, owing to high surface coverages caused by the high pressure in the reactor. In this instance, the well-known deficiency of DFT in respect of the van der Waals interactions is probably not too critical.

Moving beyond considerations of surface stability alone, Gong *et al*. also studied the hydrogenation reactions of atomic carbon, methylidyne, methylene and methyl.[174] They determined the hydrogenation of methyl ($CH_3 + H \rightarrow CH_4$) to be the most difficult step, with a reaction barrier of 1.09 eV. This rather high barrier for methane formation provides a potential explanation for the selectivity of this process towards liquid hydrocarbons, as barriers for C–C coupling are somewhat lower than this. Hydrogenation of atomic carbon to methylidyne ($C + H \rightarrow CH$) requires an activation energy of 0.85 eV, while hydrogenation of methylidyne towards methylene ($CH + H \rightarrow CH_2$) requires an activation barrier of 0.66 eV. Formation of methyl from methylene ($CH_2 + H \rightarrow CH_3$) is associated with an energy barrier of 0.63 eV.

From these results it can be seen that methylene is a rather unstable species; it is easily hydrogenated to methyl ($E_a = 0.63$ eV) or dissociates to methylidyne and hydrogen ($E_a = 0.28$ eV). The fact that CH_2 is a rather labile species already implies that reaction pathways other than CH_2 polymerisation might play an important role in the synthesis of liquid hydrocarbons.[174] It has to be mentioned that, in the contribution by Gong *et al*.,[174] the activation barriers are given with respect to separately adsorbed CH_x and H, *i.e*. neglecting adsorbate–adsorbate interaction in the initial state. The authors estimate that barriers could be up to 0.3 eV lower when the co-adsorption system is considered as the starting point. The most appropriate reference energy will, of course, depend upon the relevant surface coverages. In any case, hydrogenation will be fast under conditions that enable CO dissociation, and hence will not influence the overall reaction rate of a possible carbide mechanism; however, CH_2 will only play a minor role due to its short lifetime. We will discuss the competition between hydrogenation and C–C coupling shortly.

Meanwhile, we note that Cheng *et al*. have studied higher alkane formation by hydrogenation as part of their investigation into the adsorption of alkyl species on Co{0001}.[177] In all cases the *n*-alkyl groups migrate from the *hcp* hollow position to the atop position during the hydrogenation reaction. The hydrogen atom is bound to the same Co atom as the alkyl group in the transition state structure, and the transition state structures obtained are very similar in character to the one obtained by Gong *et al*. for the hydrogenation of methyl.[174] The distance between the reactive carbon and the approaching hydrogen is approximately 1.65 Å for all of the different transition state structures, and hence one can conclude that the hydrogenation reactions of C_1 to C_6 alkyls are all very similar.

The energetically similar initial states and the similar transition state geometries already imply that the activation barriers are likely to be in the same order: the highest barrier is indeed the hydrogenation of methyl (1.09 eV[174]), followed by ethyl (0.69 eV) and then the barriers seem to settle at around 0.66 eV for the longer-chain alkyl species.

As regards C–C coupling, Ge *et al*. studied just such a reaction starting from coadsorption of CH and CH_2 in a (2×2) unit cell of Co{0001}.[173] The two species share one metal atom in the initial structure, which leads to a repulsion owing to the bonding competition effect. Subsequently they explored the PES of the reaction to form vinyl ($CH + CH_2 \rightarrow CH_2CH$).[173] They find that the reaction proceeds *via* the classic oxidative addition mechanism: adsorbed CH_2 migrates towards the CH group and thereby overcomes the repulsive interactions between them. The activation barrier was determined to be 0.58 eV and the reaction is slightly exothermic with respect to the coadsorbed CH and CH_2 (−0.08 eV). If, however, the co-adsorbed system is not considered as the starting point of the reaction, but instead CH and CH_2 separated on the surface, the reaction is considerably endothermic. Therefore, the CH_x species have to move energetically uphill to get to the actual starting position and then have to overcome a barrier of 0.58 eV to form the vinyl species, which causes Ge *et al*. to consider the reaction rather unlikely.[173] The cleavage of the C–C bond would consequently be exothermic at low coverage, since CH_2 and CH would separate on the surface, which is energetically downhill.

Cheng *et al*. very recently also studied the coupling of C_1 species on the same surface.[175] In this study, the activation barrier of CH and CH_2 recombination was determined to be 0.76 eV (*i.e*. slightly higher than in the work by Neurock and co-workers[173]). The more drastic difference is that Cheng *et al*. determined the lowest coupling barrier for C_1 species to be for the coupling of two CH_2 species forming surface ethylene (CH_2CH_2), which has an activation barrier of 0.70 eV.[175] Also the coupling of C and CH_2 has, according to Cheng *et al*., a barrier that is slightly higher (0.74 eV)[175] than the minimum energy pathway for C_1 coupling published by Ge *et al*. (0.58 eV).[173]

Finally, before leaving flat cobalt surfaces, we mention olefin formation, since important by-products in the

Fischer–Tropsch process are olefins, mainly 1-olefins. Olefins can be formed by desorption of a substituted vinyl species (CH_2–CH–R) or by hydrogen elimination from a surface alkyl chain (–$(CH_2)_x$–CH_3). The olefin selectivity in Fischer–Tropsch synthesis, commonly described by a paraffin : olefin (P : O) ratio, is an important topic since linear 1-olefins are an important feed-stock, widely used as monomers for polymerization or as feed-stock for hydrogenation reactions.[49] Hence, steering the FT synthesis towards 1-olefin production is of considerable economic interest for commercial applications.[178]

Hu and co-workers very recently presented the first DFT study on this issue, in order to explain the α-olefin selectivity in Fischer–Tropsch synthesis on Co{0001}.[177] Barriers for the alkyl hydrogenation reaction ($C_nH_{2n+1} + H \rightarrow C_nH_{2n+2}$) are in the range of 0.65 eV to 0.67 eV, with the exception of ethyl, which requires a slightly higher activation barrier of 0.69 eV. Barriers of the dehydrogenation reaction ($C_nH_{2n+1} \rightarrow C_nH_{2n} + H$) range between 0.41–0.44 eV, ethyl again being the exception with 0.49 eV. Their calculations hence showed that the barriers for hydrogenation and dehydrogenation were essentially independent of the chain lengths for $n > 2$, as were the adsorption energies of 1-olefins of different chain length with the exception of ethene (C_2H_4). A kinetic comparison between alkyl hydrogenation and dehydrogenation based on these DFT results satisfactorily explained experimental results for the P : O ratio.[177]

Stepped and other Co surfaces: corrugated {0001}, {10$\bar{1}$0}, {11$\bar{2}$0}, {10$\bar{1}\bar{2}$}, {11$\bar{2}\bar{4}$}. Quite a few experimental studies report on the adsorption of CO on non-flat cobalt surfaces: Toomes and King, for instance, monitored CO adsorption on Co{10$\bar{1}$0} by means of RAIRS, TPD and LEED.[179] Papp, meanwhile, investigated the chemisorption of CO on Co{11$\bar{2}$0}, finding that the species dissociates above 300 K, which indicates that this surface is far more active for CO dissociation than the flat Co{0001} surface.[164] There are also a number of DFT studies concerned with the adsorption of CO on stepped cobalt surfaces. Jenkins and King, for instance, report calculations for CO adsorbed on the Co{10$\bar{1}$0} surface.[180] More detailed DFT studies that also include the reactivity of CO at stepped cobalt surfaces are, however, more scarce.

Ge and Neurock studied the adsorption and activation of CO over Co{11$\bar{2}$0}, Co{10$\bar{1}\bar{2}$} and Co{11$\bar{2}\bar{4}$} surfaces.[167] Within the descriptive scheme introduced recently by Jenkins and Pratt, the first of these would be considered a ''meandering row'' surface, the second a ''stepped'' surface, and the third a ''kinked'' surface. The meandering row surface is characterised by a zig-zag chain of atoms lying within the surface plane, the stepped surface by a linear chain, and the kinked surface by the absence of any such chain of atoms. Furthermore, the meandering row surface and this particular stepped surface share a coordination number of seven in the outermost layers (not true for all *hcp* stepped surfaces), while the atoms in the outermost layer of this particular kinked surface have a coordination number of six (again not true for all *hcp* kinked surfaces).[52]

Ge and Neurock find that CO chemisorbs onto all these surfaces, but that the strength of chemisorption strongly depends on the surface structure. The presence of the meandering row on Co{11$\bar{2}$0} enhances the reactivity slightly by reducing the barrier for CO dissociation to 2.00 eV as compared to 2.39 eV on flat Co{0001}.[167] The stepped Co{10$\bar{1}\bar{2}$} and kinked Co{11$\bar{2}\bar{4}$} surfaces are significantly more active than the flat and meandering row cobalt surfaces, however, both surfaces having activation barriers for dissociation that are lower than the desorption energy and thereby providing direct pathways for decomposition of CO. In general, the activation barriers become lower as the reaction energies become more exothermic, in accordance with the Brønsted–Evans–Polanyi relationship.[181]

These results plainly indicate that low coordination sites are generally much more reactive for CO dissociation than those found on flat Co{0001}, although the relatively low reactivity of the meandering row Co{11$\bar{2}$0} surface is something of a puzzle. It is not, however, known how C_1 hydrocarbon fragments behave at such sites. It is known for many metals that dissociation reactions are highly exothermic at steps and kinks, and additionally have rather low activation barriers. If this would be the case on meandering row, stepped and kinked cobalt surfaces, the activity would be limited by rapid dissociation of C–H bonds, which in turn blocks the formation of C_1 hydrocarbon fragments and consequently suppresses formation of longer chained hydrocarbons. In order to determine whether direct hydrogenation of CO is the main reaction route (as we believe to be the case on strictly flat Co{0001}) or whether the real synthesis is more likely to proceed *via* dissociation at steps followed by hydrogenation and polymerization, the behaviour of C_1 hydrocarbon fragments at steps has to be understood.

Gong *et al.* determined the stable adsorption sites for C_1 hydrocarbon fragments and atomic carbon on an artificially corrugated cobalt surface formed (*in silico*) by simply deleting rows of atoms from a Co{0001} slab.[174] As a model for low coordination sites on an *hcp* surface, such a scheme is computationally quite attractive, but compared with the high-index surfaces studied by Ge and Neurock[167] it suffers from the weakness that it cannot be replicated in experiment. Furthermore, only one type of low-coordination site is probed, whereas a set of high-index surfaces could reveal a variety of different types. Nevertheless, these calculations provide much important information. As expected, the authors find that the atoms/fragments are more strongly bound to the undercoordinated atoms at the step than to the terrace. Atomic carbon (C) resides on the terrace adjacent to the bottom of the step. Methylidyne (CH) resides in a very similar position with the C–H bond parallel to the step. Methylene (CH_2) and methyl (CH_3) bind most strongly to the step-edge with the carbon atom located in the bridged position. The most stable species (with respect to CH_4 in the gas phase) is, surprisingly, atomic carbon (C) in the case of the corrugated surface, in contrast to Co{0001} in which methylidyne (CH) is the most stable species, see above. The least stable species is the methylene species (CH_2) as in the case of flat Co{0001}. These results thus already raise the question whether the carbide mechanism is correct at low-coordination sites, even though

CO dissociation is more likely here: atomic carbon (C) is the most stable species, and formation of methylene (CH_2) from this species is endothermic with an energy of 0.61 eV.

Gong *et al*. also studied the hydrogenation reactions of C_1 hydrocarbon fragments at corrugated Co{0001}.[174] They considered the CH_x species to be located at the most favourable site on or at the step, with hydrogen adsorbed on the terrace, to be the initial state of all the reactions. Atomic carbon and methylidyne (C and CH) are hence adsorbed below the step, while methylene (CH_2) and methyl (CH_3) are adsorbed in the bridged position on the step-edge; atomic hydrogen in turn resides in the *fcc* hollow site in all cases.

While C, CH, and CH_2 do not move out of their initial positions during the reaction, the methyl moiety (CH_3) moves from the bridge site on the step-edge to the atop position in the course of the hydrogenation reaction. Moreover, the methyl group shares a metal atom with the approaching hydrogen, analogously to the reaction on flat Co{0001}, which destabilises the transition state due to bonding competition. Consequently, the hydrogenation of methyl ($CH_3 + H \rightarrow CH_4$) has the highest barrier of all hydrogenation steps on corrugated Co{0001} (0.96 eV), only slightly lower than on flat Co{0001} (1.9 eV[174]). The hydrogenation barriers for atomic carbon and methylidyne ($C + H \rightarrow CH$ and $CH + H \rightarrow CH_2$) are both around 0.8 eV. In the case of carbon, this barrier is only slightly lower than on flat Co{0001} where it was (0.85 eV[174]), while in the case of methylidyne the barrier is rather higher (0.66 eV[174]) on the flat surface. The hydrogenation of the least stable species ($CH_2 + H \rightarrow CH_3$) possesses a barrier of only 0.43 eV. The comparison hence shows that the hydrogenation of C_1 hydrocarbon fragments at steps will be approximately as fast at steps as on the flat Co{0001} surface. If atomic carbon (C) is formed by CO dissociation on this surface, it has to be hydrogenated to methylene (CH_2) in two endothermic steps, which both have activation barriers of around 0.8 eV. In order to fully understand the conversion, however, carbon–carbon coupling reactions at low-coordination sites have also to be considered, which we will now consider.

Cheng *et al*. very recently studied the coupling reactions of C_1 species at steps on their artificially corrugated Co{0001} surface.[175] According to this study, the lowest barrier for a coupling reaction is, in analogy to the planar surface, the combination of CH_2 species with a barrier of 0.22 eV. The transition states of the coupling reactions of all possible C_1 species are depicted in Fig. 5.

Surprisingly, however, the barriers for C_1 coupling reactions are all rather higher on the corrugated surface than on the flat surface, with the exception of the coupling of CH_2 species to either another CH_2 or to a CH_3 species. For instance, the formation of vinyl ($CHCH_2$) has a barrier of 0.76 eV on the flat surface and a barrier of 1.32 eV on the corrugated surface.[175] Having in mind that the activation barriers of dissociation reactions are generally significantly lower at steps, this result is of the utmost interest. Nevertheless, since the C_1 species are adsorbed considerably more strongly to the steps, the absolute energies of the transition state structures are lower than on the flat Co{0001} surface. According to the rate constant calculated by Cheng *et al*., the main reaction route at steps involves two pathways, *via* coupling of two CH_2 species to form ethane as well as *via* reaction of C with CH_3 (to form ethylidyne). The latter pathway, however, does not account for the general chain growth mechanism, since it would lead to short chain alkanes. Based on results from a simple kinetic model, the authors argue that the main reaction pathway depends on the external conditions and on the number of free adsorption sites at the step.[175]

To conclude our discussion on the Fischer–Tropsch process on cobalt, we note that various DFT calculations agree that

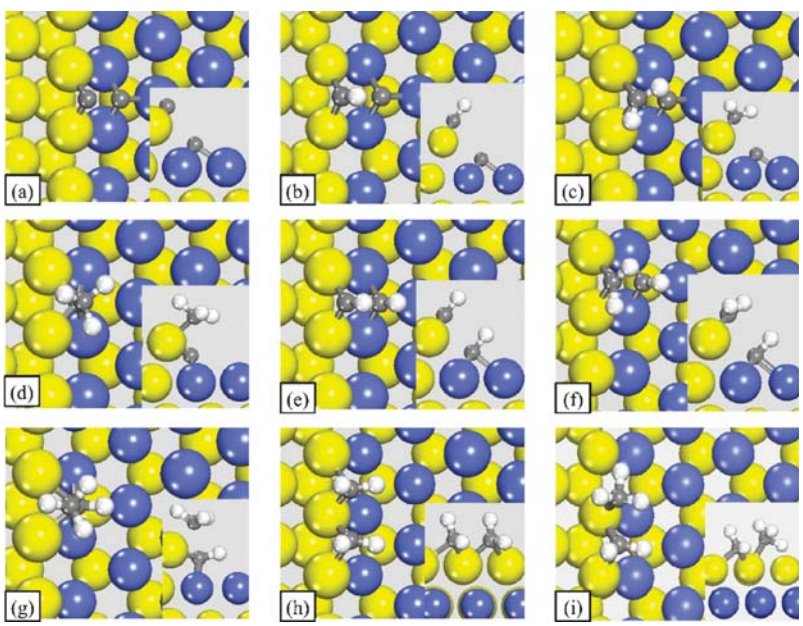

Fig. 5 Top view and side view (inserted) of the calculated TS structures of $C_1 + C_1$ coupling reactions on the stepped Co(0001). (a) C + C; (b) C + CH; (c) C + CH_2; (d) C + CH_3; (e) CH + CH; (f) CH + CH_2; (g) CH + CH_3; (h) CH_2 + CH_2; (i) CH_2 + CH_3. Reprinted from ref. 175, Copyright Elsevier Ltd. Reproduced with permission.

the dissociation barrier on a flat Co surface is much higher than the desorption barrier, in accordance with TPD spectra by Yates and co-workers,[182] and hence the carbide mechanism can definitely be excluded here. The only viable pathway on terraces of cobalt is hence the direct hydrogenation of intact CO followed by C–O bond scission. At steps, however, the desorption barrier seems to be generally higher than the dissociation barrier and hence CO dissociation can take place here, which is in agreement with experimental observations.[164] It has, however, still to be gauged if the direct hydrogenation route might be a viable alternative pathway at steps as well, in order to draw conclusions on the exact pathway of hydrocarbon formation on cobalt. Preliminary results showed that hydrogenation of CO at steps has also a lower barrier than dissociation of this species.[24] Once the labile methylene species is formed, it can either undergo further hydrogenation, dehydrogenation to CH, or polymerisation. Here it has to be investigated whether this species is sufficiently reactive to directly form a bond with adsorbed CO.

4.2 Ruthenium

Flat ruthenium surfaces: Ru{0001}. Another metal that is able to generate liquid hydrocarbons from synthesis gas is ruthenium.[12] The adsorption of CO, oxygen and hydrogen on Ru{0001} is therefore also rather well studied: LEED studies on the adsorption geometry of CO on Ru{0001} in presence or absence of oxygen are available[183] and have already been successfully benchmarked against DFT studies, *vide infra*.[184] Braun *et al*. investigated the adsorption of CO and its co-adsorption with hydrogen and oxygen on Ru{0001} using high resolution helium atom scattering.[185] Riedmuller *et al*. studied the adsorption of CO on H- and CO-precovered Ru{0001} using molecular beams.[186] Adsorbed oxygen on Ru{0001} is also well studied, not the least because ruthenium was long believed to be a good oxidation catalyst:** Ertl and co-workers published the famous real-time STM video of the random walk of oxygen adatoms on Ru{0001};[188] Nakamura *et al*. investigated the adsorption structure of oxygen using XRD;[189] and Takahashi investigated the dissociative adsorption of dioxygen utilizing molecular beams.[190]

But it is not only experimental studies of adsorption on Ru{0001} that are abundant. This surface is also quite thoroughly studied by means of DFT: Feibelman, for instance, investigated the adsorption of hydrogen (H), hydroxyl (OH) and water (H_2O) on the {0001} facet of ruthenium.[191] In this case DFT is especially helpful, owing to experimental difficulties when studying water on this surface, as Menzel points out in a perspective article.[192] Ertl, Scheffler and co-workers investigated the adsorption of oxygen by a combination of LEED and DFT, and both techniques determine atomic oxygen to be most stable in the *hcp* position of this surface. Even at up to a full monolayer coverage, which was achieved experimentally by NO_2 exposure of a surface covered with 0.5 ML O, experiment and theory agree that O resides exclusively in the *hcp* position.[193] Stampfl and Scheffler studied the adsorption of CO on bare Ru{0001} and find the atop position to be most favourable, followed by the threefold hollow positions, with a slight preference for the *hcp* site.[194] The same authors subsequently investigated the co-adsorption of atomic oxygen and CO on this facet of Ru and found that in a (2×2) elementary cell, *i.e*. at 0.5 ML coverage, the adsorbates reside in the same positions as for the single adsorption, *i.e*. *hcp* in the case of O and atop in the case of CO;[195] it is found that oxygen co-adsorption weakens the CO-surface bond. Moreover, they benchmark their DFT results[195] with LEED studies by Menzel and co-workers.[183] In comparison, the adsorption of hydrogen is not as thoroughly studied, but Luntz *et al*. have investigated the laser-induced desorption kinetics of hydrogen from Ru{0001} using an *ab initio* molecular dynamics approach.[196]

More interesting within the scope of this review, however, are studies on the adsorption and reaction of hydrocarbons as well as CO on Ru{0001}. On the experimental side, Goodman and co-workers studied methane coupling over Ru{0001}[197] as well as CO hydrogenation on Ru{0001} using HREELS.[198] Payne *et al*. studied the adsorption/desorption kinetics of CO on this surface using statistical mechanics and are able to reproduce experimental results very well.[199] Baerends and co-workers[200] calculated highly precise transition states for hydrogen adsorption on Ru{0001} on a six dimensional PES utilizing PW91 and RPBE functionals. Both functionals predict that the adsorption, *i.e*. the breaking of H–H bond, is lowest when H_2 is coordinated over an atop site, with the bond lying parallel to the surface. They conclude that the adsorption is barely activated with a barrier of just 10 meV (PW91) and 20 meV (RPBE). Van Santen and co-workers published a series of articles that are concerned with (i) the adsorption of CO and hydrogen, (ii) the adsorption of methane fragments (CH_x, $x = 1$–3), as well as (iii) the chain growth of hydrocarbon using both methylene and methylidyne as building blocks.[201–206]

Hereafter, we will, as in the case of cobalt, discuss studies on the adsorption and conversion of CO, formation of C_1 building blocks, and their polymerisation to alkane fragments with longer chain length. Other surface processes, such as the dissociation of hydrogen and the formation of water, are unlikely to determine the rate of the FT process.

Various DFT studies examined the different pathways for CO dissociation on Ru{0001}. Ciobica and van Santen studied this dissociation at two different coverages, 0.11 and 0.25 ML, (*i.e*. in (2×2) and (3×3) elementary cells); various starting points and reaction coordinates were considered in this comprehensive study.[205] They report that a path starting from CO adsorbed in an *hcp* position is the lowest energy pathway for the dissociation of CO on this surface. In the transition state structure, oxygen is located in the bridged position and carbon remains essentially at its starting point, which is in agreement with similar studies.[75] The activation barrier is 2.24 eV and 2.35 eV for coverages 0.11 ML and 0.25 ML, respectively.[205] Inderwildi *et al*. essentially confirmed these results, reporting an activation barrier of 2.23 eV for dissociation from the *hcp* position at a coverage of 0.25 ML, *i.e*. CO adsorbed in a (2×2) elementary cell of Ru{0001}.[75] As in the case of Co{0001}, the desorption barrier of CO from Ru{0001} is much lower than the dissociation barrier (1.76 eV *vs*. 2.23 eV according to Inderwildi *et al*.[75]) implying again that CO

** Meanwhile, more recent research suggests that the actually active phase is either ruthenium oxide or a ruthenium surface oxide.[187]

should desorb rather than dissociate. These findings provide a highly likely explanation for CO TPD spectra by Yates and co-workers, who observe a peak for recombinative CO desorption in the case of a stepped Ru{109} surface, while this peak is clearly not visible in a CO TPD from Ru{0001}.[182] Inderwildi *et al.*,[75] however, suggest a radically new reaction mechanism *via* a formyl species, analogous to the new mechanism suggested in the case of hydrocarbon oxidation (and that described in the previous section on cobalt). In this pathway, H attacks CO and has to overcome a barrier of 0.99 eV in order to form CHO (formyl), and a further barrier of 0.76 eV for the decomposition to CH and O (Fig. 6). This route is clearly favourable in view of the very high barrier towards CO dissociation of 2.23 eV.

These results strongly suggest that, on this facet at least, the reaction will definitely proceed *via* the formyl pathway rather than *via* the carbide mechanism. TPD spectra of a H–CO co-adsorption system would be highly valuable, but are not, to our knowledge, available in the literature at present. The DFT results by Inderwildi *et al.*, nonetheless strongly suggest that formyl formation and reaction should be included into kinetic modelling in order to produce accurate results. Apart from dissociation on Ru{0001}, the study by Ciobica and van Santen[205] also investigated the disproportionation reaction ($2CO \rightarrow C + CO_2$), which is excluded owing to a very high barrier, the hydrogen-assisted dissociation *via* CHO and dissociation at steps. The latter case will be discussed in detail in the following section.[205]

It should be noted that Morgan *et al.* had already considered the possibility of a formyl intermediate in the Fischer–Tropsch synthesis in 2004; they studied CHO adsorbed in various conformations *via* the C and O atom,[207] analogously to the recent study by Inderwildi *et al.*,[75] but concluded the species will readily dissociate to CO and H owing to rather low activation barriers for the C–H cleavage (0.18–0.32 eV).[207] The present authors do not agree with this view, since although the dissociation barrier for the C–O bond is 0.76 eV, this reaction is highly exothermic (−0.85 eV). Hence this reaction is considerably more exothermic than the C–H cleavage, and under conditions where the first barrier of 0.99 eV can be overcome, C–O cleavage will be a rather fast net process, especially because it is thermochemically favoured. Moreover, CO adsorbs rapidly under FT conditions pushing the equilibrium towards the product side. Another supporting effect might be the hydrogenation of oxygen to water and its subsequent desorption which might also pull the equilibrium to the product side. Detailed kinetic models will shed more light onto the dynamic interplay of surface processes. Nevertheless, we agree with Morgan *et al.* that CHO will not be readily observable on Ru{0001} at any temperature, due to its extremely short life time. In order to create a meaningful kinetic model, however, many more reactions have to be studied and their activation barriers have to be determined.

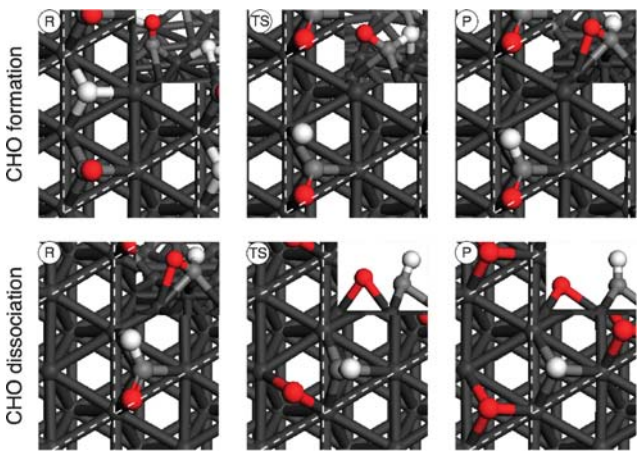

Fig. 6 Hydrogenation of CO on Ru{0001} to $CHO_{(s)}$ (top panel) and the subsequent dissociation of $CHO_{(s)}$ to $CH_{(s)}$ and $O_{(s)}$ (bottom panel). Reprinted from ref. 75, Copyright Wiley-VCH Verlag GmbH & Co. KGaA. Reproduced with permission.

In a further study, Ciobica *et al.* investigated the adsorption of hydrogen, carbon and C_1 fragments on Ru{0001}; in all cases the threefold hollow positions are favoured.[202] From estimating diffusion barriers, the authors conclude that, under Fischer–Tropsch conditions, all these species should be highly mobile. Moreover, methylidyne (CH) is found to be by far the most stable species, which is in accordance with experimental results by Wu and Goodman[208] and a similar DFT study by Liu and Hu.[209] This is also a good analogy to the close-packed {111} surfaces of many metals used for catalytic combustion of hydrocarbons (see above). C–H cleavage is therefore exothermic in all cases (*i.e.* for CH_4, CH_3 and CH_2) except for the most stable methylidyne species.[202] Mortensen *et al.* subsequently studied associative methane desorption and dissociative adsorption using molecular beams experiments[210] and compared their results to DFT results by Ciobica *et al.*,[201] finding excellent agreement. The associative desorption, as studied with LAAD is also in excellent agreement with the DFT results of Ciobica *et al.*[201] Ge *et al.* also studied the C_1 hydrocarbon fragments on Ru{0001}[173] and find methylidyne (CH) to be the most strongly adsorbed species, the preferred adsorption site being the *hcp* hollow site,[173] which is in accordance with prior studies by Ciobica *et al.*,[202] and analogous to the analogue cobalt surface. They also studied methylene (CH_2), which one might intuitively expect to adsorb in the bridged position, owing to the tetrahedral geometry the CH_2 species can adopt there, but their results suggest that again the *hcp* hollow site is the most favourable location.[173] Thus Ru, like Co, Rh and Ni, fails to conform to the "completion of tetravalency" rule of thumb.

An important C_2 hydrocarbon species is the vinyl species ($CHCH_2$), which is assumed to be an essential intermediate in the hydrocarbon polymerization process.[176] Ciobica *et al.* determined vinyl to be 0.29 eV more stable than co-adsorbed CH and CH_2.[204] The species has, however, never been unambiguously observed in surface science experiments on Ru{0001},[198,211] although a few experiments with labelled carbon indicate that vinyl might be possible.[212] Moreover, ethylidyne (CH_3CH) was also investigated by Ciobica *et al.*,[204] this species being 0.1 eV less stable than vinyl (with respect to the gas-phase molecules).[204] Ethyl (CH_2CH_3) adsorbs preferentially in the atop position, ethylene ($(CH_2)_2$) adsorbs on the bridged site, acetylene is located with its carbon atoms in two adjacent threefold positions and vinylidene (CCH_2) is

located with its less saturated carbon atom in a single hollow position according to Ciobica *et al.*[204]

Going to longer chained hydrocarbon species, the same authors also studied several C_3 species, starting with 1-propenyl ($CH_3(CH)_2$), which is formed by coupling methylmethylidyne (CH_3CH) and methylidyne (CH) and is 0.55 eV more stable than the co-adsorption system. No structural details are reported, although hydrogenation of this species has been discussed (see below). C_3 species on Ru are really not that thoroughly studied, any species with longer chain length not at all.

Liu and Hu determined the activation barriers for hydrogenation of the different C_1 species on Ru{0001}. The barrier towards the hydrogenation of carbon to methylidyne ($C + H \rightarrow CH$) is 0.7 eV and this process is slightly exothermic according to those calculations.[209] This step is the only exothermic step in the hydrogenation of carbon to methane. The subsequent hydrogenation of methylidyne to methylene ($CH + H \rightarrow CH_2$) has a barrier of 0.5 eV and is markedly endothermic. The hydrogenation of methylene to methyl ($CH_2 + H \rightarrow CH_3$) is thermoneutral and has a reaction barrier of 0.7 eV. The last step in the hydrogenation sequence, the hydrogenation of methyl to gas-phase methane ($CH_3 + H \rightarrow CH_4$) has a rather high barrier of 0.9 eV and is again endothermic. These barriers are all rather lower than for the C–C coupling reaction (see below) indicating that they are not in themselves rate-determining in the FT synthesis.

The vinyl species ($CH–CH_2$) can be hydrogenated to ethylidene ($CHCH_3$), the activation barrier for this step being negligible and the transition state very early according to Ciobica *et al.*[204] The main energy barrier that has to be overcome is actually included in forming the initial state of the reaction (*i.e.* H and $CHCH_2$ sharing a surface atom). The structure of the vinyl intermediate scarcely changes as the hydrogen atom approaches from the *fcc* hollow site; in the transition state it is bound to the atop position of the Ru atom to which the CH_2 group of vinyl is also bound. The hydrogenation reaction is endothermic with an energy of 0.25 eV. Hydrogenation of ethylidene ($CHCH_3$) to form ethyl (CH_2CH_3) can be achieved by inserting a further hydrogen atom into a Ru–C bond. This reaction has a relatively high activation barrier of 0.79 eV, and correspondingly a rather late transition state. Liu and Hu studied the hydrogenation of CCH to CCH_2 which has a barrier of roughly 0.8 eV, the subsequent hydrogenation of CCH_2 to CCH_3 has a barrier of approximately 1.0 eV.[209]

The 1-propenyl ($CH_3(CH)_2$) species can be hydrogenated to form propylidene (CH_3CH_2CH); in this reaction a activation barrier of 0.26 eV has to be overcome. As for the analogue vinyl species, the rather low activation barrier has an early transition state, the structure of propenyl hardly changes in the course of the reaction. The formed propylidene species can subsequently be hydrogenated to form surface propyl ($CH_3(CH_2)_2$), the activation energy for this step is 0.74 eV. A rather late transition state is associated with this rather high barrier.

Regarding the C–C coupling reaction, Ge *et al.* studied the reactions of CH and CH_2 to form vinyl ($CHCH_2$). The process is, however, endothermic in contrast to the equivalent cobalt surface on which it is exothermic.[173] The barrier is, at 1.20 eV, considerably higher than on Co{0001} (0.58 eV), suggesting a different pathway in the case of ruthenium. Liu and Hu confirm those results by determining the barrier to be 1.23 eV.[209] In this study, however, all other C_1 coupling reactions are considered; the lowest barrier (0.87 eV) is associated with a coupling reaction of two methylidyne species leading to an adsorbed ethyne species (CHCH).[209] Reaction of methylene with methyl to form surface ethyl ($CH_2 + CH_3 \rightarrow CH_2CH_3$), which is often considered to be the first polymerisation step, has an extraordinary barrier of 1.80 eV on Ru{0001}. Therefore, hydrogenation of the surface ethynyl species ($CCH + 4H \rightarrow CH_2CH_3$) is, according to the results presented by Liu and Hu,[209] a more viable route.

Van Santen, Neurock and co-workers also studied the chain growth on Ru{0001}:[204] They conclude, based on their DFT results, that CO dissociates, is partially hydrogenated, and will thereafter enter a C–C coupling cycle. They distinguish two different coupling cycles: in the first mechanism the resting state is alkylidene-like (*i.e.* an R–CH species), while in the second mechanism it is alkyl-like (*i.e.* an $R–CH_2$ species). Both catalytic cycles are given in Fig. 7. In both mechanisms the methylidyne species serves as building block for the hydrocarbon polymerization, which is in accordance with the results presented by Liu and Hu.[209] In mechanism 1 the β-carbon (which is indeed a secondary carbon atom) is hydrogenated leading to $R–CH_2–CH$, while in mechanism 2 the α-carbon (the primary carbon), *i.e.* the carbon that is bound to the surface is hydrogenated; herein we will refer to this latter mechanism as the alkyl cycle, and the former as the alkylidene cycle. In both mechanisms the starting species is prolonged by one methylene group during a full catalytic cycle, but this occurs *via* reaction with CH and subsequent hydrogenation, rather than by direct addition of CH_2. Both catalytic cycles have an $R–CH_2–CH$ species in common which couples both catalytic cycles and it would be possible that both catalytic cycles compete and that the predominant formation pathway varies with the conditions of the reaction.

Ciobica *et al.* implicitly assume that since CO dissociation is possible on Ru{0001}, the Fischer–Tropsch synthesis will proceed *via* the carbide mechanism and exclude from their calculations reactions such as the CO insertion mechanism or direct hydrogenation of CO.[204] We, however, think that CO dissociation is not possible on Ru{0001} since the adsorption barrier is lower than the dissociation barrier (the fact that DFT drastically overestimates the adsorption energies further supports this). Also TPD spectra of CO on Ru{0001} give no indication of CO dissociation.

In order to verify these hypothetical catalytic cycles, they were investigated by Ciobica *et al.*[204] in a comprehensive study. The mobility of the growing chain intermediate on the surface is thought to be higher than that for the CH building block, since CH is so strongly adsorbed. In the alkyl cycle, the first coupled intermediate adsorbs on the surface *via* a single carbon atom. In the alkylidene cycle, in contrast, the product of the carbon–carbon coupling reaction is bound *via* two carbons in a chelate-type manner with the surface. The activation barriers for the C–C coupling reactions are rather high in the case of the alkylidene cycle: the reaction of methylidyne (CH) and

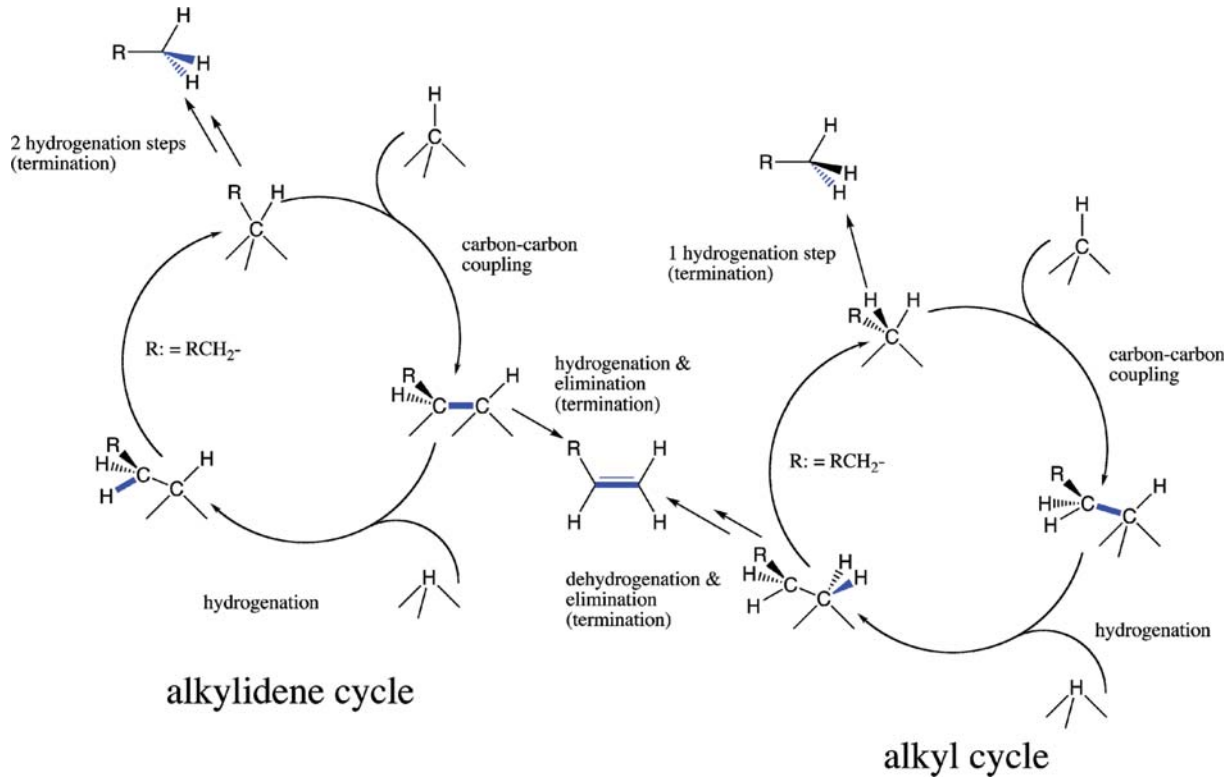

Fig. 7 Mechanism for the chain growth of hydrocarbons, adapted from the schemes presented in the work of Ciobica *et al.*[204] Formed bonds in the growth cycle are depicted in blue, dangling bonds indicate atop, twofold and threefold adsorption sites.

methylene (CH_2) to vinyl ($CHCH_2$) requires 0.74 eV; the reaction of ethylidyne ($CHCH_3$) and methylidyne (CH) to form propylene ($CHCHCH_3$) requires 0.63 eV.

In the case of the alkyl cycle, the activation barriers are considerably lower, most likely due to the labile, reactive nature of this species. The coupling of methyl (CH_3) and methylidyne (CH) to form ethylidene ($CHCH_3$) merely requires 0.05 eV and can hence be considered almost non-activated. The coupling of ethyl (CH_2CH_3) and methylidyne (CH) to form propylidene ($CHCH_2CH_3$) has to be activated by 0.23 eV. Hence, the C–C coupling reactions are with 0.05 eV and 0.23 eV kinetically the much more likely pathway as opposed to the methylidyne cycle in which barriers of 0.74 and 0.63 eV must be overcome. Moreover, these barriers are much lower than the barriers for the hydrogenation of CH_2 to CH_4 (0.7 and 0.9 eV), as determined by Liu and Hu,[209] which gives a potential explanation for the selectivity of Ru towards higher hydrocarbons with a low amount of methane. Moreover, it is noteworthy that in mechanism 1 the rate-determining step is a C–C coupling reaction, while in mechanism 2 it is a hydrogenation reaction.

Termination of the chain can either occur by hydrogenation up to saturation forming an alkane, or by elimination forming an alkene. Another possibility (that probably has a much higher activation barrier) is the recombination of two surface alkyl chains to form an alkane, which has not yet been studied.

Stepped ruthenium surfaces: {101$\bar{9}$}, corrugated {0001}. There are, as in the case of cobalt, considerably less studies on stepped than on flat ruthenium surfaces available: Yates and co-workers observed the formation of a $(\sqrt{3} \times \sqrt{3})$ CO superstructure on the terraces of Ru{101$\bar{9}$} in LEED, but noted that CO was found to dissociate at the step sites.[207,213] Moreover, the authors note that this surface reconstructs to form wide {0001} terraces and double height {101$\bar{1}$} steps. The involvement of the step sites in the CO dissociation process was demonstrated by poisoning them with carbon. Compared to the stability of CO on Ru{0001}, the activity of Ru{101$\bar{9}$} observed in this study already indicated that steps might actually be the active phase for CO dissociation. In a subsequent study, this assumption was confirmed;[182] the authors note that in TPD spectra from Ru{101$\bar{9}$}, a high temperature CO peak evolves at around 520 K. The authors attribute this to recombinative CO desorption from the step sites. In TPD spectra from CO on Ru{0001}, this peak is not present, which indicates that CO stays intact on this facet.[182]

Ciobica and van Santen performed DFT calculations for the adsorption of CO on an artificially-corrugated model of a stepped Ru{0001} surface,[205] quite unlike Ru{101$\bar{9}$}. They conclude that the geometry of CO adsorbed atop on the step edge is not different from atop CO on flat surfaces, while the geometry of CO adsorbed at the *hcp* hollow site on the step edge and at the bottom edge of the step is only slightly different from that found on the planar Ru{0001} surface.[203] Subsequently, Ciobica and van Santen studied the dissociation of CO on this surface and find that the lowest energy reaction path for CO dissociation proceeds through adsorption at the bottom of the step followed by the O atom jumping up onto the next terrace.[205] The barrier for this reaction is only 0.89 eV, as compared to around 2.2 eV on the flat Ru{0001} surface.[75,205] Hence, the activation barrier for dissociation is below the

desorption barrier in the case of corrugated Ru, while it is the other way around on flat Ru{0001}. These DFT results give thus a reasonable explanation for the lack of a recombination peak in TPD spectra from Ru{0001},[182,213] and are consistent with the interpretation that step sites have potential for dissociation. Inderwildi *et al*., however, found the barrier for hydrogenation on flat Ru(0001} to be 0.99 eV, analogously to the cobalt surface, making this reaction competitive,[75] and hence steps may not be necessary for activity when hydrogen is added to the system. It still has to be confirmed how high the barrier for hydrogenation is at steps, in order to determine which pathway will be the main reaction route in a realistic system.

Cheng *et al*. performed DFT calculations on the C–C coupling mechanism on a corrugated Ru{0001}[214] surface, analogous to the previous study on corrugated Co{0001} by Gong *et al*.[174] These calculations reveal that the initial state and transition state structures on the stepped Ru surface are very similar to those on stepped Co.

The lowest C–C coupling barrier found by Cheng *et al*. is for the association of two methylene species (CH_2), which is activated by 0.92 eV. Competitive, but higher, barriers were found for the reaction of methyl (CH_3) with CH_2 (1.17 eV) and atomic carbon (C) with CH_2 (1.13 eV).[214] Even though the structures are very similar to those found on cobalt, the energetics of the reactions are very different. For instance, the coupling of CH_3 to CH_2, and of CH_2 to CH_2, both have lower barriers on the stepped cobalt surface (0.76 eV and 0.27 eV, respectively), while the coupling of C to CH_2 is more likely on Ru than on Co (1.36 eV as opposed to 1.13 eV). The lowest energy pathway for C_1 coupling, however, remains the reaction of two methylene (CH_2) species on *both* surfaces. Based on a kinetic model, however, Cheng *et al*. assume that the main reaction route for the formation of C_2 species differs. Including not only the activation barriers of the reaction, but also the stability of the reactant structure (*i.e*. the absolute stability of the transition state), leads them to the conclusion that the main reaction pathway on Co is *via* coupling of two methylene species (CH_2) and the reaction of methyl (CH_3) with atomic carbon (C), while on Ru the coupling will mainly occur *via* association of atomic carbon (C) and methylidyne (CH) as well as methylidyne with methylidyne.[214]

The kinetic model of Cheng *et al*., however, excludes back-reaction (*i.e*. C–C bond scission), which we believe might lead to a considerable error. Nevertheless, the kinetic model proposed is definitely an important first step towards a fully computational description of the Fischer–Tropsch process on these metals.

Despite the considerable number of experimental and theoretical studies available on various Ru surfaces, essential questions remain unanswered: are the steps only more active in the CO dissociation or are they also more active in the hydrogenation of atomic carbon? Moreover, is the hydrogenation of CO also the lowest energy pathway for CO conversion? Only when these questions have been answered can it be determined which reaction pathway is the main route to liquid hydrocarbons on realistic ruthenium catalysts.

4.3 Iron

Flat iron surfaces: Fe{110}. According to the definition given by Pratt and Jenkins, the only really flat surface of a *bcc* metal is the {110} facet.[52] Jiang and Carter studied the adsorption and diffusion energetics of hydrogen on this facet of iron utilising a PAW setup.[215] At all coverages studied, atomic hydrogen is most stable in the (quasi) threefold position in agreement with experimental studies.[216] Bridge sites are found to be transition states for H diffusion,[215] which results in a low-energy zig-zag diffusion path for H atoms along either the [001] or [1$\bar{1}$0] directions on Fe{110} with an associated diffusion barrier of below 0.2 eV; for more detail, the reader is referred to the original publication.[215] In a subsequent study, the same authors employed DFT-GGA calculations to characterise CO adsorption on Fe{110}.[217] CO is found to preferentially adsorb atop on Fe{110}; at lower coverage (0.25 ML) the molecule adsorbs upright, while at higher coverage it adsorbs tilted at an angle of around 13° due to steric effects. These results reproduce experimental findings very well.[218]

In addition to adsorption, Jiang and Carter also studied the dissociation of CO on Fe{110} at 0.25 ML.[217] Even though CO is most stable in the atop site, dissociation from this site is rather unlikely, since stabilization of the transition state is facile, owing to low coordination.[217] The authors found that CO moves off the atop site into a tilted precursor state prior to dissociation, reorients itself towards the surface, and then passes through a transition state in which CO lies almost flat on the short-bridge site of Fe{110}.[217] They determined the reaction to be endothermic with 0.5 eV, and the activation barrier to be 1.52 eV. After dissociation the atomic products reside in threefold sites. The barrier of 1.52 eV is lower than the calculated desorption energy in this site (1.95 eV), but considerably higher than the experimentally determined desorption energy, 1.24 eV.[219] The discrepancy between theoretical and experimental adsorption energies is, as usual, most likely due to the known over-estimation of adsorption energies in DFT studies.

A further study by Jiang and Carter concerned itself with the fate of carbon adatoms after their generation by CO dissociation on Fe{110}; they find that carbon atoms are strongly bound to Fe{110}, and are accommodated in the long-bridge position.[220] The carbon atom is, however, slightly less strongly bound to flat Fe{110} than to the kinked Fe{100} surface. Diffusion of carbon atoms into the Fe{110} subsurface can occur *via* a fourfold coordinated transition state; the barrier for this subsurface diffusion was found to be 1.18 eV[220] and has hence a lower barrier than the antecedent dissociation (1.52 eV).[217] This implies that at temperatures at which CO dissociates, subsurface migration of carbon is to be expected on this facet.

In a subsequent study, Sorescu has extended this investigation of C_1 species chemisorption on Fe{110}.[221] He determined that CH_x (x = 0–2) species preferentially adsorb at the fourfold sites, while the CH_3 species prefers binding at the bridge site. Methane is only weakly physisorbed. The presence of atomic carbon at either a hollow or a subsurface site was found to increase the stability of all other adsorbates (C, H, O, CO, CH_x (x = 1–4)) adsorbed on the surface.[221] Sorescu also studied the minimum-energy pathway for the hydrogenation of atomic carbon (C) to gas-phase methane (CH_4) on Fe{110}. The hydrogenation of carbon to methane is a four step process ($C \rightarrow CH \rightarrow CH_2 \rightarrow CH_3 \rightarrow CH_{4(g)}$); the first three steps (*i.e*. the formation of adsorbed methyl) are all found to be endothermic; the hydrogenation of CH_3 to gas-phase methane,

however, was determined to be exothermic. The largest activation energy (corresponding to the rate-determining step in this subset of the reaction mechanism) was found to be the hydrogenation of methylene (CH_2) to methyl (CH_3), with an activation energy of 0.85 eV. The overall rate-determining step in the hydrogenation of CO is, however, the dissociation of CO, with an activation energy of 1.05 eV. From this DFT study it can be concluded that on iron the dissociation of CO is the rate-determining step, while hydrogenation reactions are relatively fast. To our knowledge, no studies of C_2 species or higher are available at the moment, hence little can be said about the hydrocarbon polymerisation on flat Fe{110}. This process has, however, been studied on the kinked Fe{100} surface, which we discuss below.

Stepped iron surfaces: Fe{211}. Before discussing kinked iron surfaces, including Fe{111} and Fe{100}, we note that only one true stepped iron surface has thus far been studied in relation to FT synthesis, namely Fe{211}. Borthwick *et al.*[239] determine six stable adsorption sites for CO on Fe{211} at 0.5 ML. On this rather open surface, CO can either absorb on the first or the second layer of metal atoms. The most favourable adsorption site, with a PW91 adsorption energy of 2.41 eV, was found to be the threefold hollow position on the step, on which the CO bond is strongly tilted at 38° from the vertical. Other less stable sites include bridged positions on the step and on the second layer, the least stable adsorption sites being the atop positions on the first and second layers. Recalculation of the adsorption energies with the RPBE functional leads, as expected, to lower values; the most stable threefold hollow site has, for instance, an adsorption energy of 1.92 eV in RPBE as opposed to 2.41 eV according to the PW91 calculations. Interestingly, in the case of CO on Fe{211}, the first-layer atop site, which is according to the PW91 results one of the least stable adsorption sites, is the second most stable site according to the RPBE calculations; the tilted threefold hollow site, however, remains the most stable site according to the RPBE calculations. Borthwick *et al.* then studied the dissociation of CO starting from this hollow position. The transition state was found at a C–O bond distance of 1.83 Å, with an energy 0.78 eV higher than the reactant structure in PW91 and 0.93 eV in RPBE. Both values are considerably lower than the desorption energy, rendering this surface facet well-suited for CO dissociation. Borthwick *et al.* believe the reason for this low activation barrier to be the highly tilted initial state of CO on Fe{211}, which is very similar to (i) the CHO species on Co{0001}, Ru{0001}, Rh{111}, Pd{111} and Pt{111} in which the carbonyl species is also tilted, *vide supra*; (ii) the precursor state of the dissociation on Fe{110}, see foregoing sub-section; and (iii) the initial state for dissociation on kinked iron surfaces, *vide infra*.

To our knowledge, however, no DFT calculations of hydrogenation or C–C coupling reactions are available for Fe{211} in the literature at present, and hence it is difficult to predict the overall activity of this facet for Fischer–Tropsch synthesis based on DFT calculations.

Kinked iron surfaces: Fe{100}, Fe{310}, Fe{111}. Sorescu studied the adsorption of hydrogen on Fe{100},[222] finding that adsorption takes place dissociatively and that atomic H adsorbs at both bridge and fourfold hollow sites only, with a slight preference for the fourfold site at lower coverage and a clear preference for the fourfold site at higher coverage. Furthermore, minimum energy pathways for the surface diffusion of atomic H between several local minima indicated that hydrogen is very mobile owing to rather low diffusion barriers (0.08 eV). Barriers for subsurface diffusion are slightly higher at approximately 0.4 eV. Absorption of H in the bulk of *bcc* Fe is overall endothermic relative to molecular gas-phase hydrogen, and takes place at tetrahedral sites. The most favourable diffusion pathway between tetrahedral sites was found to traverse through trigonal sites with an activation barrier of 0.05 eV.[222]

Sorescu *et al.* studied the adsorption, diffusion and dissociation of CO molecules on the Fe{100} surface.[223] Several possible adsorption configurations are considered in this study and the most stable configuration is determined to be a fourfold state in which the CO molecule is tilted relative to the surface normal by 50°,[223] as found also in a later study by Bromfield *et al.*[224] Adsorption in atop and twofold positions is found to be slightly less stable, the relative stability being $E_{(\text{fourfold})} > E_{(\text{bridged})} \approx E_{(\text{atop})}$ at lower surface coverage, and $E_{(\text{fourfold})} > E_{(\text{atop})} > E_{(\text{bridged})}$ at higher coverage. In the work by Sorescu *et al.*, geometries and adsorption heats calculated using the PW91 functional were compared to RPBE calculations. The geometries derived from RPBE calculations are essentially the same as for PW91, while the RPBE adsorption energies calculated are 6–10% lower than those calculated with the PW91 functional. Results from both sets of pseudopotential calculations (*i.e.* Sorescu *et al.*[223] and Bromfield *et al.*[224]) compare well with the more precise but more expensive all-electron FP-LAPW calculations reported by Blaha and co-workers.[225] All theoretical studies overestimate the experimentally determined heat of adsorption of CO on Fe{100} significantly, by more than 100%.[226]

Diffusion barriers for CO on Fe{100} are found to be rather small (<0.1 eV) indicating that CO is rather mobile on this facet of iron. One exception is, according to Sorescu *et al.*,[223] the diffusion out of the global minimum (the fourfold hollow site) where the barrier was predicted to be around 0.6 eV. Bromfield *et al.* also studied the adsorption of CO on Fe{100} and characterised the transition-state structures for CO dissociation at different coverages.[224] They calculated the activation energy of dissociation for CO to be 1.11 eV at 0.25 ML and to be 1.18 eV at 0.5 ML, whereas the desorption energy of the CO molecule is 2.54 eV and 2.41 eV for coverages of 0.25 ML and 0.5 ML, respectively. Hence, as in the case of the stepped surface, the activation barrier for dissociation is lower than the barrier for desorption on this kinked surface, additionally indicating that the carbide mechanism is indeed the most plausible reaction route for the Fischer–Tropsch process on iron. The dissociation reaction is exothermic at 0.25 ML, while it is endothermic at 0.5 ML. Consequently, molecular adsorption is stabilized with respect to dissociation when the CO coverage is increased from 0.25 ML to 0.5 ML.

Sorescu *et al.* also studied the dissociation of CO from the fourfold site[223] (as suggested by experiment[226]) and calculated the barrier to be between 1.05 eV and 1.21 eV for coverages of

0.25 ML and 0.5 ML, supporting the experimental observation that dissociation of CO bound to the surface seems to compete with CO desorption at 440 K.[227] The activation barriers reported by Sorescu *et al.*[223] are therefore in agreement with the values reported by Bromfield *et al.*,[224] which are derived from a very similar setup using a slightly lower energy cutoff (400 eV as opposed to 495 eV). Very recent results by Lo and Ziegler (using almost exactly the same setup as Bromfield *et al.*[224]) confirm the barrier of 1.1 eV at 0.25 ML coverage and determine the reaction to be exothermic; the dissociation at 0.5 ML is, however, according to Lo and Ziegler, slightly lower than at 0.25 ML[228] in contrast to the previous studies.[223,224] The difference between this and the previous studies is that the coverage was varied by changing the number of adsorbates per elementary cell, rather than changing the size of the elementary cell.

Curulla-Ferre *et al.* studied the effect of sulfur—a well-known catalyst poison—on CO dissociation over Fe{100}.[229] They conclude that the binding of CO is considerably weakened by the presence of co-adsorbed S. The relative difference between calculated adsorption energies for CO at 0.5 ML in the presence and the absence of S is in good agreement with the experimental TPD data reported by Moon *et al.*[226] The activation energy for CO dissociation is calculated as 1.29 eV in the presence of sulfur, and hence 0.15 eV larger than on the sulfur-free surface. More importantly, the presence of sulfur changes the thermochemistry from exothermic (without S) to endothermic (with S). Moreover, in the case of the non-precovered surface, O adatoms formed by dissociation of CO can diffuse into a much more stable position, leading to a 0.82 eV more stable adsorption geometry, while in the case of the precovered surface this diffusion process is essentially thermoneutral. Consequently, the overall reaction energy is −1.14 eV on the clean surface, whereas on the S precovered surface it is +0.32 eV, which makes the reaction thermochemically unlikely in the presence of sulfur.

Lo and Ziegler have recently investigated the production of methane from CO and H_2 on a clean Fe{100} surface using periodic DFT calculations in conjunction with kinetic modelling.[228] They calculate the optimal geometries for atomic carbon and for the methane fragments, and subsequently determine the activation barriers for the hydrogenation (dissociation) process. Methylidyne (CH) is found to be the most stable species on the Fe{100} surface, in analogy to many surfaces of the platinum group metals and cobalt, *vide supra*.

This study also investigated the hydrogenation of atomic carbon to methane (C + H → CH) on the {100} facet of iron. The barriers are rather similar: hydrogenation of atomic carbon requires 0.62 eV, hydrogenation of methylidyne (CH + H → CH_2) requires 0.63 eV and hydrogenation of methylene (CH_2 + H → CH_3) requires 0.80 eV. While the formation of methylidyne (CH) is exothermic, the hydrogenation of methylidyne (CH) to methylene (CH_2) is endothermic, as is the hydrogenation of methylene (CH_2) to methyl (CH_3). The very last step, the methane formation, has a rather lower energy barrier of 0.47 eV, and is exothermic with a reaction energy of −0.58 eV.[228] The rate-determining step on this facet of iron will definitely be the dissociation of CO, *vide supra*.

Based on this reaction mechanism determined by DFT, Lo and Ziegler set up a kinetic model of the methanation, which further confirms that CH is the predominant C_1 species on the surface. The production of CH_4 was found to be more favoured at a high reaction temperature and H_2 partial pressure, but suppressed by a high pressure of CO, due to self-poisoning of the reaction. These results further support the assumption that the carbide mechanism might indeed be the correct mechanism in the case of iron, while on the other FT-active metals alternative pathways have to be considered.

Lo and Ziegler also studied different C_2 species and their formation from atomic carbon and methane fragments on Fe{100}.[230] Their calculations demonstrated that the most favourable C_2 species are those containing the acetylenic carbon (*i.e.*, C–CH, C–CH_2, and C–CH_3). In order to determine which C–C coupling reaction is responsible for the chain propagation, the authors studied various possible reactions. The reaction barrier for the coupling of two atomic carbon adsorbates to C_2 was determined to be 2.16 eV, whereas the reaction of atomic carbon and methyl (C + CH_3 → C–CH_3) has a barrier of only 0.86 eV.[230] This rather large difference is entirely anticipated, because CH_3 is much more labile on the surface, which facilitates its migration towards the surface carbide species. The barriers for recombination of CH and CH_2 with C are slightly higher at 1.26 eV and 0.85 eV, respectively. Moreover, the authors determine the recombination of two carbide species to be endothermic, while the coupling reactions to yield C–CH, C–CH_2, and C–CH_3 are much more feasible; these C_2 species are, respectively 0.15 eV, 0.22 eV, and 0.23 eV more stable than the corresponding C_1 reactants.[230]

Coupling of methylidyne (CH) with other CH_x fragments is thermochemically unfavourable. Formation of ethyne from two methylidyne species (CH + CH → CHCH) has a rather high barrier of 1.42 eV and is endothermic; formation of vinyl ($CHCH_2$)) and ethylidene ($CHCH_3$) from reaction of methylidyne (CH) with methylene (CH_2) or methyl (CH_3) have barriers of 1.17 eV and 0.86 eV, respectively. The formation of ethyl (CH_2CH_3) from methylene (CH_2) and methyl (CH_3) is a slightly endothermic process with an enormous barrier of 2.3 eV, according to Lo and Ziegler,[230] and can hence be ruled out based on this study. The coupling of two methylene species (CH_2) to form chemisorbed ethene (CH_2CH_2) has an activation barrier of 1.5 eV and is considerably endothermic, which leads Lo and Ziegler to the conclusion that this pathway can be ruled out as well. The present authors, however, believe that in a high-pressure process, carried out at elevated temperature, endothermic pathways cannot *a priori* be ruled out, owing to entropic effects.

Lo and Ziegler also determined the minimum energy pathways of the hydrogenation processes that lead to the formation of different C_2H_n species.[230] They assume from their calculations that hydrogenation reactions at both carbon atoms are generally facile, with the reaction barriers varying from 0.4 eV to 0.8 eV. Intramolecular H-shift reactions are rather unlikely, in contrast, since they have activation barriers higher than 2.20 eV.[230]

In a subsequent study, the same authors reported calculations of CO dissociation on the kinked Fe{310} surface.[231] After {100} and {111}, this is the structurally simplest kinked surface facet for a *bcc* material;[52] the kink atoms are quite

closely-spaced (similar to the {100} surface), but nevertheless display the characteristic coordination number of a kinked *bcc* surface, namely four. The authors verified the stability of CO on eleven possible adsorption sites and found that only the hollow adsorption sites on the {100} terraces on Fe{310} are stable.[231] Analogously to the adsorption on Fe{100},[223] the CO atom is tilted from the surface normal by 55°. The molecule can, however, tilt into two different directions, and hence two distinct adsorption geometries can be discretised: in one adsorption geometry, the CO is tilted towards the step (called 4f by Lo and Ziegler[231]), while in the other the CO is tilted towards the adjacent fourfold hollow position (referred to as 4f2 by Lo and Ziegler[231]); the 4f position is determined to be slightly more stable. Due to surface stabilization of the rather unstable Fe{310} facet, induced by CO adsorption, the adsorption energy increases with increasing coverage.[231] Such a situation would suggest islanding behaviour under equilibrium conditions.

Two dissociation channels were investigated for coverages of 0.25 ML and 0.5 ML. At 0.25 ML coverage, CO adsorbed in the fourfold site (4f) on the terrace dissociates with the oxygen atom ending up in the fourfold site on the terrace and the carbon in the threefold site on the step. This pathway resembles the pathway on Fe{110},[217] but its activation barrier is considerably lower at 0.93 eV[231] compared to 1.52 eV.[217] The second pathway, starting from the 4f2 site, resembles the process on Fe{100} and has, with 1.13 eV, a very similar activation barrier to that determined on Fe{100} by Bromfield *et al*.[224] At 0.5 ML coverage, CO molecules occupy alternate hollow adsorption sites, but two different ordered configurations across the stepped Fe{310} are still possible according to Lo and Ziegler[231] as per Fig. 8.

Lo and Ziegler argue that the CO–CO spacing is the same in both structures and hence the structures should be equally stable. The authors therefore chose the zig-zag configuration as starting point for the dissociation of CO at 0.5 ML coverage.

The 4f configuration at hollow sites on the terrace is still the most stable adsorption site at 0.5 ML, and the calculated adsorption energy slightly increases when increasing the surface coverage. Analogously to the coverage of 0.25 ML, only two stable minima are located at 0.5 ML (the 4f and 4f2 sites). The fact that the adsorption energy increases with increasing coverage is noteworthy, since on other kinked surfaces, as for instance Fe{100}, an increase in the surface coverage is marked by a decrease in adsorption energy for all adsorption sites,[224] *vide supra*. Lo and Ziegler subsequently studied the dissociation of CO from 4f and 4f2 configurations on Fe{310}, finding pathways that are essentially equivalent to those at the lower coverage.[231] The first pathway again starts from CO adsorbed in the 4f site, and the O atom is stabilized in the transition state at the twofold position on the step-edge while the C atom migrates towards the hollow site on the step. In this case, the activation barrier is, as expected, higher at the higher coverage of 0.5 ML (0.99 eV as opposed to 0.93 eV at 0.25 ML), but still lower than the barrier on the Fe{100} surface (1.13 eV).[224] The reaction is thermoneutral at 0.5 ML as opposed to 0.18 eV exothermic at 0.25 ML, which is most likely due to bonding competition.[231]

The second pathway involves dissociation of CO from the 4f2 adsorption site on the {100} terrace. In this pathway, the CO molecule dissociates from a tilted geometry and the O atom diffuses to an adjacent 4f2 site, which is identical to the dissociation pathway on Fe{100}. The activation barriers for this process on {100} and {310} are equal (1.13 eV) and hence are almost 0.2 eV higher than the dissociation barrier from the 4f position, which makes the first pathway much more likely. Just as for the adsorption energies, the surface coverage dependence of the activation energies is also noteworthy: in the case of a low-index surface such as Fe{100},[224] the activation barrier increases with increasing surface coverage, as one would *a priori* expect. Lo and Ziegler's study on Fe{310} shows the reverse effect.[231] The activation energy for the first pathway increases slightly, while in the case of the second pathway the barrier is significantly reduced as the surface coverage is increased from 0.25 ML to 0.5 ML. Lo and Ziegler attribute the smaller barriers on Fe{310} (compared to those on Fe{100}) to the lower surface density of the higher-index surface and the increased energy gain by surface relaxation during CO dissociation.[231] The substantial reduction of the dissociation barrier for the second pathway may, according to the authors, be attributed to a better stabilisation of the

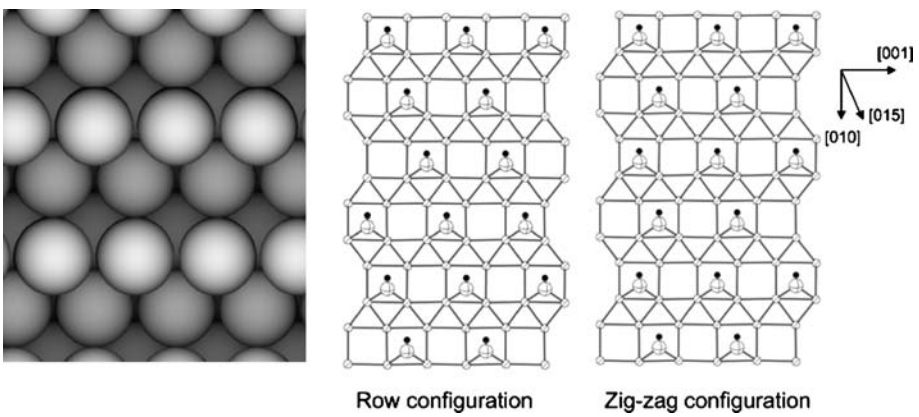

Fig. 8 The Fe{310} surface (left) and the different CO adsorption overlayers taken from Lo and Ziegler[231] (right). We note that the directions indicated are projections onto the (100) plane, not vectors lying within the macroscopic surface plane.

oxygen atom in the transition state structure. Once again these DFT calculations suggest that low-coordination sites are more active in the dissociation of CO.

Jiao and co-workers studied the adsorption properties of CO on Fe{111} and showed that both preferred site and binding strength are strongly dependent on the coverage.[232] At 0.33 ML, for instance, the most stable adsorption site is a hollow site (*i.e.* the lowest hollow site on Fe{111}), a bridge-like (or tilted atop) site is 0.20 eV less stable, while other adsorption sites are significantly less stable according to this study.[233] Subsequently, a study on the co-adsorption of CO with hydrogen was published by the same group.[232] At low coverage (*i.e.* one CO and one H per elementary cell) the hollow site is still the preferred adsorption site for CO. With increasing H coverage, however, CO shifts to the atop position on Fe{111}.[232]

In a further study, Jiao and co-workers reported on the dissociation of CO on Fe{111}[234] starting from adsorption sites determined in their earlier work.[232,233] Firstly, they investigated dissociation of CO adsorbed in the bridge-like site and took five probable pathways into account. The energetically most likely pathway on this surface is the one in which C and O end up in high-coordination sites (for the exact structure the interested reader is referred to the original publication[234]); the reaction is exothermic, with an energy of 0.36 eV, and the activation barrier is 1.53 eV, which is considerably lower than the desorption barrier from the bridge-like site (1.88 eV).[234] The authors also note that carbon atoms move into the subsurface region after formation, analogous to the subsurface migration found by Niemantsverdriet and co-workers[235] and in accordance with experimental results.[236]

Secondly, Jiao and co-workers studied dissociation from the most stable hollow site. They found that CO would have to overcome a barrier of 2.71 eV from this position, which is significantly higher than the desorption barrier of 2.08 eV.[234] Diffusion to the slightly less stable bridge-like site, however, is essentially non-activated according to the authors. It is therefore anticipated that a diffusion pre-equilibrium is involved in the dissociation reaction. Inderwildi *et al.* have recently found that also in the case of the nitrogen recombination on Rh{211} the most stable site is not the most reactive site.[237]

In the scope of the studies discussed above, Jiao and co-workers also investigated the co-adsorption of CO with hydrogen and the hydrogen-assisted CO dissociation.[232] They determined co-adsorption structures of CO with hydrogen molecularly or dissociatively adsorbed. As a starting point for the hydrogen-assisted dissociation, the authors chose a co-adsorption structure in which CO is adsorbed in a bridge-like position (due to the low dissociation barrier from this position) and two hydrogen atoms adsorbed in hollow positions.[232] Three plausible paths for CO dissociation in the presence of hydrogen were taken into account: (i) dissociation with H as spectator species (*i.e.* the carbide mechanism); (ii) dissociation to form atomic (C) and hydroxyl (OH); as well as (iii) a two step scenario, in which a surface formyl species (CHO) is formed followed by dissociation into CH and O. Dissociation in the presence of H has a rather high barrier (1.76 eV as opposed to 1.53 eV on the clean surface) due to repulsive interactions of the CO with the coadsorbates. Dissociation to form a surface hydroxyl species (OH) is a process in which the C–O bond is cleaved and an O–H bond formed concertedly, previously suggested by Bianchi and Bennett.[238] According to Jiao and co-workers, this process has an activation barrier of 1.79 eV, rather similar to the barrier for direct dissociation in presence of hydrogen.[232] In the formyl pathway, however, the formation of CHO has to overcome an activation barrier of merely 0.99 eV, and the reaction is only slightly endothermic. Dissociation of the CHO species has an activation barrier of 1.17 eV and is highly exothermic, with a reaction energy of −0.82 eV.

To recap, according to Jiang and Carter's study,[217] CO dissociation on flat Fe{110} starts from CO adsorbed upright in an atop site at 0.25 ML and goes through a transition state in which the molecule is adsorbed side-on; the associated barriers are 1.52 eV (PBE) and 1.83 eV (RPBE). On the more open kinked Fe{100} surface, CO adsorbs in the fourfold hollow site and is already tilted from the surface normal by up to 50°. Owing to this rather large tilt, the interaction of the O atom with the surface is enhanced, and consequently the activation barrier on Fe{100} is considerably lower at 1.05 eV[223] or 1.11 eV[224] in the different studies. Naturally, one would expect the more open kinked Fe{111} surface (the least stable of the low-index iron surfaces) to have an even lower barrier. The calculations of Jiao and co-workers, however, reveal that the C–O bond is more activated on Fe{100} than on Fe{111} (the lowest barrier on Fe{111} being reported as 1.53 eV). Interestingly, the lowest reported barrier of all occurs from Fe{211}, where Borthwick *et al.* claim values of just 0.78 eV (PW91) and 0.93 eV (RPBE).[239] Thus the stepped surface (*i.e.* {211}) is expected to be at least as active as the kinked surfaces (*i.e.* {100}, {111}, {310}), if not more so.

4.4 Nickel

Flat Ni surfaces: {111}, {100}. Ni is the "joker" among the metals discussed within this review, since it is able to combust hydrocarbons and is also able to catalyse the methanation reaction, the formation of methane from different feedstocks. Owing to this "ambiguity", the properties of methane fragments and their reactions on the low-index Ni surfaces were already discussed in the first chapter of this review article. Since microscopic reversibility applies in this instance, we will not discuss again the mechanistic details of the formation of methane fragments and methane. What has, however, still to be understood when trying to elucidate the mechanism of methanation on nickel is the activation of the CO bond, which we will now address.

Remediakis *et al.* studied the adsorption of CO in the presence and the absence of atomic hydrogen on Ni{111}.[240] They found that in a (2 × 2) supercell CO is most stable in the *hcp* threefold position, with an adsorption energy of −1.56 eV and a C–O bond length of 1.20 Å.[240] The *fcc* threefold position is only 0.02 eV less stable, the bridged position is around 0.1 eV less stable, and the atop site is considerably less stable with an adsorption energy of just −1.29 eV.[240] The calculated values are hence in excellent agreement with experimental results (as for instance SCAC measurements by King and

co-workers, which range between 1.35 and 1.55 eV[241]). However, Sholl and co-workers,[242] as well as Bengaard *et al.*,[157] determined CO on Ni{111} to be considerably more strongly adsorbed, with an adsorption energy of around 1.9 eV at the same coverage.

Hydrogen meanwhile adsorbs preferentially in the *fcc* threefold position on Ni{111}, with a dissociative adsorption energy of −0.39 eV per atom relative to hydrogen in the gas phase.[240] The *hcp* threefold position is merely 0.01 eV less stable, making both adsorption sites competitive. These adsorption energies, calculated by Nørskov and co-workers,[240] are in reasonable agreement with experimental isosteric heat obtained by Christmann *et al.*[243] Sholl and Bhatia confirmed these results; also in their study the hollow positions on Ni{111} are the most stable adsorption site, the heat of adsorption is in both cases 0.48 eV,[244] in broad agreement with the previous results.[240] In the study by Sholl and Bhatia, Ni{100} and Ni{110} were also studied, and again the hollow positions are preferred; in the case of Ni{100} the adsorption energy on the fourfold hollow site is 0.54 eV; in the case of Ni{110} the pseudo-threefold position is favoured with an adsorption energy of 0.37 eV.

Morikawa *et al.* determined the lowest activation barrier for CO dissociation on Ni{111} to be 2.80 eV on a fully constrained surface using a DFT-LDA approach for geometrical optimisations, with GGA-corrected energy values.[245] Analogously to other metals, C stays in its adsorption site at the transition state, while O shifts to a bridged position. The experimentally determined activation barrier is much lower,[246] and the authors attribute this discrepancy to the neglect of surface relaxation and spin-polarisation, which was a common simplification at the time of publication. However, later results by Bengaard *et al.* which *include* surface relaxation and spin effects, determine the barrier for CO dissociation to be 3.1 eV from a threefold adsorption site. Desorption from this threefold site is activated by 1.83 eV and hence these results conclude that CO should desorb rather than dissociate on this surface facet.[157] Sholl and co-workers studied the same reaction including spin-polarisation and determined the activation barrier to be 2.96 eV and a desorption energy of 1.9 eV.[148] A very recent DFT study by Andersson *et al.* confirms this extremely high barrier; in this contribution the activation barrier is determined to be 2.85 eV at low CO coverage.[33] The transition state structure of CO dissociation on Ni{111} is very similar to the structures on the {0001} facets of the *hcp* metals Co and Ru.

The adsorption energy reported in these contributions ranges from 1.4 eV to 1.9 eV, while the dissociation barrier is between 2.8 eV and 3.1 eV. Hence, based on the DFT data available at this point, desorption should be significantly faster than dissociation. Andersson *et al.* recently extended a similar observation to Ni{100}, the activation barrier for CO dissociation on this facet varying from 1.87 eV to 2.17 eV when going from low to high coverage, significantly higher than the desorption barrier.[241] In this respect, flat Ni surfaces are very similar to those of both Ru and Co in having much higher theoretical dissociation barriers[148,240,245] than desorption barriers,[243] implying that CO dissociation is not a viable reaction route. Very recently, Wang *et al.* proposed an alternative formyl route analogous to the routes mentioned earlier in this review.[159,160] Such a formyl species was investigated earlier by Nørskov and co-workers in the scope of a formaldehyde synthesis study.[240] They determined the optimal adsorption geometry for HCO and its structural isomers: the adsorption energy for COH (C–O–H) was determined to be −2.07 eV relative to the free formyl radical, compared to −1.79 eV for HCO (*i.e.* H–C–O).[240] Wang *et al.* followed this up in a study on CO_2 reforming on Ni{111};[159] the hydrogenation of CO to CHO has an activation barrier of 1.49 eV as opposed to 3.15 eV for the dissociation of CO (determined within the same study). Moreover, CHO formation is energetically more favourable than the dissociation of CO.

Based on this DFT study, Wang *et al.* propose a simplified mechanism for the reforming of CO_2 to CH_4 on Ni{111}. Firstly, CO_2 is dissociated forming adsorbed CO and O, and CH_4 is sequentially dehydrogenated into methylidyne (CH) and atomic hydrogen (H). Secondly, CH is oxygenated to formyl (CHO), and this oxygenation facilitates the cleavage of the C–H bond. Thirdly, CHO is dissociated into CO and H. Finally, H_2 and CO desorb from the surface. This reaction pathway is entirely in line with the previous one by thermodynamic analyses.[160] The reverse process (the formation of methylidyne from CO) is an endothermic process, with an activation barrier of 1.47 eV. The subsequent cleavage of the CO bond to form methylidyne and oxygen (CHO → CH + O) is activated by 1.31 eV, which makes this route much more likely than the direct dissociation of CO (associated with a barrier of 2.8 eV or more[148,160,240,245]).

On Ni{100}, matters seem to be slightly different. Andersson *et al.* considered formation of a COH species, an alcohol-type species,[33] to be 1.21 eV in the low coverage regime, and 1.29 eV in the high-coverage regime. These barriers are hence also significantly lower than the corresponding CO dissociation barriers of 1.87 eV and 2.17 eV. Moreover, as in the case of formyl formation on Ni{111}, the hydrogenation barriers are lower than the experimentally determined desorption energies, while the dissociation barriers are considerably higher.[241] The reason why Andersson *et al.* believe this will not be the main reaction pathway is the fact that hydrogen coverages on Ni{100} are low at methanation conditions.[33]

Stepped and kinked nickel surfaces: {110}, {211}, {531}, {321}. King and co-workers studied the adsorption of CO on the stepped Ni{211} surface by means of DFT and microcalorimetry experiments.[247] CO initially adsorbs at the bridged position at the step-edge, but adsorption proceeds on terraces at higher coverage. The adsorption energy is moderate, at 2.09 eV (as opposed to 2.38 eV on Pt{211}), and is quite close to calculated adsorption energies at 0.25 ML coverage on the low-index surfaces Ni{111} and Ni{110}.[248] The adsorption energy determined by microcalorimetric measurements, however, is considerably lower at just 1.46 eV,[247] which is in agreement with the general observation that DFT-GGA calculations significantly overestimate the adsorption energies of molecules.[249] Although DFT overestimates the heat of adsorption of CO on Ni{211}, as determined by microcalorimetry, the adsorption energy relative to the analogous Pt surface is in good agreement.[247] Bengaard *et al.* subsequently determined the

adsorption energy of CO on this facet of Ni to be 1.96 eV, which is in accordance with the earlier results by King and co-workers.[247] They also determine the dissociation barrier on this facet of Ni, which is, at 2.07 eV, only slightly higher than the calculated desorption barrier. This could lead to the conclusion that on Ni{211} dissociation and desorption are competitive, in contrast to the low-index surface, *vide supra*. Hence, CO dissociation is, according to this DFT calculation, possible at steps. However, the experimentally determined adsorption energy is considerably lower than the calculated dissociation barrier (1.46 eV *vs*. 2.07 eV), so in this case it seems more likely that CO would desorb rather than dissociate.

Andersson *et al*., in a very recent study, determined the activation barrier to be slightly lower, at 1.94 eV.[33] In this contribution, however, the already mentioned formyl pathway was for the first time investigated at a stepped surface. The activation barrier for the reaction *via* CHO is 1.33 eV at the Ni{211} surface, and consequently this barrier is actually lower than the experimentally determined adsorption energy reported by King and co-workers (1.46 eV).[247] Moreover, Andersson *et al*. also investigated other stepped surfaces such as the Ni{311} surface, on which the oxygen atom of CO is hydrogenated to form COH. This route has also a considerably lower activation barrier than the dissociation of CO (1.24 eV *vs*. 1.66 eV).[33]

These studies can thus explain the ability of steps on Ni surfaces to convert CO in the presence of hydrogen. The work by Andersson *et al*. is, moreover, especially valuable because it, for the first time, illustrates that the hydrogenation of CO has a lower barrier than the dissociation at surface defects.[33]

Sholl and co-workers have studied the dissociation of CO on the kinked Ni{531} surface. As initial state for the mapping of the CO dissociation, they did not choose the most stable site for the CO, but instead the configuration from which CO can dissociate most easily into the most stable adsorption sites for atomic C and O.[148] In the initial state the CO is adsorbed on the terrace at the bottom of the step with the O atom leaning towards the step edge. After dissociation the C atom resides in the same position as before, while O is adsorbed at the step edge. The authors employed a very precise setup for the determination of the transition state and determined it to be merely 0.02 eV higher in energy than the initial state, making the reaction quasi non-activated. The authors furthermore argue that, owing to the similar adsorption energies of CO on Ni{531} and Ni{111}, the difference of approximately 1 eV between activation energies is also the difference in the absolute energy barriers to dissociation. Hence, reaction rates on the two different surfaces would, we believe, differ by approximately nine orders of magnitude at 500 K.

Andersson *et al*., in addition to their work on stepped Ni{211} and Ni{311}, also studied CO dissociation and hydrogenation at the kinked Ni{321} surface.[33] They found a considerably higher barrier for dissociation than for desorption on this surface. In the low-coverage regime, they calculated the dissociation activation barrier to be 1.77 eV, while hydrogenation of CO to COH is activated by merely 1.22 eV. Hence, this study provides further DFT evidence that the hydrogenation route is the actual reaction route at surface defects as well as flat surfaces.

5. Conclusions

In this review, we have summarised results from more than 200 publications concerned with DFT calculations relating to alkane combustion and synthesis on precious metal surfaces. Despite this impressive amount of scientific effort by many authors over several years, and the wide variety of individual processes studied, many essential questions remain incompletely answered to date. Nevertheless, certain general features may be identified, leading towards a view of combustion and synthesis as inverse processes, driven in opposite directions by the particular catalyst involved and the conditions of the reaction. Trends within the periodic table, and between different surface facets, are thus of the utmost importance, and DFT calculations are ideally suited to investigating just these factors. Here we summarise what may be gleaned from existing work, and highlight areas where further study is likely to be rewarded with new insight.

In the case of the Fischer–Tropsch process, CO dissociation has been quite well studied within DFT on both flat and stepped surfaces of Co, Ru, Fe and Ni, and it can be concluded that CO can only dissociate readily at steps and/or kinks, since only here is the desorption barrier higher than the dissociation barrier. An alternative pathway, whereby CO is directly hydrogenated to formyl (CHO), prior to dissociation into methylidyne (CH) and oxygen adatoms (O), has been proposed based on DFT calculations for various of the flat surfaces, where it is found to be dominant over the dissociative route for Co and Ru. On stepped Ni and kinked Fe surfaces, the formyl route has also been found to be competitive with CO dissociation. Hydrogenation of carbon adatoms or of C_1 hydrocarbons has been studied extensively on the flat surfaces of Co, Ru, Fe and Ni, but not as yet on any stepped or kinked surfaces of these metals. It seems to us likely that the dissociative route may well be dominant on Fe surfaces, but that the formyl route would be preferred on the Co, Ru and Ni surfaces. Either way, we anticipate that the rate of CO conversion will be highest at step sites.

Calculations relating to carbon–carbon coupling reactions have been reported in the literature on the flat Co{0001} and Ru{0001} surfaces, and plausible mechanistic cycles have been proposed in which either surface alkylidene (CHR) or surface alkyl (CH_2R) species are progressively augmented by addition of surface methylidyne (CH). Similar reactions have not, however, been so thoroughly investigated on stepped surfaces, which is, of course, precisely where one would expect methylidyne to be created most readily. Only once such studies have been reported will the full picture of chain growth and (equally importantly) chain termination start to emerge.

In the case of alkane combustion, DFT results from various groups suggest that surface methyl (CH_3) should dissociate readily to methylidyne (CH) below the hydrogen desorption temperature on flat Pt, Rh, Pd and Ni surfaces of {111} type; further dissociation to carbon adatoms (C) can be driven only by the entropy of hydrogen desorption at elevated temperatures. On the flat Pd{100} and Ni{100} surfaces, similar calculations suggest full dissociation into carbon adatoms would occur even at moderate temperatures, and we anticipate that the same will be true for Pt{100} and Rh{100}. The

picture on stepped surfaces is rather more mixed, with methylidyne (CH) being favoured on Pt{110}-(1 × 2), and methyl (CH_3) being the favoured surface species on Ni{110}. Calculations on Rh{110} and Pd{110} are currently lacking from the literature, and few other stepped surfaces have been studied in much detail. The principle of fourfold carbon coordination (loosely described as "tetravalency" in the literature) holds rather well for adsorption of methane and its dissociation products on Pt and Pd surfaces, but not on those of Rh or Ni (nor those of Co, Ru or Fe, studied within the context of alkane synthesis). Fewer DFT calculations exist for heavier hydrocarbons on these surfaces, but the "tetravalency" principle holds for ethane dissociation products on Pt{111} and Pt{110}-(1 × 2). In the latter case, thermodynamic analysis predicts ethene (CH_2CH_2) to be the preferred surface species under atmospheric pressure in the temperature range 300–600 K, with ethylidyne (CCH_3) becoming competitive at higher temperature; under typical UHV conditions, by way of contrast, both ethene (CH_2CH_2) and ethylidyne (CCH_3) are predicted to be stable at room temperature, with ethynyl (CCH) becoming more stable in the range 400–600 K. In summary, the carbon-containing surface species will vary depending upon the feedstock (methane, ethane, or other alkanes) but also upon the surface facet and the prevailing conditions of temperature and pressure. It is by no means certain that dissociation will occur all the way to carbon, and indeed some residual hydrogen content appears to be the norm. Thus, combustion at moderate temperatures is likely to be dominated by the oxidation and subsequent dehydrogenation of surface hydrocarbon; oxidation of carbon adatoms is, for most surfaces, a high-temperature pathway only.

Oxidation of methylidyne (CH) to formyl (CHO) has been identified *via* DFT as the most probable main reaction route on the flat {111} surfaces of Pt, Pd, Rh and Ni, together with the stepped {211} surface of Rh. In light of the important role of steps in reaction mechanisms, however, further calculations of this process and the alternative adatom oxidation process on additional stepped and kinked surfaces are urgently required. Furthermore, experimental verification of a formyl intermediate is still awaited. We might also note that alkane oxidation on Pd is very likely to occur on a somewhat oxidised surface, and that calculations relating to adsorption, dissociation and oxidation on the surface oxide might well be more relevant than those on the metallic surface.

One conclusion that can definitely be drawn, based on the DFT results summarised herein, is that both CO and CH have to be activated prior to cleavage; the necessary weakening of the C–O or C–H bond can be achieved in two ways (Fig. 9). In the case of the simple dissociation, the molecule must coordinate its O or H atom to a metal atom, which on the flat surface requires a significant tilt but which is facilitated by the presence of a step or kink. In the cases involving a formyl intermediate, the addition of either H or O weakens the pre-existing C–O or C–H bond and activates it. The effect is twofold in the instance of CO hydrogenation, since the addition of H also induces a strong tilt in the C–O bond and consequent coordination of O to the metal surface. The crucial event in alkane combustion or synthesis is the reaction whereby carbon changes from an oxygenated to a hydrogenated

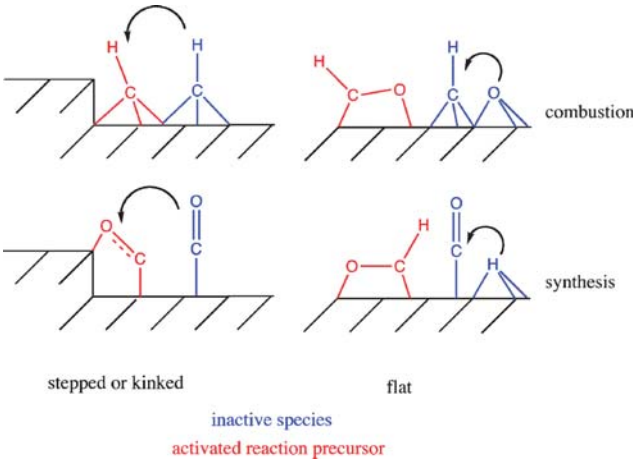

Fig. 9 Scheme of the activation of CO on a metal surface.

form (or *vice versa*). DFT calculations have revealed that activation of the breaking bond can be achieved either by the geometric sites, or by virtue of the electronic properties pertaining to the formyl intermediate. Calculations involving formyl on stepped and kinked surfaces are keenly awaited. Closing we feel obliged to mention that even though the reactions on the active surface are the most crucial factor of a catalytic reactor, many other factors influence the activity. Hence, surface science studies lay the foundation of more complex studies on more realistic, polymorphic surfaces or particles at more realistic pressures.

References

1 D. A. King, *Science*, 2004, **303**, 176.
2 G. Walker and D. A. King, *'The Hot Topic: What We Can Do about Global Warming'*, Harvest Books, Bloomsbury, London, 2008.
3 *'Climate Change 2007: The Physical Science Basis'*, ed. D. Q. S. Solomon, M. Manning, M. Marquis, K. Averyt, M. M. B. Tignor and H. Leroy Miller, Cambridge University Press, New York, 2007.
4 N. Nakicenovic and R. Swart, in *'Special Report on Emissions Scenarios'*, http://www.ipcc.ch/ipccreports/sres/emission/index.htm, 2007.
5 http://www.savedarfur.org/pages/background.
6 T. Flannery, *'The Weather Makers: The History and Future Impact of Climate Change'*, Penguin Books Ltd, London, 2007.
7 D. A. Stainforth, T. Aina, C. Christensen, M. Collins, N. Faull, D. J. Frame, J. A. Kettleborough, S. Knight, A. Martin, J. M. Murphy, C. Piani, D. Sexton, L. A. Smith, R. A. Spicer, A. J. Thorpe and M. R. Allen, *Nature*, 2005, **433**, 403; M. R. Allen and W. J. Ingram, *Nature*, 2002, **419**, 224.
8 E. B. I. Association, http://www.eubia.org, 2008.
9 G. W. Huber and A. Corma, *Angew. Chem., Int. Ed.*, 2007, **46**, 7184; G. W. Huber, P. O'Connor and A. Corma, *Appl. Catal., A*, 2007, **329**, 120.
10 G. Buntrock, *'Cheap No More—Rising incomes in Asia and ethanol subsidies in America have put an end to a long era of falling food prices'*, The Economist, London, 6 December 2007.
11 K. Gordon, R. Holroyd, J. N. Perquin, D. Morten, D. A. C. Dewdney, A. R. M. Murray, K. Stock and F. A. Williams, in *Synthetic Oil Production in Germany; Interrogation of Dr. Butefisch*, British Intelligence Objectives Sub-Committee Final Report No. 1697, Interrogation 667 Item No. 30, 1946.
12 H. Schulz, *Appl. Catal., A*, 1999, **186**, 3.
13 R. J. Farrauto and R. M. Heck, *Catal. Today*, 2000, **55**, 179.
14 L. D. Schmidt and P. J. Dauenhauer, *Nature*, 2007, **447**, 914; Y. Roman-Leshkov, C. J. Barrett, Z. Y. Liu and J. A. Dumesic,

Nature, 2007, **447**, 982; G. W. Huber, S. Iborra and A. Corma, *Chem. Rev*., 2006, **106**, 4044.
15 J. Wolff, A. G. Papathanasiou, I. G. Kevrekidis, H. H. Rotermund and G. Ertl, *Science*, 2001, **294**, 134; H. Over, Y. D. Kim, A. P. Seitsonen, S. Wendt, E. Lundgren, M. Schmid, P. Varga, A. Morgante and G. Ertl, *Science*, 2000, **287**, 1474; M. Bonn, S. Funk, C. Hess, D. N. Denzler, C. Stampfl, M. Scheffler, M. Wolf and G. Ertl, *Science*, 1999, **285**, 1042; J. Wintterlin, S. Volkening, T. V. W. Janssens, T. Zambelli and G. Ertl, *Science*, 1997, **278**, 1931; T. Zambelli, J. Wintterlin, J. Trost and G. Ertl, *Science*, 1996, **273**, 1688; H. H. Rotermund, G. Haas, R. U. Franz, R. M. Tromp and G. Ertl, *Science*, 1995, **270**, 608.
16 M. Mavrikakis, M. Baumer, H. J. Freund and J. K. Norskov, *Catal. Lett*., 2002, **81**, 153.
17 R. T. Vang, K. Honkala, S. Dahl, E. K. Vestergaard, J. Schnadt, E. Laegsgaard, B. S. Clausen, J. K. Norskov and F. Besenbacher, *Surf. Sci*., 2006, **600**, 66.
18 Z. P. Liu, *Phys. Rev. B: Condens. Matter Mater. Phys*., 2006, **73**, 233410; Z. P. Liu, X. Q. Gong, J. Kohanoff, C. Sanchez and P. Hu, *Phys. Rev. Lett*., 2003, **91**, 266102.
19 N. D. Lang and W. Kohn, *Phys. Rev. B: Solid State*, 1970, **1**, 4555.
20 N. D. Lang and A. R. Williams, *Phys. Rev. Lett*., 1975, **34**, 531.
21 S. P. Walch and W. A. Goddard, *Solid State Commun*., 1977, **23**, 907.
22 J. K. Norskov and N. D. Lang, *Phys. Rev. B: Condens. Matter Mater. Phys*., 1980, **21**, 2131.
23 H. Rabaa, J. Y. Saillard and R. Hoffmann, *J. Am. Chem. Soc*., 1986, **108**, 4327.
24 O. R. Inderwildi, S. J. Jenkins and D. A. King, *J. Phys. Chem. C*, 2008, **112**, 1305.
25 M. A. Petersen, S. J. Jenkins and D. A. King, *J. Phys. Chem. B*, 2004, **108**, 5909.
26 M. A. Petersen, S. J. Jenkins and D. A. King, *J. Phys. Chem. B*, 2004, **108**, 5920.
27 T. A. Halgren and W. N. Lipscomb, *Chem. Phys. Lett*., 1977, **49**, 225.
28 N. Govind, M. Petersen, G. Fitzgerald, D. King-Smith and J. Andzelm, *Comput. Mater. Sci*., 2003, **28**, 250.
29 G. Mills, H. Jonsson and G. K. Schenter, *Surf. Sci*., 1995, **324**, 305.
30 G. Henkelman, B. P. Uberuaga and H. Jonsson, *J. Chem. Phys*., 2000, **113**, 9901.
31 D. J. Wales, *'Energy Landscapes'*, Cambridge University Press, Cambridge, 2003.
32 B. Hammer, K. W. Jacobsen and J. K. Norskov, *Phys. Rev. Lett*., 1992, **69**, 1971.
33 M. P. Andersson, F. Abild-Pedersen, I. Remediakis, T. Bligaard, G. Jones, J. Engbæk, O. Lytken, S. Horch, J. H. Nielsen, J. Sehested, J. R. Rostrup-Nielsen, J. K. Nørskov and I. Chorkendorff, *J. Catal*., 2008, **255**, 6.
34 A. T. Anghel, S. J. Jenkins, D. J. Wales and D. A. King, *J. Phys. Chem. B*, 2006, **110**, 4147.
35 A. T. Anghel, D. J. Wales, S. J. Jenkins and D. A. King, *Chem. Phys. Lett*., 2005, **413**, 289.
36 A. T. Anghel, D. J. Wales, S. J. Jenkins and D. A. King, *Phys. Rev. B: Condens. Matter Mater. Phys*., 2005, **71**, 113410.
37 T. Bligaard, J. K. Norskov, S. Dahl, J. Matthiesen, C. H. Christensen and J. Sehested, *J. Catal*., 2004, **224**, 206; M. L. Bocquet, A. Michaelides, D. Loffreda, P. Sautet, A. Alavi and D. A. King, *J. Am. Chem. Soc*., 2003, **125**, 5620; J. Greeley, J. K. Norskov, L. A. Kibler, A. M. El-Aziz and D. M. Kolb, *ChemPhysChem*, 2006, **7**, 1032; A. Gross, *Top. Catal*., 2006, **37**, 29; B. Hammer, *J. Catal*., 2001, **199**, 171; B. Hammer, *Top. Catal*., 2006, **37**, 3; D. Loffreda, D. Simon and P. Sautet, *J. Catal*., 2003, **213**, 211; A. Michaelides, A. Alavi and D. A. King, *J. Am. Chem. Soc*., 2003, **125**, 2746; M. Neurock, in *Catalytic surface reaction pathways and energetics from first principles: Proceedings of the International Symposium, Antwerp, Belgium, 15-17 September 1997*, ed. G. F. Froment and K. C. Waugh, Elsevier, Amsterdam, 1997; J. M. Ricart, F. Ample, A. Clotet, D. Curulla, J. W. Niemantsverdriet, J. F. Paul and J. Perez-Ramirez, *J. Catal*., 2005, **232**, 179; A. Vargas, F. Hoxha, N. Bonalumi, T. Mallat and A. Baiker, *J. Catal*., 2006, **240**, 203.
38 Z. P. Liu and P. Hu, *J. Am. Chem. Soc*., 2003, **125**, 1958.
39 M. D. Rasmussen, L. M. Molina and B. Hammer, *J. Chem. Phys*., 2004, **120**, 988; D. Vogtenhuber, R. Podloucky, J. Redinger, E. L. D. Hebenstreit, W. Hebenstreit and U. Diebold, *Phys. Rev. B: Condens. Matter Mater. Phys*., 2002, **65**, 125411; O. R. Inderwildi and M. Kraft, *ChemPhysChem*, 2007, **8**, 444.
40 P. Broqvist, L. M. Molina, H. Gronbeck and B. Hammer, *J. Catal*., 2004, **227**, 217; L. M. Molina and B. Hammer, *Phys. Rev. Lett*., 2003, **90**, 206102; Y. Wang, E. Florez, F. Mondragon and T. N. Truong, *Surf. Sci*., 2006, **600**, 1703; H. Gronbeck and P. Broqvist, *J. Chem. Phys*., 2003, **119**, 3896; N. Lopez, J. K. Norskov, T. V. W. Janssens, A. Carlsson, A. Puig-Molina, B. S. Clausen and J. D. Grunwaldt, *J. Catal*., 2004, **225**, 86; Z. P. Liu, S. J. Jenkins and D. A. King, *Phys. Rev. Lett*., 2004, **93**, 156102.
41 G. Ertl, H. Knoezinger and J. E. Weitkamp, *'Handbook of Heterogeneous Catalysis'*, VCH Verlagsgesellschaft mbH, Weinheim, 1997.
42 A. Klust and R. J. Madix, *Surf. Sci*., 2006, **600**, 5025; R. L. Cropley, F. J. Williams, O. P. H. Vaughan, A. J. Urquhart, M. S. Tikhov and R. M. Lambert, *Surf. Sci*., 2005, **578**, L85.
43 R. Schwiedernoch, S. Tischer, C. Correa and O. Deutschmann, *Chem. Eng. Sci*., 2003, **58**, 633; J. D. Grunwaldt, S. Hannemann, C. G. Schroer and A. Baiker, *J. Phys. Chem. B*, 2006, **110**, 8674; S. Hannemann, J. D. Grunwaldt, N. van Vegten, A. Baiker, P. Boye and C. G. Schroer, *Catal. Today*, 2007, **126**, 54.
44 R. Burch, J. P. Breen and F. C. Meunier, *Appl. Catal., B*, 2002, **39**, 283; M. D. Amiridis, C. Mihut, M. Maciejewski and A. Baiker, *Top. Catal*., 2004, **28**, 141.
45 M. Azar, V. Caps, F. Morfin, J. L. Rousset, A. Piednoir, J. C. Bertolini and L. Piccolo, *J. Catal*., 2006, **239**, 307; M. J. Kahlich, H. A. Gasteiger and R. J. Behm, *J. Catal*., 1997, **171**, 93.
46 M. D. Hughes, Y. J. Xu, P. Jenkins, P. McMorn, P. Landon, D. I. Enache, A. F. Carley, G. A. Attard, G. J. Hutchings, F. King, E. H. Stitt, P. Johnston, K. Griffin and C. J. Kiely, *Nature*, 2005, **437**, 1132; X. P. Xu and C. M. Friend, *J. Phys. Chem*., 1991, **95**, 10753.
47 F. Zaera, *Chem. Rec*., 2005, **5**, 133; F. Zaera, *Catal. Lett*., 2003, **91**, 1.
48 H. Ostrom, L. Triguero, M. Nyberg, H. Ogasawara, L. G. M. Pettersson and A. Nilsson, *Phys. Rev. Lett*., 2003, **91**, 046102.
49 B. K. Hodnett, F. J. J. G. Janssen, J. W. Niemantsverdriet, V. Ponec, R. A. Van Santen and J. A. R. Van Veen, in *'Heterogeneous Catalysis'*, ed. R. A. Van Santen, P. W. N. M. Van Leeuwen, J. A. Moulijn and B. A. Averill, Elsevier, Amsterdam, 1999.
50 B. Eisenberg, R. A. Fiato, C. H. Mauldin, G. R. Say and S. L. Soled, 'Exxon's advanced gas-to-liquids technology', , in *Natural Gas Conversion V, 119: Proceedings of the 5th Natural Gas Conversion Symposium, Giardini Naxos - Taormina, Sicily, Italy, 20-25 September 1998*, ed. A. Parmaliana, D. Sanfilippo, F. Frusteri, A. Vaccari and F. Arena, Elsevier, Amsterdam, 1998.
51 J. F. Weaver, A. F. Carlsson and R. J. Madix, *Surf. Sci. Rep*., 2003, **50**, 107.
52 S. J. Jenkins and S. J. Pratt, *Surf. Sci. Rep*., 2007, **62**, 373.
53 S. J. Pratt, S. J. Jenkins and D. A. King, *Surf. Sci*., 2005, **585**, L159.
54 F. Zaera, *Langmuir*, 1996, **12**, 88.
55 D. J. Oakes, M. R. S. McCoustra and M. A. Chesters, *Faraday Discuss*., 1993, **96**, 325; D. H. Fairbrother, X. D. Peng, M. Trenary and P. C. Stair, *J. Chem. Soc., Faraday Trans*., 1995, **91**, 3619; D. H. Fairbrother, X. D. Peng, R. Viswanathan, P. C. Stair, M. Trenary and J. Fan, *Surf. Sci*., 1993, **285**, L455; D. J. Oakes, H. E. Newell, F. J. M. Rutten, M. R. S. McCoustra and M. A. Chesters, *J. Vac. Sci. Technol., A*, 1996, **14**, 1439.
56 T. Fuhrmann, M. Kinne, B. Trankenschuh, C. Papp, J. F. Zhu, R. Denecke and H. P. Steinruck, *New J. Phys*., 2005, **7**, 107.
57 C. Papp, B. Trankenschuh, R. Streber, T. Fuhrmann, R. Denecke and H. P. Steinruck, *J. Phys. Chem. C*, 2007, **111**, 2177; C. Papp, T. Fuhrmann, B. Trankenschuh, R. Denecke and H. P. Steinruck, *Chem. Phys. Lett*., 2007, **442**, 176.
58 E. Herceg, H. Celio and M. Trenary, *Rev. Sci. Instrum*., 2004, **75**, 2545; R. P. Deng, E. Herceg and M. Trenary, *Surf. Sci*., 2004, **573**, 310.
59 J. Kua, F. Faglioni and W. A. Goddard, *J. Am. Chem. Soc*., 2000, **122**, 2309.

60 J. Kua and W. A. Goddard, *J. Phys. Chem. B*, 1999, **103**, 2318.
61 J. Kua and W. A. Goddard, *J. Phys. Chem. B*, 1998, **102**, 9492.
62 R. M. Watwe, B. E. Spiewak, R. D. Cortright and J. A. Dumesic, *J. Catal*., 1998, **180**, 184.
63 C. Minot, M. A. Van Hove and G. A. Somorjai, *Surf. Sci*., 1983, **127**, 441.
64 T. Jacob and W. A. Goddard, *J. Phys. Chem. B*, 2005, **109**, 297.
65 D. C. Ford, Y. Xu and M. Mavrikakis, *Surf. Sci*., 2005, **587**, 159.
66 G. Papoian, J. K. Norskov and R. Hoffmann, *J. Am. Chem. Soc*., 2000, **122**, 4129.
67 A. Michaelides and P. Hu, *J. Am. Chem. Soc*., 2000, **122**, 9866.
68 A. Michaelides and P. Hu, *J. Chem. Phys*., 2001, **114**, 2523.
69 M. L. Bocquet, J. Cerda and P. Sautet, *Phys. Rev. B: Condens. Matter Mater. Phys*., 1999, **59**, 15437.
70 M. Chen, S. P. Bates, R. A. van Santen and C. M. Friend, *J. Phys. Chem. B*, 1997, **101**, 10051.
71 A. Eichler, F. Mittendorfer and J. Hafner, *Phys. Rev. B: Condens. Matter Mater. Phys*., 2000, **62**, 4744.
72 A. Eichler and J. Hafner, *Phys. Rev. Lett*., 1997, **79**, 4481.
73 A. Gross, A. Eichler, J. Hafner, M. J. Mehl and D. A. Papaconstantopoulos, *Surf. Sci*., 2003, **539**, L542.
74 A. Gross, A. Eichler, J. Hafner, M. J. Mehl and D. A. Papaconstantopoulos, *J. Chem. Phys*., 2006, **124**, 174713.
75 O. R. Inderwildi, S. J. Jenkins and D. A. King, *Angew. Chem., Int. Ed*., 2008, **47**, 5253.
76 R. M. Watwe, R. D. Cortright, J. K. Norskov and J. A. Dumesic, *J. Phys. Chem. B*, 2000, **104**, 2299.
77 R. M. Watwe, R. D. Cortright, M. Mavrikakis, J. K. Norskov and J. A. Dumesic, *J. Chem. Phys*., 2001, **114**, 4663.
78 J. M. Essen, J. Haubrich, C. Becker and K. Wandelt, *Surf. Sci*., 2007, **601**, 3472.
79 J. W. Medlin and M. D. Allendorf, *J. Phys. Chem. B*, 2003, **107**, 217.
80 P. S. Moussounda, M. F. Haroun, B. M'Passi-Mabiala and P. Legare, *Surf. Sci*., 2005, **594**, 231.
81 P. S. Moussounda, M. F. Haroun, G. Rakotovelo and P. Legare, *Surf. Sci*., 2007, **601**, 3697.
82 P. D. Szuromi, J. R. Engstrom and W. H. Weinberg, *J. Phys. Chem*., 1985, **89**, 2497.
83 J. A. Stinnett, M. C. McMaster, S. L. M. Schroeder and R. J. Madix, *Surf. Sci*., 1996, **365**, 683.
84 M. C. McMaster, S. L. M. Schroeder and R. J. Madix, *Surf. Sci*., 1993, **297**, 253.
85 M. C. McMaster and R. J. Madix, *J. Chem. Phys*., 1993, **98**, 9963.
86 M. C. McMaster and R. J. Madix, *Surf. Sci*., 1993, **294**, 420; M. C. McMaster and R. J. Madix, *Surf. Sci*., 1992, **275**, 265.
87 S. Schroeder, M. C. McMaster, J. A. Stinnett and R. J. Madix, *Surf. Sci*., 1993, **297**, L148.
88 A. V. Walker and D. A. King, *Phys. Rev. Lett*., 1999, **82**, 5156; A. V. Walker and D. A. King, *J. Chem. Phys*., 2000, **112**, 4739.
89 A. V. Walker and D. A. King, *Surf. Sci*., 2000, **444**, 1; A. V. Walker and D. A. King, *J. Phys. Chem. B*, 2000, **104**, 6462; D. T. P. Watson, Q. Ge and D. A. King, *J. Chem. Phys*., 2001, **115**, 11306; D. T. P. Watson, J. van Dijk, J. J. W. Harris and D. A. King, *Surf. Sci*., 2002, **506**, 243; D. T. P. Watson, J. J. W. Harris and D. A. King, *J. Phys. Chem. B*, 2002, **106**, 3416.
90 A. V. Walker and D. A. King, *J. Chem. Phys*., 2000, **112**, 1937; D. T. P. Watson, J. J. W. Harris and D. A. King, *Surf. Sci*., 2002, **505**, 58.
91 M. A. Petersen, D. T. P. Watson, S. J. Jenkins and D. A. King, *J. Chem. Phys*., 2002, **117**, 3951.
92 D. T. P. Watson, S. Titmuss and D. A. King, *Surf. Sci*., 2002, **505**, 49.
93 J. J. W. Harris, V. Fiorin, C. T. Campbell and D. A. King, *J. Phys. Chem. B*, 2005, **109**, 4069.
94 F. R. Laffir, J. J. W. Harris, V. Fiorin and D. A. King, *Chem. Phys. Lett*., 2007, **439**, 342.
95 A. T. Anghel, D. J. Wales, S. J. Jenkins and D. A. King, *J. Chem. Phys*., 2007, **126**, 044710.
96 M. A. Petersen, S. J. Jenkins and D. A. King, *J. Phys. Chem. B*, 2006, **110**, 11962.
97 A. Stuck, C. E. Wartnaby, Y. Y. Yeo and D. A. King, *Phys. Rev. Lett*., 1995, **74**, 578.
98 Y. Ohno, T. Matsushima, S. Tanaka, E. Yagasaki and M. Kamada, *Surf. Sci*., 1992, **275**, 281.
99 K. C. Prince, K. Duckers, K. Horn and V. Chab, *Surf. Sci*., 1988, **200**, L451.
100 J. Fusy and R. Ducros, *Surf. Sci*., 1989, **214**, 337; R. Ducros and J. Fusy, *Appl. Surf. Sci*., 1990, **44**, 59.
101 T. Yamanaka, T. Matsushima, S. Tanaka and M. Kamada, *Surf. Sci*., 1996, **349**, 119.
102 M. Sano, Y. Seimiya, Y. Ohno, T. Matsushima, S. Tanaka and M. Kamada, *Appl. Surf. Sci*., 1998, **132**, 518; M. Sano, Y. Seimiya, Y. Ohno, T. Matsushima, S. Tanaka and M. Kamada, *Surf. Sci*., 1999, **421**, 386.
103 S. Wako, M. Sano, Y. Ohno, T. Matsushima, S. Tanaka and M. Kamada, *Surf. Sci*., 2000, **461**, L537.
104 S. Helveg, H. T. Lorensen, S. Horch, E. Laegsgaard, I. Stensgaard, K. W. Jacobsen, J. K. Norskow and F. Besenbacher, *Surf. Sci*., 1999, **430**, L533.
105 E. Janin, H. von Schenck, M. Gothelid, U. O. Karlsson and M. Svensson, *Phys. Rev. B: Condens. Matter Mater. Phys*., 2000, **61**, 13144.
106 M. A. Petersen, PhD Thesis, University of Cambridge, 2003.
107 M. A. Petersen, S. J. Jenkins and D. A. King, unpublished.
108 A. T. Gee, B. E. Hayden, C. Mormiche, A. W. Kleyn and B. Riedmuller, *J. Chem. Phys*., 2003, **118**, 3334.
109 R. Kose and D. A. King, *Chem. Phys. Lett*., 1999, **313**, 1; S. J. Jenkins, M. A. Petersen and D. A. King, *Surf. Sci*., 2001, **494**, 159.
110 M. Chen, C. M. Friend and R. A. van Santen, *Catal. Today*, 1999, **50**, 621.
111 M. Mavrikakis, J. Rempel, J. Greeley, L. B. Hansen and J. K. Norskov, *J. Chem. Phys*., 2002, **117**, 6737.
112 E. J. Walter and A. M. Rappe, *Surf. Sci*., 2004, **549**, 265.
113 H. Y. Xiao and D. Q. Xie, *Surf. Sci*., 2004, **558**, 15.
114 A. Kokalj, N. Bonini, C. Sbraccia, S. de Gironcoli and S. Baroni, *J. Am. Chem. Soc*., 2004, **126**, 16732.
115 B. S. Bunnik and G. J. Kramer, *J. Catal*., 2006, **242**, 309.
116 M. M. Yang, X. H. Bao and W. X. Li, *J. Chem. Phys*., 2007, **127**, 024705.
117 J. P. Perdew, J. A. Chevary, S. H. Vosko, K. A. Jackson, M. R. Pederson, D. J. Singh and C. Fiolhais, *Phys. Rev. B: Condens. Matter Mater. Phys*., 1992, **46**, 6671.
118 J. P. Perdew, K. Burke and M. Ernzerhof, *Phys. Rev. Lett*., 1996, **77**, 3865.
119 B. Hammer, L. B. Hansen and J. K. Norskov, *Phys. Rev. B: Condens. Matter Mater. Phys*., 1999, **59**, 7413.
120 T. Kecskes, R. Barthos, J. Rasko and J. Kiss, *Vacuum*, 2003, **71**, 107.
121 O. R. Inderwildi, S. J. Jenkins and D. A. King, *J. Am. Chem. Soc*., 2007, **129**, 1751.
122 D. Loffreda, D. Simon and P. Sautet, *J. Chem. Phys*., 1998, **108**, 6447.
123 M. V. Ganduglia-Pirovano, K. Reuter and M. Scheffler, *Phys. Rev. B: Condens. Matter Mater. Phys*., 2002, **65**, 245426; M. V. Ganduglia-Pirovano and M. Scheffler, *Phys. Rev. B: Condens. Matter Mater. Phys*., 1999, **59**, 15533; M. V. Ganduglia-Pirovano, M. Scheffler, A. Baraldi, S. Lizzit, G. Comelli, G. Paolucci and R. Rosei, *Phys. Rev. B: Condens. Matter Mater. Phys*., 2001, **63**, 205415.
124 M. Todorova, W. X. Li, M. V. Ganduglia-Pirovano, C. Stampfl, K. Reuter and M. Scheffler, *Phys. Rev. Lett*., 2002, **89**, 096103.
125 E. J. Walter, S. P. Lewis and A. M. Rappe, *J. Chem. Phys*., 2000, **113**, 4388.
126 O. R. Inderwildi, D. Lebiedz, O. Deutschmann and J. Warnatz, *J. Chem. Phys*., 2005, **122**, 154702.
127 Z. P. Liu, P. Hu and M. H. Lee, *J. Chem. Phys*., 2003, **119**, 6282.
128 G. Fratesi and S. de Gironcoli, *J. Chem. Phys*., 2006, **125**, 044701.
129 B. McAllister and P. Hu, *J. Chem. Phys*., 2005, **122**, 084709.
130 T. Bhattacharjee, O. R. Inderwildi, S. J. Jenkins, U. Riedel and J. Warnatz, *J. Phys. Chem. C*, 2008, **112**, 8751.
131 J. F. Paul and P. Sautet, *J. Phys. Chem. B*, 1998, **102**, 1578.
132 C. J. Zhang and P. Hu, *J. Chem. Phys*., 2002, **116**, 322.
133 K. Honkala and K. Laasonen, *J. Chem. Phys*., 2001, **115**, 2297.
134 M. Todorova, K. Reuter and M. Scheffler, *J. Phys. Chem. B*, 2004, **108**, 14477.
135 K. Reuter and M. Scheffler, *Appl. Phys. A: Mater. Sci. Process*., 2004, **78**, 793.

136 E. Lundgren, G. Kresse, C. Klein, M. Borg, J. N. Andersen, M. De Santis, Y. Gauthier, C. Konvicka, M. Schmid and P. Varga, *Phys. Rev. Lett.*, 2002, **88**, 246103.
137 M. Todorova, K. Reuter and M. Scheffler, *Phys. Rev. B: Condens. Matter Mater. Phys.*, 2005, **71**, 195403.
138 M. Saidy, O. L. Warren, P. A. Thiel and K. A. R. Mitchell, *Surf. Sci.*, 2001, **494**, L799; D. T. Vu, K. A. R. Mitchell, O. L. Warren and P. A. Thiel, *Surf. Sci.*, 1994, **318**, 129.
139 M. Todorova, E. Lundgren, V. Blum, A. Mikkelsen, S. Gray, J. Gustafson, M. Borg, J. Rogal, K. Reuter, J. N. Andersen and M. Scheffler, *Surf. Sci.*, 2003, **541**, 101.
140 J. N. Carstens, S. C. Su and A. T. Bell, *J. Catal.*, 1998, **176**, 136; S. C. Su, J. N. Carstens and A. T. Bell, *J. Catal.*, 1998, **176**, 125.
141 K. Fujimoto, F. H. Ribeiro, M. Avalos-Borja and E. Iglesia, *J. Catal.*, 1998, **179**, 431.
142 H. Y. Li, Y. L. Guo, Y. Guo, G. Z. Lu and P. Hu, *J. Chem. Phys.*, 2008, **128**, 051101.
143 A. Hirsimaki, S. Paavilainen, J. A. Nieminen and M. Valden, *Surf. Sci.*, 2001, **482**, 171; S. Paavilainen and J. A. Nieminen, *Surf. Sci.*, 2001, **486**, L489.
144 S. Paavilainen and J. A. Nieminen, *Phys. Rev. B: Condens. Matter Mater. Phys.*, 2002, **66**, 155409.
145 M. Lahti, N. Nivalainen, A. Puisto and M. Alatalo, *Surf. Sci.*, 2007, **601**, 3774.
146 P. Junell, K. Honkala, M. Hirsimaki, M. Valden and K. Laasonen, *Surf. Sci.*, 2003, **546**, L797.
147 S. Yamagishi, S. J. Jenkins and D. A. King, *Surf. Sci.*, 2003, **543**, 12.
148 T. Li, B. Bhatia and D. S. Sholl, *J. Chem. Phys.*, 2004, **121**, 10241.
149 M. Pedio, L. Becker, B. Hillert, S. Daddato and J. Haase, *Phys. Rev. B: Condens. Matter Mater. Phys.*, 1990, **41**, 7462; M. A. Mendez, W. Oed, A. Fricke, L. Hammer, K. Heinz and K. Muller, *Surf. Sci.*, 1991, **253**, 99; C. Schwennicke and H. Pfnur, *Surf. Sci.*, 1996, **369**, 248.
150 S. Y. Hong, A. Kara, T. S. Rahman, R. Heid and K. P. Bohnen, *Phys. Rev. B: Condens. Matter Mater. Phys.*, 2004, **69**, 195403.
151 M. J. Harrison, D. P. Woodruff and J. Robinson, *Surf. Sci.*, 2008, **602**, 226.
152 W. Oed, H. Lindner, U. Starke, K. Heinz, K. Muller and J. B. Pendry, *Surf. Sci.*, 1989, **224**, 179.
153 A. Michaelides and P. Hu, *Surf. Sci.*, 1999, **437**, 362.
154 A. Michaelides and P. Hu, *J. Chem. Phys.*, 2000, **112**, 6006.
155 A. Michaelides and P. Hu, *J. Chem. Phys.*, 2000, **112**, 8120.
156 R. M. Watwe, H. S. Bengaard, J. R. Rostrup-Nielsen, J. A. Dumesic and J. K. Norskov, *J. Catal.*, 2000, **189**, 16.
157 H. S. Bengaard, J. K. Norskov, J. Sehested, B. S. Clausen, L. P. Nielsen, A. M. Molenbroek and J. R. Rostrup-Nielsen, *J. Catal.*, 2002, **209**, 365.
158 S.-G. Wang, D.-B. Cao, Y.-W. Li, J. Wang and H. Jiao, *Surf. Sci.*, 2006, **600**, 3226.
159 S. G. Wang, X. Y. Liao, J. Hu, D. B. Cao, Y. W. Li, J. G. Wang and H. J. Jiao, *Surf. Sci.*, 2007, **601**, 1271.
160 S. G. Wang, D. B. Cao, Y. W. Li, J. Wang and H. Jiao, *J. Phys. Chem. B*, 2006, **110**, 9976.
161 F. Abild-Pedersen, O. Lytken, J. Engbaek, G. Nielsen, I. Chorkendorff and J. K. Norskov, *Surf. Sci.*, 2005, **590**, 127.
162 D. J. Klinke and L. J. Broadbelt, *Surf. Sci.*, 1999, **429**, 169.
163 K. Christmann, *Surf. Sci. Rep.*, 1988, **9**, 1.
164 H. Papp, *Surf. Sci.*, 1985, **149**, 460.
165 J. Lahtinen, J. Vaari, K. Kauraala, E. A. Soares and M. A. Van Hove, *Surf. Sci.*, 2000, **448**, 269.
166 S. Pick, *Surf. Sci.*, 2007, **601**, 5571.
167 Q. F. Ge and M. Neurock, *J. Phys. Chem. B*, 2006, **110**, 15368.
168 H. Papp, *Surf. Sci.*, 1983, **129**, 205.
169 X. Q. Gong, R. Raval and P. Hu, *Surf. Sci.*, 2004, **562**, 247.
170 H. Oosterbeek, *Phys. Chem. Chem. Phys.*, 2007, **9**, 3570.
171 J. J. C. Geerlings, M. C. Zonnevylle and C. P. M. de Groot, *Surf. Sci.*, 1991, **241**, 302.
172 S. J. Jenkins and D. A. King, *J. Am. Chem. Soc.*, 2000, **122**, 10610.
173 Q. Ge, M. Neurock, H. A. Wright and N. Srinivasan, *J. Phys. Chem. B*, 2002, **106**, 2826.
174 X. Q. Gong, R. Raval and P. Hu, *J. Chem. Phys.*, 2005, **122**, 024711.
175 J. Cheng, X.-Q. Gong, P. Hu, C. M. Lok, P. Ellis and S. French, *J. Catal.*, 2008, **254**, 285.
176 B. E. Bent, *Chem. Rev.*, 1996, **96**, 1361.
177 J. Cheng, T. Song, P. Hu, C. M. Lok, P. Ellis and S. French, *J. Catal.*, 2008, **255**, 20.
178 M. E. Dry, *Catal. Today*, 2002, **71**, 227.
179 R. L. Toomes and D. A. King, *Surf. Sci.*, 1996, **349**, 1.
180 S. J. Jenkins and D. A. King, *Surf. Sci.*, 2002, **504**, 138.
181 O. R. Inderwildi, D. Lebiedz and J. Warnatz, *Phys. Chem. Chem. Phys.*, 2005, **7**, 2552; J. K. Nørskov, T. Bligaard, A. Logadottir, S. Bahn, L. B. Hansen, M. Bollinger, H. Bengaard, B. Hammer, Z. Sljivancanin, M. Mavrikakis, Y. Xu, S. Dahl and C. J. H. Jacobsen, *J. Catal.*, 2002, **209**, 275; A. Michaelides, Z. P. Liu, C. J. Zhang, A. Alavi, D. A. King and P. Hu, *J. Am. Chem. Soc.*, 2003, **125**, 3704.
182 Y. K. Kim, G. A. Morgan and J. T. Yates, *Chem. Phys. Lett.*, 2006, **431**, 317.
183 B. Narloch, G. Held and D. Menzel, *Surf. Sci.*, 1995, **340**, 159; B. Narloch, G. Held and D. Menzel, *Surf. Sci.*, 1994, **317**, 131.
184 C. Stampfl and M. Scheffler, *Isr. J. Chem.*, 1998, **38**, 409.
185 J. Braun, K. L. Kostov, G. Witte and C. Woll, *J. Chem. Phys.*, 1997, **106**, 8262.
186 B. Riedmuller, I. M. Ciobica, D. C. Papageorgopoulos, F. Frechard, B. Berenbak, A. W. Kleyn and R. A. van Santen, *J. Chem. Phys.*, 2001, **115**, 5244; B. Riedmuller, I. M. Ciobica, D. C. Papageorgopoulos, B. Berenbak, R. A. van Santen and A. W. Kleyn, *Surf. Sci.*, 2000, **465**, 347.
187 D. W. Goodman, C. H. F. Peden and M. S. Chen, *Surf. Sci.*, 2007, **601**, L124; K. Reuter, *Oil Gas Sci. Technol.*, 2006, **61**, 471; K. Reuter and M. Scheffler, *Phys. Rev. B: Condens. Matter Mater. Phys.*, 2006, **73**, 045433.
188 J. Wintterlin, J. Trost, S. Renisch, R. Schuster, T. Zambelli and G. Ertl, *Surf. Sci.*, 1997, **394**, 159.
189 M. Nakamura, H. Kato, N. Hoshi, K. Sumitani and O. Sakata, *J. Phys. Chem. C*, 2007, **111**, 977.
190 S. Takahashi, Y. Fujimoto, Y. Teraoka, A. Yoshigoe, H. Okuyama and T. Aruga, *Surf. Sci.*, 2007, **601**, 3809.
191 P. J. Feibelman, *Science*, 2002, **295**, 99.
192 D. Menzel, *Science*, 2002, **295**, 58; D. Menzel, *Science*, 2002, **296**, 264.
193 C. Stampfl, S. Schwegmann, H. Over, M. Scheffler and G. Ertl, *Phys. Rev. Lett.*, 1996, **77**, 3371.
194 C. Stampfl and M. Scheffler, *Phys. Rev. B: Condens. Matter Mater. Phys.*, 2002, **65**, 155417.
195 C. Stampfl and M. Scheffler, *Phys. Rev. B: Condens. Matter Mater. Phys.*, 1996, **54**, 2868.
196 A. C. Luntz, M. Persson, S. Wagner, C. Frischkorn and M. Wolf, *J. Chem. Phys.*, 2006, **124**, 244702.
197 M. C. Wu, P. Lenzsolomun and D. W. Goodman, *J. Vac. Sci. Technol., A*, 1994, **12**, 2205.
198 M. C. Wu, D. W. Goodman and G. W. Zajac, *Catal. Lett.*, 1994, **24**, 23.
199 S. H. Payne, J. S. McEwen, H. J. Kreuzer and D. Menzel, *Surf. Sci.*, 2005, **594**, 240.
200 M. Luppi, R. A. Olsen and E. J. Baerends, *Phys. Chem. Chem. Phys.*, 2006, **8**, 688.
201 I. M. Ciobica, F. Frechard, R. A. van Santen, A. W. Kleyn and J. Hafner, *J. Phys. Chem. B*, 2000, **104**, 3364.
202 I. M. Ciobica, F. Frechard, R. A. van Santen, A. W. Kleyn and J. Hafner, *Chem. Phys. Lett.*, 1999, **311**, 185.
203 I. M. Ciobica, A. W. Kleyn and R. A. Van Santen, *J. Phys. Chem. B*, 2003, **107**, 164.
204 I. M. Ciobica, G. J. Kramer, Q. Ge, M. Neurock and R. A. van Santen, *J. Catal.*, 2002, **212**, 136.
205 I. M. Ciobica and R. A. van Santen, *J. Phys. Chem. B*, 2003, **107**, 3808.
206 I. M. Ciobica and R. A. van Santen, *J. Phys. Chem. B*, 2002, **106**, 6200.
207 G. A. Morgan, D. C. Sorescu, T. Zubkov and J. T. Yates, *J. Phys. Chem. B*, 2004, **108**, 3614.
208 M. C. Wu and D. W. Goodman, *Surf. Sci.*, 1994, **306**, L529.
209 Z. P. Liu and P. Hu, *J. Am. Chem. Soc.*, 2002, **124**, 11568.
210 H. Mortensen, L. Diekhoner, A. Baurichter and A. C. Luntz, *J. Chem. Phys.*, 2002, **116**, 5781.

211 M. C. Wu and D. W. Goodman, *J. Am. Chem. Soc*., 1994, **116**, 1364.
212 H. C. Long, M. L. Turner, P. Fornasiero, J. Kaspar, M. Graziani and P. M. Maitlis, *J. Catal*., 1997, **167**, 172; P. M. Maitlis, H. C. Long, R. Quyoum, M. L. Turner and Z. Q. Wang, *Chem. Commun*., 1996, 1.
213 T. Zubkov, G. A. Morgan, J. T. Yates, O. Kuhlert, M. Lisowski, R. Schillinger, D. Fick and H. J. Jansch, *Surf. Sci*., 2003, **526**, 57.
214 J. Cheng, P. Hu, P. Ellis, S. French, G. Kelly and C. M. Lok, *J. Phys. Chem. C*, 2008, **112**, 6082.
215 D. E. Jiang and E. A. Carter, *Surf. Sci*., 2003, **547**, 85.
216 A. M. Baro and W. Erley, *Surf. Sci*., 1981, **112**, L759.
217 D. E. Jiang and E. A. Carter, *Surf. Sci*., 2004, **570**, 167.
218 W. Erley, *J. Vac. Sci. Technol*., 1981, **18**, 472.
219 G. Wedler and R. Ruhmann, *Appl. Surf. Sci*., 1983, **14**, 137.
220 D. E. Jiang and E. A. Carter, *Phys. Rev. B: Condens. Matter Mater. Phys*., 2005, **71**, 045402.
221 D. C. Sorescu, *Phys. Rev. B: Condens. Matter Mater. Phys*., 2006, **73**, 155420.
222 D. C. Sorescu, *Catal. Today*, 2005, **105**, 44.
223 D. C. Sorescu, D. L. Thompson, M. M. Hurley and C. F. Chabalowski, *Phys. Rev. B: Condens. Matter Mater. Phys*., 2002, **66**, 035416.
224 T. C. Bromfield, D. C. Ferre and J. W. Niemantsverdriet, *ChemPhysChem*, 2005, **6**, 254.
225 S. K. Nayak, M. Nooijen, S. L. Bernasek and P. Blaha, *J. Phys. Chem. B*, 2001, **105**, 164.
226 D. W. Moon, S. L. Bernasek, J. P. Lu, J. L. Gland and D. J. Dwyer, *Surf. Sci*., 1987, **184**, 90.
227 S. D. Cameron and D. J. Dwyer, *J. Vac. Sci. Technol., A*, 1988, **6**, 796.
228 J. M. H. Lo and T. Ziegler, *J. Phys. Chem. C*, 2007, **111**, 11012.
229 D. Curulla-Ferre, A. Govender, T. C. Bromfield and J. W. Niemantsverdriet, *J. Phys. Chem. B*, 2006, **110**, 13897.
230 J. M. H. Lo and T. Ziegler, *J. Phys. Chem. C*, 2007, **111**, 13149.
231 J. M. H. Lo and T. Ziegler, *J. Phys. Chem. C*, 2008, **112**, 3692.
232 Z. Y. Ma, C. F. Huo, X. Y. Liao, Y. W. Li, J. G. Wang and H. J. Jiao, *J. Phys. Chem. C*, 2007, **111**, 4305.
233 Y. H. Chen, D. B. Cao, Y. Jun, Y. W. Li, J. G. Wang and H. J. Jiao, *Chem. Phys. Lett*., 2004, **400**, 35.
234 C. F. Huo, J. Ren, Y. W. Li, J. G. Wang and H. J. Jiao, *J. Catal*., 2007, **249**, 174.
235 D. L. S. Nieskens, M. M. M. Jansen, A. P. van Bavel, D. Curulla-Ferre and J. W. Niemantsverdriet, *Phys. Chem. Chem. Phys*., 2006, **8**, 624; D. L. S. Nieskens, D. Curulla-Ferre and J. W. Niemantsverdriet, *ChemPhysChem*, 2006, **7**, 1022.
236 M. Watanabe and T. Kadowaki, *Appl. Surf. Sci*., 1987, **28**, 147.
237 O. R. Inderwildi, S. J. Jenkins and D. A. King, *J. Am. Chem. Soc*., 2008, **130**, 2213.
238 D. Bianchi and C. O. Bennett, *J. Catal*., 1984, **86**, 433.
239 D. Borthwick, V. Fiorin, S. J. Jenkins and D. A. King, *Surf. Sci*., 2008, **602**, 2325.
240 I. N. Remediakis, F. Abild-Pedersen and J. K. Norskov, *J. Phys. Chem. B*, 2004, **108**, 14535.
241 J. T. Stuckless, N. Alsarraf, C. Wartnaby and D. A. King, *J. Chem. Phys*., 1993, **99**, 2202.
242 V. Shah, T. Li, K. L. Baumert, H. Cheng and D. S. Sholl, *Surf. Sci*., 2003, **537**, 217.
243 K. Christmann, O. Schober, G. Ertl and M. Neumann, *J. Chem. Phys*., 1974, **60**, 4528.
244 B. Bhatia and D. S. Sholl, *J. Chem. Phys*., 2005, **122**, 204707.
245 Y. Morikawa, J. J. Mortensen, B. Hammer and J. K. Norskov, *Surf. Sci*., 1997, **386**, 67.
246 R. D. Kelley and D. W. Goodman, *Surf. Sci*., 1982, **123**, L743; D. W. Goodman, R. D. Kelley, T. E. Madey and J. M. White, *J. Catal*., 1980, **64**, 479.
247 A. D. Karmazyn, V. Fiorin, S. J. Jenkins and D. A. King, *Surf. Sci*., 2003, **538**, 171.
248 Q. F. Ge, S. J. Jenkins and D. A. King, *Chem. Phys. Lett*., 2000, **327**, 125.
249 Q. F. Ge, R. Kose and D. A. King, *Adv. Catal*., 2000, **45**, 207.